



CHORUS

This is the accepted manuscript made available via CHORUS. The article has been published as:

Coulomb drag

B. N. Narozhny and A. Levchenko

Rev. Mod. Phys. **88**, 025003 — Published 10 May 2016

DOI: [10.1103/RevModPhys.88.025003](https://doi.org/10.1103/RevModPhys.88.025003)

Coulomb drag

B.N. Narozhny

*Institut für Theorie der Kondensierten Materie,
Karlsruhe Institute of Technology,
76128 Karlsruhe,
Germany*

*National Research Nuclear University MEPhI (Moscow Engineering Physics Institute),
Kashirskoe shosse 31,
115409 Moscow,
Russia*

A. Levchenko

*Department of Physics,
University of Wisconsin-Madison,
Madison, Wisconsin 53706,
USA*

*Institut für Nanotechnologie,
Karlsruhe Institute of Technology,
76021 Karlsruhe,
Germany*

(Dated: October 28, 2015)

Coulomb drag is a transport phenomenon whereby long-range Coulomb interaction between charge carriers in two closely spaced but electrically isolated conductors induces a voltage (or, in a closed circuit, a current) in one of the conductors when an electrical current is passed through the other. The magnitude of the effect depends on the exact nature of the charge carriers and microscopic, many-body structure of the electronic systems in the two conductors. Drag measurements have become part of the standard toolbox in condensed matter physics that can be used to study fundamental properties of diverse physical systems including semiconductor heterostructures, graphene, quantum wires, quantum dots, and optical cavities.

PACS numbers: 73.63.-b, 73.43.Cd, 81.05.ue

CONTENTS

I. Frictional drag	2	A. Perturbative regime in ballistic samples	27
II. Coulomb drag in semiconductor heterostructures	4	1. Nonlinear susceptibility in graphene	27
A. Interlayer Coulomb interaction	5	2. Lowest-order perturbation theory	28
B. Kinetic theory of ballistic drag	6	3. Energy-dependent scattering time	31
1. Electron-hole asymmetry and rectification	7	4. Plasmon contribution	31
2. Drag resistivity in ballistic samples.	8	5. Drag between massless and massive fermions	32
3. Plasmon contribution	9	6. Numerical evaluation of the drag coefficient	32
C. Effects of potential disorder	10	B. Hydrodynamic regime	33
1. Drag resistivity in diffusive regime	10	1. Collinear scattering singularity	33
2. Weak localization corrections	11	2. Macroscopic linear-response theory in graphene	34
D. Third-order drag effect	12	3. Coulomb drag in weakly disordered graphene.	35
E. Transconductance due to tunneling bridges	13	C. Diffusive regime	36
F. Comparison to experiment	14	D. Giant magneto-drag in graphene	36
1. Phonon effects	16	E. Hall drag in graphene	38
2. Interlayer interaction beyond RPA	17	F. Higher-order effects in graphene	38
G. Single-particle drag in magnetic field	17	1. Third-order drag in graphene	39
1. Hall drag in weak (classical) magnetic field	18	2. Interlayer disorder correlations	40
2. Coulomb drag of composite fermions	18	V. Coulomb drag at the nanoscale	41
III. Mesoscopic fluctuations of Coulomb drag	20	A. Quantum dots and quantum point contacts	41
A. Drag fluctuations in conventional diffusive samples	20	B. Optical cavities	43
B. Giant fluctuations of Coulomb drag	23	VI. Coulomb drag between parallel nanowires	44
C. Drag fluctuations at the half-filled Landau level	24	VII. Novel many-body states in double-layer systems	47
IV. Drag in graphene-based double-layer devices	26	A. Quantum Hall Effect in double-layer systems	47
		B. Interlayer exciton formation	49

VIII. Open questions and perspectives	51
Acknowledgments	52
References	53

I. FRICTIONAL DRAG

Inner workings of solids are often studied with the help of transport measurements. Within linear response, the outcome of such measurements is determined by the properties of the unperturbed system, which are often the object of study. In a typical experiment a current is driven through a conductor and the voltage drop along the conductor is measured. In conventional conductors at low temperatures the resulting Ohmic resistance is mostly determined by disorder (which is always present in any sample) (Lifshitz and Pitaevskii, 1981; Ziman, 1965), while interactions between charge carriers lead to corrections that affect the temperature dependence of transport coefficients (Altshuler and Aronov, 1985).

In his pioneering work, Pogrebinskii (1977) suggested an alternative measurement that involves two closely spaced, but electrically isolated conductors (hereafter referred to as “layers”). In such a system, an electric current I_1 flowing through one of the layers, known as the “active” layer, induces a current (or, in an open circuit, a voltage V_2 , see Fig. 1) in the other, “passive” layer by means of “mutual friction”. By this one typically understands scattering between charge carriers belonging to different layers due to long-range interactions. These scattering events are accompanied by energy and momentum transfer from the carriers in the active layer to the carriers in the passive layer, effectively “dragging” them along. At the simplest level, such friction effects can be described by introducing a phenomenological relaxation rate. In the case of frictional drag, the corresponding rate τ_D^{-1} generally depends on the exact nature of the charge carriers, interlayer interaction, and microscopic structure of the electronic system. Thus, measurements of this relaxation rate provide additional insight into microscopic properties of interacting many-body systems.

A related phenomenon, where a quasiparticle flow instigates a partial transfer of energy and momentum between separate, but interacting subsystems of quasiparticles, is known as “phonon drag” (Gurevich, 1946a,b; Herring, 1954) and manifests itself in a rising thermoelectric power in semiconductors at low temperatures (Fredrikse, 1953a,b; Geballe, 1953; Geballe and Hull, 1954). In the presence of a temperature gradient, lattice vibrations become anisotropic since the phonons travel preferentially from hot to cold (providing a mechanism for thermal conduction). Interacting with electrons, the phonons effectively drag them towards the cold end of the sample, creating an excess charge density (this process will continue until the electrostatic field created by the accumu-

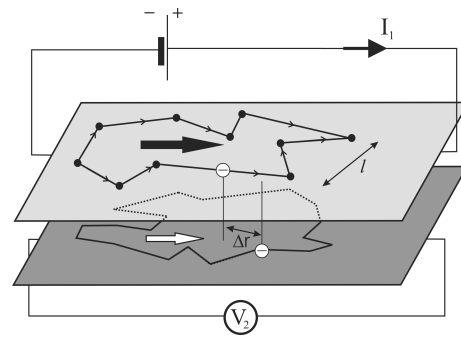


FIG. 1 Schematic showing the drag signal V_2 induced by the current I_1 . [From Price *et al.* (2007). Reprinted with permission from AAAS.]

lated charge will counterbalance the drag effect). In a nonequilibrium system of electrons and phonons, their mutual drag is intertwined with heating effects and affects charge transport (Gurevich and Mashkevich, 1989). The resulting correction to the standard transport theory is important in thermoelectric measurements.

In contrast, frictional drag in double-layer systems is *not a correction*: in the absence of the interlayer interaction, charge carriers in two disjointed conductors are insensitive to each other (therefore, any drag effect should necessarily vanish in the limit of infinitely remote layers). In other words, *the drag phenomenon simply does not exist in noninteracting systems!* Consequently, initial experimental work on mutual drag was devoted to quantitative measurement of the strength of interactions between quasiparticle subsystems in various semiconductor devices including p -modulation-doped GaAs quantum wells (Höpfel and Shah, 1988; Höpfel *et al.*, 1986), capacitively coupled two- and three-dimensional (2D-3D) electron systems in AlGaAs/GaAs heterostructures (Solomon and Laikhtman, 1991; Solomon *et al.*, 1989), 2D electron systems in AlGaAs/GaAs double quantum wells (Eisenstein, 1992; Gramila *et al.*, 1991, 1992, 1994; Solomon and Laikhtman, 1991), and electron-hole bilayers (Sivan *et al.*, 1992). Drag between 3D systems was numerically simulated in Jacoboni and Price (1988). At low temperatures and for closely spaced layers, the interlayer scattering rate τ_D^{-1} appeared to be dominated by the Coulomb interaction (Price, 1983, 1988).

Coulomb drag between spatially separated electron systems is ultimately caused by fluctuations (or inhomogeneities) of the charge density in the two layers (Zheng and MacDonald, 1993). Indeed, an infinite layer with uniformly distributed electric charge creates a uniform electric field in the normal direction that does not exert any lateral force upon the carriers in another layer. If both layers are in the Fermi-liquid state, then the usual phase-space argument (Gramila *et al.*, 1991) yields the quadratic temperature dependence $\tau_D^{-1} \propto T^2$ in qualita-

tive agreement with the observed behavior at low enough temperatures. More detailed analysis of the experimental data revealed the presence of additional mechanisms leading to frictional drag, such as the indirect interlayer interaction mediated by phonons (Gramila *et al.*, 1993; Noh *et al.*, 1999; Rubel *et al.*, 1995, 1996), plasmon effects (Hill *et al.*, 1997; Noh *et al.*, 1998), and thermoelectric phenomena (Solomon and Laikhtman, 1991).

Theoretically, it was realized early on that mutual Coulomb scattering between electrons in the two layers results in the *exchange of both energy and momentum* (Boiko and Sirenko, 1988; Maslov, 1992; Price, 1983). Initial calculations aimed at energy and momentum relaxation in a nondegenerate 2D electron gas (2DEG) due to proximity to a 3D conductor (Boiko and Sirenko, 1988, 1990) were followed by investigation of transport properties in coupled 2D and 3D systems (Boiko *et al.*, 1992; Laikhtman and Solomon, 1990), 1D systems coupled to conductors of arbitrary dimensionality (Sirenko and Vasilopoulos, 1992), coupled 1D wires (Gurevich *et al.*, 1998; Tanatar, 1996, 1998; Tso and Vasilopoulos, 1992), and quantum Hall edge states (Orgad and Levit, 1996). Following the groundbreaking experiments in AlGaAs/GaAs double quantum wells (Eisenstein, 1992; Gramila *et al.*, 1991), a lot of work was devoted to drag between two degenerate 2DEGs. While the purely Coulomb mechanism (Flensberg *et al.*, 1995; Jauho and Smith, 1993; Kamenev and Oreg, 1995; Zheng and MacDonald, 1993) does capture the most qualitative features of the effect, other mechanisms of momentum transfer may also contribute to the observed behavior. In samples with larger interlayer spacing ($d \sim 50\text{-}500\text{nm}$) as much as 30% of the measured signal was attributed to phonon-mediated interactions (Gramila *et al.*, 1993). These measurements appeared to be consistent with the virtual-phonon exchange mechanism (Tso *et al.*, 1992, 1994). Other suggested scattering mechanisms involved acoustic (Bønsager *et al.*, 1998a) and optical (Hu, 1998) phonons, plasmon effects (Flensberg and Hu, 1994) and coupled plasmon-phonon modes (Güven and Tanatar, 1997a). Bilayers subject to strong magnetic fields were shown to form interlayer correlated states (Girvin and MacDonald, 1997; Varma *et al.*, 1994). For superconducting layers, interlayer magnetic interaction due to spontaneously created vortices has also been suggested (Shimshoni, 1995).

Mutual Coulomb scattering has been studied also in a hybrid device (Huang *et al.*, 1995) comprising normal (Au/Ti) and superconducting (AlO_x) 2D films separated by an insulating (Al_2O_3) layer. In that case, as well as in “cross-talk” measurements in superconductor–insulator–normal-metal trilayers (Giordano and Monnier, 1994), the phenomenological Drude-like description of drag in terms of τ_D^{-1} does not apply. The Drude description also fails when the system is subjected to a strong magnetic field: in contrast to the naive description, numerous experiments (Feng *et al.*, 1998; Hill *et al.*, 1996, 1998; Jörger

et al., 2000c; Lok *et al.*, 2001a,b; Patel *et al.*, 1997; Rubel *et al.*, 1997a,b) show significant dependence of the measured drag resistivity ρ_D on the applied field, especially in the extreme quantum regime (Lilly *et al.*, 1998). More sophisticated theoretical calculations on Coulomb drag in quantum Hall states (Shimshoni and Sondhi, 1994), superfluid condensates in paired electron-hole layers (Vignale and MacDonald, 1996), drag of composite fermions (Kim and Millis, 1999; Ussishkin and Stern, 1997, 1998; Zhou and Kim, 1999), vortex drag (Vitkalov, 1998), non-dissipative drag (Rojo and Mahan, 1992), supercurrent drag (Duan and Yip, 1993), as well as drag between charged Bose gases (Tanatar and Das, 1996) and mesoscopic rings (Baker *et al.*, 1999; Shahbazyan and Ulloa, 1997a,b) have confirmed the expectation that *the drag resistivity reflects not only the exact character of interlayer interaction, but also the nature of elementary excitations in each layer and their fundamental properties.*

After the turn of the century, drag measurements became part of the standard toolbox in condensed matter physics. They have been used to investigate properties of electron-electron scattering in low-density 2D electron systems (An *et al.*, 2006; Kellogg *et al.*, 2002a); signatures of metal-insulator transition in dilute 2D hole systems (Jörger *et al.*, 2000a,b; Pillarisetty *et al.*, 2002, 2005a,b); quantum coherence of electrons (Kim *et al.*, 2011; Price *et al.*, 2008, 2007) and composite fermions (Price *et al.*, 2010); exciton effects in electron-hole bilayers (Croxall *et al.*, 2008; Keogh *et al.*, 2005; Morath *et al.*, 2009; Seamons *et al.*, 2009); exotic bilayer collective states (Eisenstein, 2014), especially the quantum Hall effect (QHE) at the total filling factor $\nu_T = 1$ (Finck *et al.*, 2010; Kellogg *et al.*, 2003, 2002b; Schmult *et al.*, 2010; Spielman *et al.*, 2004; Tutuc *et al.*, 2009); compressible quantum Hall (QH) states at half-integer filling factor (Muraki *et al.*, 2004; Zelakiewicz *et al.*, 2000); integer QH regime (Lok *et al.*, 2002); Luttinger liquid effects (Debray *et al.*, 2001; Laroche *et al.*, 2008, 2014); Wigner crystallization in quantum wires (Yamamoto *et al.*, 2002, 2006, 2012); and one-dimensional (1D) sub-bands in quasi 1D wires (Debray *et al.*, 2000; Laroche *et al.*, 2011). More generally, interlayer interaction and corresponding transport properties have been studied in hybrid devices comprising a quantum wire and a quantum dot (Krishnaswamy *et al.*, 1999); a SC film and a 2D electron gas (Farina *et al.*, 2004); Si metal-oxide-semiconductor systems (Laikhtman and Solomon, 2005); quantum point contacts (Khrapai *et al.*, 2007); insulating a-SiNb films (Elsayad *et al.*, 2008); ferromagnetic-antiferromagnetic-SC trilayers (Cuoco *et al.*, 2009); nanosize CdSe-CdS semiconductor tetrapods (Mauser *et al.*, 2010); electron-hole scattering in quantum wells (Prunnila *et al.*, 2008; Takashina *et al.*, 2009; Yang *et al.*, 2011); graphene monolayers (Gorbachev *et al.*, 2012; Kim *et al.*, 2011; Kim and Tutuc, 2012; Titov *et al.*, 2013a); and hybrid graphene-semiconductor systems (Gamucci *et al.*, 2014).

On the theory side, the variety of suggested extensions and generalizations of the original drag problem is even richer. The theory of Coulomb drag between two 2DEGs was extended to dilute 2D hole systems (Hwang *et al.*, 2003) and to the cases where one allows for certain tunneling processes between the layers (Oreg and Halperin, 1999; Oreg and Kamenev, 1998), interlayer disorder correlations (Gornyi *et al.*, 1999; Hu, 2000a), in-plane potential modulation (Alkauskas *et al.*, 2002), and disorder inhomogeneities (Apalkov and Raikh, 2005; Spivak and Kivelson, 2005; Zou *et al.*, 2009, 2010). Theory of Coulomb drag between composite fermions was generalized to include phonon-mediated coupling (Bønsager *et al.*, 2000; Khveshchenko, 2000). Mutual friction was also suggested to occur between non-Fermi-Liquid phases including Luttinger liquids (Flensberg, 1998; Klesse and Stern, 2000; Nazarov and Averin, 1998), Wigner crystals (Baker and Rojo, 2001; Braude and Stern, 2001), and strongly localized electrons (Raikh and von Oppen, 2002). Drag or similar measurements of interlayer interactions were also considered for composite (or hybrid) systems comprising ballistic quantum wires (Gurevich and Muradov, 2000, 2005; Raichev and Vasilopoulos, 2000a; Wang *et al.*, 2005), coupled 2D-1D systems (Lyo, 2003), nonequilibrium charged gases (Wang and da Cunha Lima, 2001), multi-wall nanotubes (Lunde *et al.*, 2005; Lunde and Jauho, 2004), quantum point contacts (Levchenko and Kamenev, 2008a), few level quantum dots (Moldoveanu and Tanatar, 2009), optical cavities (Berman *et al.*, 2010a, 2014), coupled mesoscopic rings (Yang and MacDonald, 2001), superconductors (Levchenko and Norman, 2011), and normal-metal-ferromagnet-normal-metal structures (Zhang and Zhang, 2012). Other developments include mesoscopic fluctuations of Coulomb drag (Narozhny and Aleiner, 2000; Narozhny *et al.*, 2001), frictional drag mediated by virtual photons (Donarini *et al.*, 2003) and plasmons (Badalyan *et al.*, 2007), exciton effects in semiconductors (Laikhtman and Solomon, 2006) and topological insulators (Mink *et al.*, 2012), interlayer Seebeck effect (Lung and Marinescu, 2011) and spin drag (Badalyan and Vignale, 2009; D’Amico and Vignale, 2000; Duine *et al.*, 2011, 2010; Duine and Stoof, 2009; Flensberg *et al.*, 2001; Glazov *et al.*, 2011; Pustilnik *et al.*, 2006; Tse and Das Sarma, 2007; Vignale, 2005). Recently, the focus of the theoretical work was shifted towards the drag effect in graphene-based devices (Narozhny, 2007; Narozhny *et al.*, 2015; Song *et al.*, 2013; Tse *et al.*, 2007) and strongly interacting high-mobility double-layers with low-density carrier concentration (Apostolov *et al.*, 2014; Chen *et al.*, 2015).

Given the rather large amount of literature devoted to frictional drag, it seems unreasonable to cover all possible angles in a single paper. Early work on frictional drag was reviewed by Rojo (1999). Various experimental aspects were discussed in reviews on exciton conden-

sates (Eisenstein, 2014; Snoko, 2002), electron-hole bilayers (Das Gupta *et al.*, 2011), strongly-correlated 2D electron fluids (Spivak *et al.*, 2010), and 1D ballistic electron systems (Debray *et al.*, 2002). A discussion of drag in strong magnetic fields was included in a review of magnetotransport in 2D electron systems (Dmitriev *et al.*, 2008). In the present review, we limit ourselves to the discussion of standard (“electrical”) Coulomb drag. Spin-related phenomena and thermoelectric effects are beyond the scope of this review.

II. COULOMB DRAG IN SEMICONDUCTOR HETEROSTRUCTURES

In an idealized experiment, a constant (dc) current I_1 is passed through the active layer, keeping the passive layer isolated at the same time (such that no current is allowed to flow in it), see Fig. 1. The voltage V_2 induced in the passive layer is proportional to I_1 and the coefficient¹

$$R_D = -V_2/I_1, \quad (1)$$

is a direct measure of interlayer interactions.

In his original paper, Pogrebinskii (1977) derived the Drude-like description of transport in double-layer systems comprising two coupled equations of motion

$$\frac{d\mathbf{v}_1}{dt} = \frac{e}{m_1} \mathbf{E}_1 + \frac{e}{m_1 c} [\mathbf{v}_1 \times \mathbf{B}] - \frac{\mathbf{v}_1}{\tau_1} - \frac{\mathbf{v}_1 - \mathbf{v}_2}{\tau_D}, \quad (2a)$$

$$\frac{d\mathbf{v}_2}{dt} = \frac{e}{m_2} \mathbf{E}_2 + \frac{e}{m_2 c} [\mathbf{v}_2 \times \mathbf{B}] - \frac{\mathbf{v}_2}{\tau_2} - \frac{\mathbf{v}_2 - \mathbf{v}_1}{\tau_D}, \quad (2b)$$

where e is the electric charge, \mathbf{v}_i , m_i , and \mathbf{E}_i are the drift velocities, effective masses, and electric fields in the two layers, and the nonquantizing magnetic field \mathbf{B} is assumed to be uniform. Intralayer impurity scattering processes yielding the Drude resistivity in the two layers are described by the mean free times τ_i . The last term in each of Eqs. (2) describes the mutual friction between the charge carriers in the two layers that tends to equalize drift velocities. If treated phenomenologically, the model (2) describes two distinct types of carriers coupled by the friction term, but does not explicitly require them to be spatially separated (Cui *et al.*, 1988; Hänsch and Mahan, 1983; Söderström *et al.*, 1996).

Solving the equations (2), one finds the resistivity matrix $\rho_{\alpha\beta}^{(ij)}$ [hereafter the indices $i, j = 1, 2$ denote the two layers and $\alpha, \beta = x, y$ – spatial coordinates orthogonal to $\mathbf{B} = B\mathbf{e}_z$; the “layers” described by Eqs. (2) can represent 2D or 3D conductors, see Sec. VI for the 1D case].

¹ The minus sign in Eq. (1) is motivated by Eq. (3a). An alternative definition without the explicit minus sign is also widely used in literature.

The “drag resistivity” (also called the transresistivity or the drag coefficient) is given by the Drude-like formula

$$\rho_D = -\rho_{xx}^{(12)} = m_2/(e^2 n_1 \tau_D). \quad (3a)$$

The expression (3a) is *independent of the magnetic field*. This statement has the same status as the absence of the classical magnetoresistance². Indeed, the single-layer longitudinal resistivity derived from Eqs. (2) is given by

$$\rho_{xx}^{(11)} = \frac{m_1}{e^2 n_1} \left(\frac{1}{\tau} + \frac{1}{\tau_D} \right). \quad (3b)$$

In most cases, drag is rather weak ($\tau_D \gg \tau$) and the usual Drude formula remains a good approximation for $\rho_{xx}^{(11)}$ (Eisenstein, 1992; Rojo, 1999). The single-layer Hall coefficient is unaffected by the presence of the second layer and is determined solely by the carrier density

$$\rho_{yx}^{(11)} = B/(n_1 e c). \quad (3c)$$

Within the applicability of the Drude model, frictional drag is purely longitudinal: “Hall drag” does not occur³

$$\rho_D^H = \rho_{yx}^{(12)} = 0. \quad (3d)$$

At the phenomenological level, the drag resistivity (3a) is independent of the disorder strength. Moreover, in the “clean” limit $\tau \rightarrow \infty$ the inter- and intralayer resistivities tend to the same value and the resistivity matrix becomes degenerate (the corresponding conductivities diverge):

$$\rho_{xx}^{(11)}(\tau \rightarrow \infty) = \rho_D(\tau \rightarrow \infty). \quad (4)$$

Thus a system comprising two capacitively coupled, ideal conductors is characterized by non-zero resistivity and exhibits *perfect drag!*

A. Interlayer Coulomb interaction

The “Drude formula” (3a) for the drag resistivity becomes falsifiable provided that something is known about the properties of the “drag rate” τ_D^{-1} (e.g. its dependence on temperature, carrier density, interlayer separation, and other experimentally relevant parameters). To the leading order, the contribution of the interlayer Coulomb interaction to τ_D^{-1} can be calculated within the Born approximation (or equivalently, using Fermi’s Golden Rule) (Jauho and Smith, 1993; Laikhtman and Solomon,

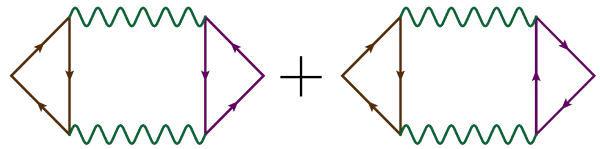


FIG. 2 (Color online) Aslamazov-Larkin diagrams describing the lowest-order contribution to drag. The solid lines refer to quasiparticle Green’s functions and the wavy lines describe the interlayer interaction. The left and right triangles correspond to non-linear susceptibilities of the two layers.

1990). In the language of Feynman diagrams, the corresponding process (Flensberg *et al.*, 1995; Kamenev and Oreg, 1995; Zheng and MacDonald, 1993) is described by the Aslamazov-Larkin diagrams (Aslamazov and Larkin, 1968) shown in Fig. 2.

The effective interlayer interaction can be found as a solution to the Poisson equation for the potential of a point source belonging to one of the layers. In principle, this can be done for any system of coupled conductors. Coupling between a 2DEG and a 3DEG was considered in Laikhtman and Solomon (1990). A double quantum well system was discussed in Jauho and Smith (1993) where the finite width of the wells was taken into account by assuming a specific form of the electron wave function in the direction perpendicular to the layers. However, the obtained results are qualitatively the same as in the simplest case of purely two-dimensional layers.

If electrons in each layer are confined to move in a 2D plane, the “bare” Coulomb potential⁴ has the form⁵

$$V_{11} = V_{22} = 2\pi e^2/q, \quad V_{12}(q) = (2\pi e^2/q)e^{-qd}. \quad (5)$$

Here e is the electron charge and d is the interlayer separation that determines the maximum value (or rather, the order of magnitude thereof) of the momentum q that can be transferred between the layers⁵:

$$q \ll 1/d. \quad (6)$$

Taking into account dynamical screening within the usual Random Phase Approximation (RPA) modifies the interlayer interaction (Das Sarma and Madhukar, 1981; Halperin *et al.*, 1993; Santoro and Giuliani, 1988; Stern and Halperin, 1995), but does not change the exponential decay at large q . The resulting retarded interaction propagator can be written as

$$\mathcal{D}_{12}^R = -\frac{1}{\Pi_1^R \Pi_2^R \frac{4\pi e^2}{q} \sinh qd + \left[\frac{q}{2\pi e^2} + \Pi_1^R + \Pi_2^R \right] e^{qd}}. \quad (7)$$

² In this Section we are discussing the simplest situation, where both τ_D and τ are unaffected by weak enough magnetic fields.

³ Under the assumptions of the present Section, magnetic field has no effect on drag. Hence, up until Sec. II.G we focus on the zero-field, longitudinal transport. Drag in magnetic field is discussed in Secs. II.G, IV.E, and VII.A.

⁴ Although electrons are confined to move in two dimensions, they interact by means of “real, 3D” Coulomb interaction.

⁵ While discussing the theory, we use the natural units where temperature and relaxation rates are measured in energy units ($\hbar = k_B = 1$). We attempt to restore the Planck’s constant in final expressions for the drag resistivity and while discussing experimental findings.

Here Π_i^R is the single-layer retarded polarization operator. It is quite common [see, e.g., Jauho and Smith (1993) and Laikhtman and Solomon (1990)], to include the dielectric constant ϵ of the insulating spacer into the “bare” potential. Since the same ϵ should enter the expression for the inverse Thomas-Fermi screening length

$$\kappa = 2\pi e^2 \nu = 2\pi e^2 \Pi^R(q < 2k_F, \omega = T = 0), \quad (8)$$

the dielectric environment can be taken into account by expressing the results in terms of κ (ν denotes the thermodynamic density of states of the 2DEG). For high carrier densities (Gramila *et al.*, 1991), Eq. (7) can be simplified (Kamenev and Oreg, 1995) by assuming the small screening length, $\kappa d \gg 1$ [see Eqs. (20) and (33b) below].

The condition (6) allows one to distinguish the following two regimes (Kamenev and Oreg, 1995):

- (i) if the interlayer separation is large compared to the mean-free path $d \gg \ell$, then it follows from Eq. (6) that $q \ll 1/\ell$; in this case the motion of charge carriers is *diffusive*;
- (ii) in the opposite case, $d \ll \ell$, transport is dominated by *ballistic* propagation of charge carriers with $1/d \gg q \gg 1/\ell$, see Eq. (36) below. Most measurements (Gorbachev *et al.*, 2012; Gramila *et al.*, 1991) are performed on ballistic samples.

The majority of analytic (Rojo, 1999) and numerical (Moško *et al.*, 1992) work on Coulomb drag in semiconductor heterostructures was performed treating the interaction (7) in the lowest order of perturbation theory. For generalizations see Secs. II.D and II.F.

B. Kinetic theory of ballistic drag

Ballistic motion of charge carriers in semiconductors can be described by using the kinetic equation approach, where impurity scattering is taken into account within the simplest τ -approximation (Jauho and Smith, 1993; Laikhtman and Solomon, 1990; Pogrebinskii, 1977). One starts with the generic Boltzmann equation

$$\frac{\partial f_i}{\partial t} + \mathbf{v}_i \cdot \nabla f_i + \left(e \mathbf{E}_i + \frac{e}{c} [\mathbf{v}_i \times \mathbf{B}] \right) \frac{\partial f_i}{\partial \mathbf{p}} = -\frac{\delta f_i}{\tau} + \mathcal{I}_{ij}, \quad (9)$$

where f_i is the distribution function (in layer $i = 1, 2$), \mathcal{I}_{ij} is the collision integral due to interlayer Coulomb interaction, τ is the transport impurity scattering time, and δf_i is the nonequilibrium correction to the distribution

function. Here we will only consider *degenerate* electron systems [as realized in semiconductor heterostructures (Gramila *et al.*, 1991)]. Weak deviations from the equilibrium Fermi-Dirac distribution function $f_i^{(0)}$ (as appropriate within linear response) are described by (Lifshitz and Pitaevskii, 1981)

$$\delta f_i \equiv f_i - f_i^{(0)} \equiv f_i^{(0)} [1 - f_i^{(0)}] h_i = -T [\partial f_i^{(0)} / \partial \epsilon] h_i. \quad (10)$$

Here we only consider the steady state and uniform fields

$$\partial f_i / \partial t = 0, \quad \nabla f_i = 0. \quad (11)$$

The latter condition physically means that the sample size is large compared to the length scale of typical relaxation processes in the system, see also Sec. IV.D.

In the absence of interlayer interaction, the task of finding linear-response transport coefficients from Eq. (9) is a textbook problem (Seeger, 2002; Smith and Jensen, 1989; Ziman, 1965). Under the above assumptions, the theory is qualitatively equivalent to the Drude theory (2) yielding the standard results (3b) and (3c). Not surprisingly, taking into account the collision integral \mathcal{I}_{ij} leads to the Drude-like description of the drag resistivity (3a) and (3d). The advantage of the present “microscopic” calculation is that now we can determine the phenomenological relaxation time τ_D in terms of the model parameters.

The standard perturbative calculation (Boiko *et al.*, 1992; Jauho and Smith, 1993; Laikhtman and Solomon, 1990; Lifshitz and Pitaevskii, 1981) amounts to finding the nonequilibrium distribution functions h_i in the two layers to the leading order in the interlayer interaction and the electric field \mathbf{E}_1 applied to the active layer. Then one uses the definition of the electric current (here the sum runs over all of the single-particle states)

$$\mathbf{j}_i = e \sum \mathbf{v} \delta f_i, \quad (12)$$

and finds the current \mathbf{j}_2 in the passive layer. The coefficient of proportionality between j_{2x} and E_{1x} defines the drag conductivity σ_D . The drag coefficient ρ_D can then be obtained by inverting the 2×2 conductivity matrix³

$$\rho_D = \frac{\sigma_D}{\sigma_1 \sigma_2 - \sigma_D^2} \approx \frac{\sigma_D}{\sigma_1 \sigma_2}, \quad (13)$$

where σ_i is the longitudinal conductivity in layer i ; the latter relation follows from the smallness of the effect

$$\sigma_D \ll \sigma_i, \quad (14)$$

as observed in experiment (Eisenstein, 1992; Rojo, 1999). This way, one finds for the phenomenological “drag rate”

$$\tau_D^{-1} = \frac{m_1}{16\pi e^2 \tau^2 n_2 T} \int_{-\infty}^{\infty} \frac{d\omega}{\sinh^2[\omega/(2T)]} \int \frac{d^2 q}{(2\pi)^2} |\mathcal{D}_{12}(\omega, \mathbf{q})|^2 \Gamma_1^x(\omega, \mathbf{q}) \Gamma_2^x(\omega, \mathbf{q}). \quad (15)$$

Similar expression⁶ can be derived for ρ_D and σ_D . The nonlinear susceptibility (also known as the rectification function) $\Gamma_i(\omega, \mathbf{q})$ (in layer i) is a response function relating a voltage $V(r_i)e^{i\omega t}$ to a dc current it induces by the quadratic response:

$$\mathbf{J} = \int d\mathbf{r}_1 \int d\mathbf{r}_2 \Gamma(\omega; \mathbf{r}_1, \mathbf{r}_2) V(\mathbf{r}_1) V(\mathbf{r}_2), \quad (16)$$

with \mathbf{J} being the induced dc current. From gauge invariance $\int d\mathbf{r}_1 \Gamma(\omega) = \int d\mathbf{r}_2 \Gamma(\omega) = 0$.

The same result follows from the standard Kubo formula approach within the diagrammatic perturbation theory (Flensberg *et al.*, 1995; Kamenev and Oreg, 1995), memory function formalism (Zheng and MacDonald, 1993), and more general Boltzmann-Langevin theory of stochastic kinetic equation (Chen *et al.*, 2015).

1. Electron-hole asymmetry and rectification

The rectification function $\Gamma(\omega, \mathbf{q})$ is the central object in the perturbative theory of Coulomb drag. The expression (15) of the interlayer relaxation rate in terms of $\Gamma(\omega, \mathbf{q})$ explicitly demonstrates the key role of electron-hole asymmetry in the leading-order drag effect⁷.

Indeed, in order to induce a voltage (or generate a current) in the passive layer, one needs to somehow move the charge carriers. This is achieved by transferring momentum from the active layer. The macroscopic state of the electronic system in the active layer is characterized by the finite electric current driven by an external source. In a typical electron gas, there are two kinds of excitations - “electron-like”, with energies $\epsilon > E_F$ above the Fermi energy (i.e. the occupied states outside the Fermi surface), and “hole-like”, with $\epsilon < E_F$. These quasiparticles are oppositely charged. As the current is driven through the active layer they move in opposite directions, see Fig. 3. Then the active layer can be characterized by a nonzero total momentum only if there is some asymmetry between electron-like and hole-like quasiparticles. Likewise, in the passive layer the momentum is transferred equally to electrons and holes, such that the resulting state can carry current only in the case of electron-hole asymmetry. In conventional semiconductors (Kamenev and Oreg, 1995), the electron-hole asymmetry appears due to curvature of the conduction band spectrum [leading to the energy dependence of the density of states

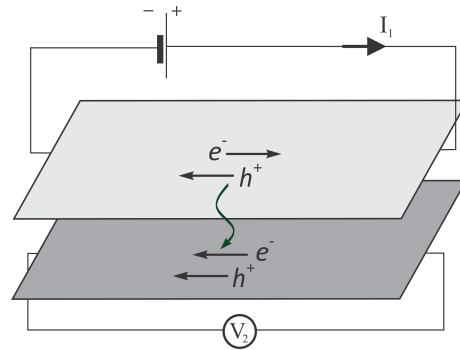


FIG. 3 Schematic illustration of the momentum transfer due to interlayer interaction. As the current I_1 is driven through the active layer, electrons and holes are moving in the opposite directions since they carry the opposite charge. Such a state has non-zero total momentum only due to electron-hole asymmetry. Once the momentum is transferred to the passive layer, the electrons and holes there are pushed in the same direction. This process can induce a voltage again only due to electron-hole asymmetry.

(DoS) and/or diffusion coefficient]. Consequently, in the Fermi-liquid theory the electron-hole asymmetry can be expressed (Narozhny *et al.*, 2001) as a derivative of the single-layer conductivity $\sigma_{1(2)}$ with respect to the chemical potential (assuming either a constant impurity scattering time or diffusive transport). The simple estimate $\partial\sigma_{1(2)}/\partial\mu \sim \sigma_{1(2)}/\mu$ then explains the typical smallness of the effect (Gramila *et al.*, 1991; Sivan *et al.*, 1992; Solomon *et al.*, 1989), see Eq. (14).

The same arguments can be applied to any system containing carriers with opposite signs of the electric charge. For instance, one can consider semimetals (or even band insulators at high enough temperature) where the electric current can be carried by electrons from the conduction band and holes from the valence band. A particularly interesting example is graphene (see Sec. IV), which exhibits exact particle-hole symmetry at the charge neutrality point (Katsnelson, 2012). At that point, the nonlinear susceptibility of graphene (73) vanishes (Narozhny, 2007; Tse *et al.*, 2007) implying the absence of the drag effect. In contrast, experiment (Gorbachev *et al.*, 2012) shows nonzero drag resistivity at charge neutrality, which in addition is greatly enhanced by the external magnetic field (Titov *et al.*, 2013a).

Indeed, the outlined physical picture is not universal. In fact, it only describes a particular (although often dominant) scattering process, where momentum is transferred from an electron-hole pair in the active layer to another electron-hole pair in the passive layer. Technically, this process is described by the leading-order perturbation theory, see Fig. 2, yielding Eq. (15). Higher-order processes [including the so-called “third-order” drag (Levchenko and Kamenev, 2008b; Schütt *et al.*, 2013), see Sec. II.D, and the effect of the corre-

⁶ The three quantities ρ_D , σ_D , and τ_D^{-1} are proportional to each other and differ only by trivial prefactors, see Eqs. (3a) and (13). All three are used in literature on equal footing.

⁷ Another known effect of the electron-hole asymmetry in electronic systems is the thermopower described by the Mott formula (Lunde *et al.*, 2006, 2007; Mott and Jones, 1936).

lated disorder (Gornyi *et al.*, 2000, 1999; Schütt *et al.*, 2013; Song *et al.*, 2013), see Sec. IV.F] may result in additional contributions which are less sensitive to electron-hole symmetry.

In conventional heterostructures, higher-order processes remain subleading at least within the temperature range where most of the experiments are performed, see Sec. II.D. Specifically in the ballistic regime, the dominant contribution to drag is indeed given by Eq. (15) [with the corresponding drag resistivity (3a)] and is determined by the nonlinear susceptibility, which in the simplest case of energy-independent impurity-scattering time τ is given by (Kamenev and Oreg, 1995)

$$\Gamma(\mathbf{q}, \omega) = \frac{2}{\pi} e\tau \mathbf{q} \frac{\omega}{v_F q} \theta(v_F q - \omega). \quad (17)$$

As shown in Kamenev and Oreg (1995), the resulting expression (17) for the nonlinear susceptibility is proportional to the imaginary part of the single-layer polarization operator

$$\Gamma(\mathbf{q}, \omega) = \frac{2e\tau \mathbf{q}}{m} \text{Im}\Pi^R(\mathbf{q}, \omega), \quad (18)$$

where (for two-dimensional, noninteracting electron gas in the ballistic regime)

$$\text{Im}\Pi^R(\mathbf{q}, \omega) = \nu \frac{\omega}{v_F q} \theta(v_F q - \omega). \quad (19)$$

Within the kinetic theory, one can observe Eq. (18) already at the level of the collision integral (Giuliani and Quinn, 1982); hence many authors [see, e.g. Jauho and Smith (1993); Shimshoni and Sondhi (1994); Ussishkin and Stern (1997); and Zheng and MacDonald (1993)] proceed to express Eq. (15) in terms of $\text{Im}\Pi^R(\mathbf{q}, \omega)$ instead of the nonlinear susceptibility. Under the assumption of energy-independent impurity-scattering time τ and neglecting intralayer correlations (Flensberg *et al.*, 1995; Kamenev and Oreg, 1995), such calculations lead to the correct result [see Eq. (21) below]. At the same time, within such an approach the physics of electron-hole asymmetry remains hidden. Generalization to more general settings is also nontrivial: the relation (18) is by no means a general theorem (Flensberg *et al.*, 1995; Kamenev and Oreg, 1995; Narozhny and Aleiner, 2000; Narozhny *et al.*, 2012); for explicit examples of the two quantities being inequivalent see Secs. III and IV.

2. Drag resistivity in ballistic samples.

In the limit of strong screening, $\kappa d \gg 1$, one can approximate (Kamenev and Oreg, 1995) the interlayer interaction propagator (7) by the expression

$$\mathcal{D}_{12}^R = -\frac{\pi e^2}{\kappa_1 \kappa_2} \frac{q}{\sinh qd}. \quad (20)$$

Combining Eq. (20) and the nonlinear susceptibility (18) with the interlayer relaxation rate (15) and Eq. (3a), one finds the following expression for the drag resistivity (Flensberg and Hu, 1994; Jauho and Smith, 1993; Kamenev and Oreg, 1995; Zheng and MacDonald, 1993)

$$\rho_D = \frac{\hbar}{e^2} \frac{\pi^2 \zeta(3)}{16} \frac{T^2}{E_{F1} E_{F2}} \frac{1}{\kappa_1 \kappa_2 k_{F1} k_{F2} d^4}. \quad (21a)$$

The same result can be also expressed⁸ in terms of the interlayer relaxation rate (15) [e.g., using Eq. (3a)]

$$\tau_D^{-1} = \frac{\pi^2 \zeta(3)}{16} \frac{n_1}{m_2} \frac{T^2}{E_{F1} E_{F2}} \frac{1}{\kappa_1 \kappa_2 k_{F1} k_{F2} d^4}. \quad (21b)$$

Physically, these expressions⁸ can be understood based on the Fermi Golden Rule [which was explicitly used in the solution of the kinetic equation (Jauho and Smith, 1993; Laikhtman and Solomon, 1990)]. Indeed, there are three basic elements that combine into the result (21): (i) the phase space available for electron-hole pairs in the two layers, which is limited by temperature, hence $\tau_D^{-1} \propto T^2$; (ii) the electron-hole asymmetry, which results in the overall smallness of the effect, $\tau_D^{-1} \propto (E_{F1} E_{F2})^{-1}$; and (iii) the matrix element of the interlayer interaction, determining the dependence on the interlayer separation; in the ballistic case the matrix element is dominated by small-angle scattering (Gramila *et al.*, 1991).

The drag resistivity (21) – and especially the quadratic temperature dependence – is often quoted as the “Fermi-liquid” result. However, Eq. (21) was obtained under a number of assumptions: (i) $\kappa d \gg 1$, (ii) $d \gg \ell$, and (iii) $T \ll T_d \sim v_F/d \sim E_F/(k_F d)$. The latter assumption appears only implicitly and is often overlooked.

Indeed, substituting the interaction propagator (20) and the nonlinear susceptibility (17) into Eq. (15), one finds that except for the θ -function in Eq. (17) the frequency and momentum integrals factorize. The exponential decay of the corresponding integrands allows one to estimate the typical values of transferred energy $\omega \sim T$ and momentum $q \sim 1/d$. Assuming $T \ll T_d$, this yields $\omega < v_F q$, which automatically satisfies the θ -function. Based on this observation, one may omit the θ -function and subsequently extend the integration limits in both integrals in Eq. (15) to infinity. The remaining integration is straightforward and yields Eq. (21).

At higher temperatures, $T \gg T_d$, the θ -function in Eq. (17) is not satisfied automatically. Physically, it represents kinematic restrictions on the phase space available to electron-hole pairs associated with predominantly

⁸ Most expressions for ρ_D (Flensberg and Hu, 1994; Flensberg *et al.*, 1995; Jauho and Smith, 1993; Rojo, 1999; Zheng and MacDonald, 1993) can be reduced to Eqs. (21) using the following simple relations, valid under the assumptions of this Section: $E_F = \pi n/m$, $n = E_F \nu$, $\nu D = E_F \tau/\pi$, where $D = v_F^2 \tau/2$ is the diffusion constant and $\nu = m/\pi$ is the density of states.

small-angle scattering (Gramila *et al.*, 1991). The frequency integration is now cut off at $v_F q$ (or T_d), rather than T , which leads to the *linear* temperature dependence [first reported in Gramila *et al.* (1991) and Solomon and Laikhtman (1991), see also Jauho and Smith (1993), and recently rediscovered in Chen *et al.* (2015)],

$$\rho_D(T \gg T_d) = \frac{\hbar \pi^3}{e^2 360} \frac{1}{(k_F d)^3 (\varkappa d)^2} \frac{T}{E_F}. \quad (22)$$

This behavior may be observable in samples with either nondegenerate 2DEGs or large interlayer separation. In the latter case, $T_d \ll T \ll E_F$, both layers are perfectly described by the Fermi liquid theory which is not synonymous with quadratic temperature dependence of transport coefficients.

3. Plasmon contribution

The approximate form of the interlayer Coulomb interaction (20) appears justified in the “ballistic” regime where the dominant interlayer relaxation processes are characterized by relatively large momentum transfers $\omega < v_F q$. The imaginary part of the single-particle polarization operator (19) vanishes at smaller momenta (or larger frequencies) making the above calculations consistent. At the same time, approximating the interlayer interaction propagator (7) by Eq. (20) one completely neglects a possible contribution of plasmon modes, that (within the simplest RPA approach) can be found by setting the denominator of Eq. (7) to zero. At zero temperature and for $\omega \gg v_F q$ (where $\text{Im}\Pi^R = 0$), the polarization operator is known to be given by (Stern, 1967)

$$\Pi(\mathbf{q}, \omega) \simeq -nq^2/(m\omega^2).$$

Using this expression and expanding the bare Coulomb potential in small momenta, yields the acoustic (“−”) and optical (“+”) plasmon modes with dispersions

$$\omega_- = eq\sqrt{2\pi nd/m}, \quad \omega_+ = e\sqrt{4\pi nq/m}.$$

Both of these modes lie outside of the particle-hole continuum and in the parameter region, where the nonlinear susceptibility (17) vanishes. Hence, one may conclude that the plasmons cannot contribute to frictional drag.

However (Flensberg and Hu, 1994), at finite temperatures thermally excited quasiparticles and plasmons may coexist in the same parameter region, which may result in an additional contribution to drag. In order to accurately describe the plasmon contribution to ρ_D , one has to consider intralayer equilibration due to electron-electron collisions (Chen *et al.*, 2015) which gives rise to two important features: (i) the polarization operator acquires nonvanishing spectral weight within the high frequency part of the spectrum at $\omega > v_F q$ (Flensberg and

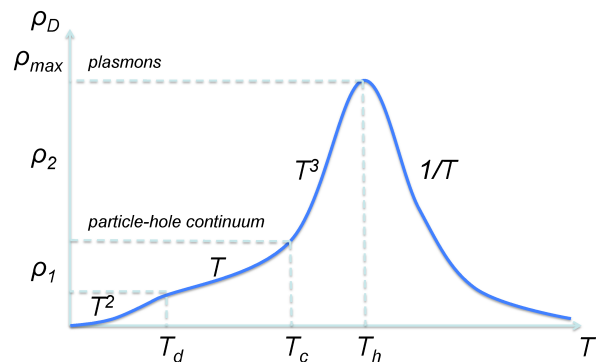


FIG. 4 (Color online) Schematic illustration for the drag resistivity at high temperatures showing the plasmon peak at $T \sim T_h$. The asymptotic dependences are exaggerated for clarity. Definitions of the three crossover scales are given in the main text. [Reproduced from Chen *et al.* (2015).]

Hu, 1994); and (ii) the plasmons acquire finite life-time (Hruska and Spivak, 2002; Mishchenko *et al.*, 2004) that regularizes the pole in the interaction propagator.

The theory discussed in the preceding Sections is based on the implicit assumption that the intralayer equilibration is the fastest process in the system. Characterizing inelastic electron-electron scattering by the quasiparticle lifetime τ_{ee} , one finds that the standard theory – and hence Eq. (22) – is valid as long as the time τ_{ee} is much smaller than the interlayer scattering time, $\tau_{ee} \ll \tau_D$ and at temperatures below the corresponding threshold $T \ll T_c \sim E_F \sqrt{k_F / (\varkappa^2 d)}$.

At higher temperatures, $T > T_c$, the system enters the collision-dominated regime, where Coulomb drag is dominated by plasmons. In this regime, Chen *et al.* (2015) find a stronger temperature dependence

$$\rho_D(T_c < T < T_h) \simeq \frac{\hbar}{e^2} \frac{1}{(k_F d)^4} \frac{T^3}{E_F}. \quad (23)$$

The rise of the plasmon contribution to drag persists so long as the quasiparticle decay rate remains small compared to the plasma frequency (at the wave vector $1/d$), i.e. up to the third crossover temperature $T_h \sim E_F \sqrt{k_F / \varkappa^4 \sqrt{1/\varkappa d}}$. At temperatures above the crossover, $T > T_h$, the electronic system enters the hydrodynamic regime that can be understood on the basis of the classical Navier-Stokes hydrodynamics (Apostolov *et al.*, 2014). In this limit the drag resistivity decays as

$$\rho_D(T > T_h) \simeq \frac{\hbar}{e^2} \frac{1}{(k_F d)^2 (\varkappa d)^3} \frac{E_F}{T}. \quad (24)$$

The resulting temperature dependence of the drag coefficient is summarized in Fig. 4. The nonmonotonicity of ρ_D originates from the delicate interplay of various scattering channels in the electronic system. Perhaps the most striking feature of the theory of Chen *et al.* (2015) is

that intralayer collisions promote stronger drag. Indeed, should one naively continue Eq. (22) up to the temperatures of the order T_h one would underestimate the actual maximum value of ρ_D by $\sqrt{k_F d} \gg 1$.

C. Effects of potential disorder

In ballistic samples, potential disorder played a very limited role. In fact, the resulting drag resistivity (21) is independent of the impurity scattering time τ . In diffusive samples with $d \gg \ell$ only small momenta $q \ll 1/\ell$ can be transferred between the layers. Typically this results in a small contribution to the drag resistivity, which in ballistic samples can be neglected. This is not always the case – at low enough temperatures drag is dominated by mesoscopic fluctuations which are mostly due to processes with small momentum transfers, see Sec. III.

Coulomb drag in diffusive systems was considered in Zheng and MacDonald (1993) using the memory function formalism and in Kamenev and Oreg (1995) using the diagrammatic technique. To the lowest order in interlayer interaction, one can use the Kubo formula analysis (Kamenev and Oreg, 1995; Narozhny and Aleiner, 2000) to derive the expression for the drag conductivity (S is the area of the sample)

$$\sigma_D = \frac{1}{16\pi TS} \int \frac{d\omega}{\sinh^2 \frac{\omega}{2T}} D_{12}^R \Gamma_{23}^x D_{34}^A \Gamma_{41}^{x*}, \quad (25)$$

where numerical subscripts indicate spatial coordinates, and are implied to be integrated over. Averaging over disorder restores translational invariance. In the absence of interlayer disorder correlations [this special case was considered in Gornyi *et al.* (1999)], the nonlinear susceptibilities in each layer have to be averaged independently of each other. Then one recovers the drag relaxation rate (15), where each quantity should be understood as disorder-averaged, i.e. $\langle \Gamma_{23}^x \rangle \rightarrow \Gamma^x(\mathbf{q})$.

1. Drag resistivity in diffusive regime

In the diffusive regime, the nonlinear susceptibility Γ can be found from Ohm's law (Landau *et al.*, 1984),

$$\mathbf{j} = \hat{\sigma} \mathbf{E} - eD \nabla n, \quad (26)$$

where $\hat{\sigma}$ is the conductivity matrix and D is the diffusion coefficient (in two dimensions $D = v_F^2 \tau / 2$). Combining Eq. (26) with the continuity equation, one finds the linear response of the carrier density n to the electric field \mathbf{E}

$$\langle n(\mathbf{q}, \omega) \rangle = \frac{1}{e} \frac{i q^\alpha \sigma^{\alpha\beta} E^\beta(\mathbf{q}, \omega)}{-i\omega + Dq^2}. \quad (27)$$

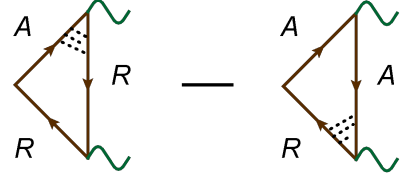


FIG. 5 (Color online) Disorder averaging of the nonlinear susceptibility (Kamenev and Oreg, 1995). The dotted lines represent the diffuson ladder (Altshuler and Aronov, 1985).

where $\langle \dots \rangle$ indicates averaging over disorder. Nonlinear response follows from the density dependence of the conductivity $j_{dc} = \text{Re}(\partial\sigma/\partial n) n(\mathbf{q}, \omega) E(-\mathbf{q}, -\omega)$, and yields

$$\langle \Gamma^\gamma \rangle = \frac{2\nu}{e} \frac{\partial \langle \sigma^{\gamma\delta} \rangle}{\partial n} q^\delta \frac{\omega D q^2}{\omega^2 + D^2 q^4}. \quad (28)$$

In the absence of a magnetic field $\langle \sigma^{\alpha\beta} \rangle = \sigma \delta^{\alpha\beta}$, and the nonlinear susceptibility (28) is parallel to \mathbf{q} . The disorder-averaged conductivity is linear in the carrier density, $\partial\sigma^{\alpha\beta}/\partial n \approx \sigma^{\alpha\beta}/n$. As a result,

$$\langle \Gamma \rangle = 2\mathbf{q} \frac{e\nu D}{E_F} \frac{\omega D q^2}{\omega^2 + D^2 q^4}. \quad (29)$$

This expression can be recast into two equivalent forms. Noting the similarity between Eq. (29) and the standard diffusive form of the polarization operator (Altshuler and Aronov, 1985; Smith and Jensen, 1989)

$$\Pi^R(\mathbf{q}, \omega) = \nu \frac{Dq^2}{-i\omega + Dq^2}, \quad (30)$$

one finds (Kamenev and Oreg, 1995)

$$\langle \Gamma \rangle = 2\mathbf{q} \frac{eD}{E_F} \text{Im} \Pi^R(\mathbf{q}, \omega). \quad (31)$$

Furthermore, one can emphasize the fact that the density dependence of the conductivity σ is a manifestation of electron-hole asymmetry by rewriting the fraction in Eq. (31) as (Narozhny and Aleiner, 2000)

$$\langle \Gamma \rangle = 2e\mathbf{q}D \frac{\partial \ln(\nu D)}{\partial \mu} \text{Im} \Pi^R(\mathbf{q}, \omega). \quad (32)$$

In the simplest case⁸, this expression can be obtained directly from Eq. (28) by noticing that $\partial\sigma^{\alpha\beta}/\partial n = (\partial\sigma^{\alpha\beta}/\partial\mu)(\partial\mu/\partial n) = (\partial\sigma^{\alpha\beta}/\partial\mu)(1/\nu)$ and using the Einstein relation. The same result can be found evaluating diagrams shown in Fig. 5.

The diffusive approximation for the interlayer interaction follows from Eqs. (7) and (30). Focusing on small momenta $q \ll 1/d$, one can obtain alternative expressions for the interaction propagator by either expanding the bare matrix element (5) in small qd (and subsequently

limiting the momentum integration from above) or keeping the exponential in Eq. (5) intact, leaving the momentum integral converging in the ultraviolet. The former approach was taken in Narozhny and Aleiner (2000). Generalizing to inequivalent layers one finds

$$\mathcal{D}_{12}^R = -\frac{1}{q^2} \frac{(-i\omega + D_1 q^2)(-i\omega + D_2 q^2)}{(\nu_1 D_1 + \nu_2 D_2)[-i\omega + (1 + \varkappa^* d)D^* q^2]}, \quad (33a)$$

where

$$\varkappa^* = 4\pi e^2 \frac{\nu_1 \nu_2}{\nu_1 + \nu_2}, \quad D^* = \frac{(\nu_1 + \nu_2)D_1 D_2}{\nu_1 D_1 + \nu_2 D_2}.$$

The latter alternative was taken in Kamenev and Oreg (1995), where in addition (just as in the ballistic case) the limit $\varkappa d \gg 1$ was used. As a result, the interaction propagator takes the form

$$\mathcal{D}_{12}^R = -\frac{\pi e^2 q}{\varkappa_1 \varkappa_2 \sinh qd} \frac{-i\omega + D_1 q^2}{D_1 q^2} \frac{-i\omega + D_2 q^2}{D_2 q^2}. \quad (33b)$$

With logarithmic accuracy, the resulting drag coefficient is independent of the distinction between the two and can be written as (Kamenev and Oreg, 1995)

$$\langle \rho_D \rangle = \frac{\hbar}{e^2} \frac{\pi^2 T^2}{12 E_{F1} E_{F2}} \frac{1}{\varkappa_1 \varkappa_2 k_{F1} k_{F2} \ell_1 \ell_2 d^2} \ln \frac{T_0}{2T}. \quad (34a)$$

The only difference between using the two expressions for the interaction propagator in Eq. (33) is the exact value of T_0 . Using Eq. (33a) in the limit $\varkappa^* d \gg 1$, one finds

$$T_0 = \frac{4\pi e^2 \nu_1 D_1 \nu_2 D_2}{(\nu_1 D_1 + \nu_2 D_2) d},$$

while Eq. (33b) leads to (Kamenev and Oreg, 1995)

$$T_0 = \min\{\varkappa_1 D_1, \varkappa_2 D_2\} / d.$$

Both expressions are of the same order of magnitude and coincide for the case of identical layers.

The result can be expressed also in terms of the inter-layer relaxation rate (Zheng and MacDonald, 1993)

$$\frac{1}{\tau_D} = \frac{\pi^2}{12} \frac{n_1}{m_2} \frac{T^2}{E_{F1} E_{F2}} \ln \frac{T_0}{2T} \frac{1}{\varkappa_1 \varkappa_2 k_{F1} k_{F2} \ell_1 \ell_2 d^2}. \quad (34b)$$

Equivalently, one can use Eq. (32) and express the drag conductivity (Narozhny and Aleiner, 2000) as (here the layers are assumed to be identical for simplicity)

$$\sigma_D = \frac{e^2}{\hbar} \frac{\pi^2}{3} \frac{(\hbar T)^2}{g^2 (\varkappa d)^2} \left(\frac{\partial}{\partial \mu} (\nu D) \right)^2 \ln \frac{T_0}{2T}, \quad (35)$$

where the derivative highlights the crucial role of the electron-hole asymmetry in the leading-order drag effect.

The diffusive result for the drag resistivity (34) appears to be rather similar to its ballistic counterpart Eq. (21). Indeed, disregarding the numerical prefactors and the logarithm in Eq. (34), one finds

$$\rho_D^{diff} / \rho_D^{bal} \sim d^2 / (\ell_1 \ell_2). \quad (36)$$

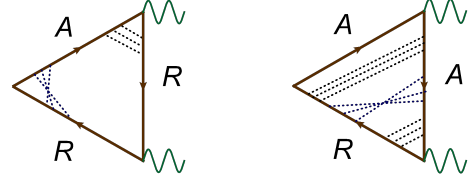


FIG. 6 (Color online) Leading weak localization corrections to the nonlinear susceptibility (Kamenev and Oreg, 1995). The black, parallel dotted lines represent the diffuson ladder (Aleiner *et al.*, 1999; Altshuler and Aronov, 1985). The blue, crossing lines represent the Cooperon (Gorkov *et al.*, 1979).

This relation may serve as an *a posteriori* justification for the statement that the drag effect in samples with $d \ll \ell$ is dominated by ballistic propagation of carriers with momenta $\ell^{-1} \ll q \ll d^{-1}$. Carriers with small momenta $q \ll \ell^{-1}$ also participate in drag, but their contribution is small [according to Eq. (36)] and is typically neglected.

2. Weak localization corrections

The nonlinear susceptibility (29) and drag coefficient (34) were obtained as the leading approximation in the standard perturbation theory of disordered metals (Altshuler and Aronov, 1985), controlled by the large parameter $g = 25.8k\Omega/R_{\square}$ representing the dimensionless conductance of the layers (with R_{\square} being the layer (sheet) resistance). Within the assumptions adopted in this Section⁸ $g \sim \nu D \sim k_F \ell \sim E_F \tau \gg 1$.

The next-order terms in the perturbation theory are known as quantum corrections to transport coefficients (Aleiner *et al.*, 1999; Altshuler and Aronov, 1985). Physically, they describe leading interference processes that arise in the course of subsequent scattering events. Although the resulting contribution to transport is proportional to a small factor $1/g$, quantum corrections dominate the temperature and magnetic field dependence of transport coefficients at low temperatures.

To the leading order in $1/g$, one may distinguish three types of corrections: (i) interference between self-intersecting, time-reversed scattering paths leads to a positive correction to resistivity, known as the weak localization correction (Abrahams *et al.*, 1979; Altshuler *et al.*, 1980; Gorkov *et al.*, 1979); (ii) coherent scattering off Friedel oscillations yields the Altshuler-Aronov correction (Altshuler and Aronov, 1979; Finkelstein, 1983, 1984; Zala *et al.*, 2001); and (iii) in small, mesoscopic samples interference between scattering paths gives rise to universal conductance fluctuations (Altshuler, 1985; Lee and Stone, 1985). The latter effect has a direct counterpart in double-layer systems, namely mesoscopic fluctuations of Coulomb drag discussed in Sec. III. At

the time of writing, no qualitative interference effect due to electron-electron interaction has been identified for drag measurements. At the technical level, the third-order drag effect (see the following Section) bears certain resemblance to the Altshuler-Aronov diagrams (Gornyi and Narozhny, 2014). Here we discuss the weak localization correction to Coulomb drag (Flensberg *et al.*, 1995; Kamenev and Oreg, 1995).

In the absence of interlayer disorder correlations [such effects were discussed in Gornyi *et al.* (1999)], impurity scattering is confined to each individual layer. It should come as no surprise that the same mechanism behind the weak localization correction to single-layer conductivity (i.e., interference between time-reversed, self-intersecting paths) yields a correction to the nonlinear susceptibility. Technically, this interference mechanism is described by a “maximally crossed” element of the diagram technique known as the Cooperon (Gorkov *et al.*, 1979). Diagrams for the corresponding corrections to the nonlinear susceptibility are shown in Fig. 6 [further corrections, e.g. two-Cooperon diagrams, considered in Flensberg *et al.* (1995) and Kamenev and Oreg (1995) were found to be subleading]. The resulting nonlinear susceptibility is given by

$$\langle \Gamma \rangle = 2q \frac{e\nu D(\tau_\varphi^{-1}, 0)}{E_F} \frac{\omega D(\omega, \mathbf{q}) q^2}{\omega^2 + D^2(\omega, \mathbf{q}) q^4}, \quad (37)$$

where the renormalized diffusion coefficient in two dimensions in (Gorkov *et al.*, 1979)

$$D(\omega, \mathbf{q}) = D \left(1 - \frac{1}{\pi k_F \ell} \ln \frac{1}{\omega \tau} \right), \quad (38)$$

and τ_φ is the dephasing time (Altshuler *et al.*, 1980). The result (37) is valid in the first order in $\delta D = D(\omega, \mathbf{q}) - D$.

The resulting leading-order weak localization correction to Coulomb drag is (Kamenev and Oreg, 1995)

$$\frac{\delta \rho_D}{\rho_D} = -\frac{1}{\pi k_{F1} \ell_1} \ln \frac{1}{2T\tau_1} - \frac{1}{\pi k_{F2} \ell_2} \ln \frac{1}{2T\tau_2}, \quad (39)$$

where ρ_D is given by Eq. (34). The result (39) is similar to the weak localization corrections in 2D (Altshuler *et al.*, 1980; Gorkov *et al.*, 1979), except that in Eq. (39) the logarithmic singularity is cut by temperature rather than by the dephasing time.

In conventional 2DEG, weak localization effects result in a dependence on a weak magnetic field (Altshuler *et al.*, 1980). Here, the characteristic scale of the magnetic field would be $H_c \sim T/(eD)$. Similar scale describes intralayer interaction corrections to magnetoresistance (Altshuler and Aronov, 1985), making the weak localization corrections to the drag coefficient hard to observe experimentally (Kamenev and Oreg, 1995).

D. Third-order drag effect

The leading contribution to Coulomb drag, Eqs. (15), (25), describes the effect to the lowest order in the inter-

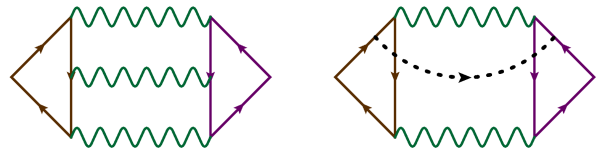


FIG. 7 (Color online) Typical diagrams describing higher-order drag effects. Left: third-order drag (Levchenko and Kamenev, 2008b). Right: the effect of interlayer disorder correlations (Gornyi *et al.*, 1999; Hu, 2000a).

layer Coulomb interaction, see Fig. 2. Since the particles belonging to different layers interact through a layer of an insulating material, certain weakness of the effective interaction is intuitively expected. In many-body electron systems the Coulomb interaction is usually screened and the perturbative analysis gives a reasonable account of most basic observable quantities (Altshuler and Aronov, 1985; Ziman, 1965). Consequently, the vast majority of theoretical studies of Coulomb drag are devoted to the investigation of the lowest-order effect. Notable exceptions are given by the studies of the interlayer correlated states, either in the context of quantum Hall devices (Girvin and MacDonald, 1997; Kim *et al.*, 2001; Stern and Halperin, 2002; Stern *et al.*, 2000; Yang, 1998; Yang and MacDonald, 2001) or quantum wires (Klesse and Stern, 2000; Nazarov and Averin, 1998), as well as strongly correlated intralayer states, such as Wigner crystals (Baker and Rojo, 2001; Braude and Stern, 2001) or Anderson insulators (Raikh and von Oppen, 2002).

The “single-particle” drag resistivity, Eqs. (21), (34), is determined (besides the interlayer interaction) by the quasiparticle phase space, electron-hole asymmetry (see Sec. II.B), and disorder effects (see Secs. II.C and III). At $T = 0$ or at a point of exact electron-hole symmetry (e.g., in neutral graphene, see Sec. IV), these factors may conspire to nullify the effect. Then ρ_D may be determined by higher orders of the perturbation theory, implying that saturation of drag resistivity at low temperatures should not necessarily point towards a strongly correlated state.

To the third order in interlayer interaction (see Fig. 7 for the “skeleton” diagram), Coulomb drag was first discussed in Levchenko and Kamenev (2008b) in the diffusive regime, $T\tau \ll 1$. It was shown that the third-order drag contribution remains finite at zero temperature⁹:

$$\rho_D^{(3)}(T < h/\tau) = 0.27(h/e^2)g^{-3}(\kappa d)^{-2}. \quad (40)$$

This surprising result was attributed (Levchenko and Kamenev, 2008b) to the singular behavior of matrix elements in the diffusive regime. In single-layer systems,

⁹ More precisely, the result is valid down to lowest temperatures $T \sim \tau^{-1} e^{-\pi g}$. Below this scale the diffusive approximation breaks down.

similar enhancement of the matrix elements leads to singular interaction effects (Altshuler and Aronov, 1985). Here, the divergence of the matrix elements is compensated by the smallness of the phase space yielding the T -independent contribution to the drag resistivity.

The third-order effect (40) does not rely on electron-hole asymmetry (technically, the third-order diagram in Fig. 7 contains four-point vertices instead of the triangular vertices in Fig. 2). Hence, $\rho_D^{(3)}$ is independent of E_F . This provides an additional explanation of the T -independent result (40): in the diffusive regime there is no other scale for a temperature dependence.

Another contribution to drag that is insensitive to electron-hole symmetry is due to interlayer disorder correlations (Gornyi *et al.*, 1999; Hu, 2000a). For temperatures higher than the inverse interlayer coherence time, but still in the diffusive regime, $\tau_g^{-1} \ll T \ll \tau$, one finds

$$\rho_D(\tau_g^{-1} \ll T \ll \tau_{tr}^{-1}) \sim (h/e^2)(k_F^2 d^2 \kappa \ell)^{-2} \ln(T\tau_g), \quad (41)$$

which might dominate over Eq. (34).

While the above higher-order effect have not been observed in semiconductor samples, they may provide an explanation of the observed nonzero drag resistivity in neutral graphene (Gorbachev *et al.*, 2012), see Sec. IV.

E. Transconductance due to tunneling bridges

A qualitatively different mechanism of transconductance takes place in the double-layer systems with point-like shortages (bridges) or when the insulating layer is sufficiently thin such that electrons may tunnel between the two layers (Oreg and Halperin, 1999; Oreg and Kamenev, 1998; Raichev, 1997). Such bridges can be present in metallic double-layer systems due to device fabrication imperfections, or they can be introduced on purpose (Giordano and Monnier, 1994).

One should distinguish two mechanisms of transresistivity due to tunneling. The first one is essentially classical and originates from a voltage drop in the passive layer due the current leaking directly from the active layer. This mechanism can be simply visualized and understood using a resistive network model where the two layers are connected in parallel by a set of resistors (Raichev, 1997). Applying the Kirchhoff's laws to such a circuit, one finds that for sufficiently long samples, $L > \sqrt{D}\tau_{12}$ (here τ_{12} is the mean intralayer scattering time associated with the interlayer tunneling conductance per unit area $\sigma_{\perp} = e^2\nu/\tau_{12}$), half of the current supplied to the active layer leaks into the passive one. In this case, the *sign* of the drag effect is *reversed* compared to the standard result (3a) and ρ_D is given by the resistance of a single layer of a doubled width. This classical effect is practically insensitive to temperature. Furthermore, the tunneling rate τ_{12} is strongly dependent to a Fermi-surface

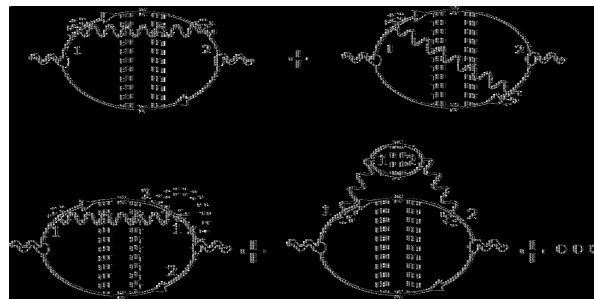


FIG. 8 Top: two diagrams contributing to the transconductance that are second order in tunneling matrix element denoted by a cross. Full lines with arrows are electron Green functions, dashed lines represent diffusons, and wavy lines screened interactions. Two additional diagrams with arrows in the opposite direction should be included. The numbers indicate the layer index. Bottom: examples of diagrams contributing to the transconductance that are fourth order in tunneling. Diagrams with interaction lines connecting “upper” and “lower” Green functions, as well as diagrams with an opposite direction of electron lines are also implicit. [Reproduced from Oreg and Kamenev (1998).]

mismatch between the layers, and thus may be affected by a gate voltage or an in-plane magnetic field (Berk *et al.*, 1995; Boebinger *et al.*, 1991), which gives an experimental knob to control the magnitude of the classical tunnel drag resistivity.

The second, purely quantum effect was suggested by Oreg and Halperin (1999) and Oreg and Kamenev (1998). Here drag originates from the intralayer exchange correlations due to wave-functions overlap of carriers in different layers (that may exist in the presence of interlayer tunneling). The sign of the quantum effect is *negative* for the carriers of the same charge, i.e. the same as in the above classical effect. This mechanism yields a strongly temperature dependent drag resistivity, which saturates to a constant value at zero temperature. The latter feature is an indication that the exchange contribution to drag resistivity does not require electron-hole asymmetry. Hence, even for a small tunneling rate, this mechanism may become stronger than the standard effect (3a) at low enough temperatures.

The interplay between tunneling, Coulomb interaction, and intralayer disorder scattering yields the three energy scales: τ_{12}^{-1} , $\kappa d\tau_{12}^{-1}$, and τ^{-1} . Here the factor of κd stems from the screening effects. At high temperatures, $T > \tau^{-1}$, the quantum drag resistivity can be computed to the lowest order in tunneling (the corresponding diagrams are shown in Fig. 8, top panel). Furthermore, since for $T\tau \gg 1$ the motion of electrons is ballistic, one can omit disorder ladders (diffusons) in these diagrams. Then the transconductance is given by the temperature-

independent expression (Oreg and Kamenev, 1998)

$$\sigma_D = -\frac{e^2}{\hbar} \frac{\pi}{32} \frac{1}{\kappa d} \frac{v_F \tau^2}{d\tau_{12}}. \quad (42)$$

At lower temperatures, $T < \tau^{-1}$, the diffusive character of the electron motion should be taken into account. The drag resistivity can be still computed to the leading order in tunneling using the same set of diagrams in Fig. 8 (top panel), but with insertion of disorder renormalizations. As a result, one finds the following temperature-dependent contribution to the transconductance (Oreg and Kamenev, 1998)

$$\sigma_D = -\frac{e^2}{\hbar} \frac{1}{24\pi} \frac{\ln(\kappa d)}{\kappa d} \frac{1}{T\tau_{12}}. \quad (43)$$

In the diffusive limit, such singular temperature dependence is not entirely unexpected. Indeed, the diagrams in Fig. 8 (top) are analogous to the Altshuler-Aronov corrections to the conductivity of 2D systems, which are known to be logarithmically singular (Altshuler and Aronov, 1985; Zala *et al.*, 2001). In the present context, the interplay of tunneling and Coulomb interaction makes this singularity stronger.

The above quantum physics becomes even more pronounced at lower yet temperatures, $T < \kappa d\tau_{12}^{-1}$, where the quantum drag mechanism is dominated by coherent tunneling of electrons to the passive layer and back to the active one accompanied by intralayer Coulomb interactions, see Fig. 8 (bottom). In this regime, the temperature dependence is even stronger (Oreg and Kamenev, 1998)

$$\sigma_D = -\frac{e^2}{\hbar} \frac{3\zeta(3)}{8\pi^4} \frac{\ln(T\tau_{12})}{(T\tau_{12})^2}. \quad (44)$$

The low-temperature divergence in the transconductance (43) and (44) should be cut off by the finite size effects at the Thouless energy, $E_T = D/L^2$. Interestingly enough, for large systems, $L \gg \sqrt{D\tau_{12}}$, there is an additional temperature range, $E_T < T < \tau_{12}^{-1}$, where the exchange contribution to σ_D is due to multiple tunneling processes. In that case, the transconductance becomes logarithmic in temperature (Oreg and Kamenev, 1998)

$$\sigma_D = -\frac{e^2}{\hbar} \frac{1}{8\pi^2} \ln \frac{1}{T\tau_{12}}. \quad (45)$$

Up to the factor of 1/4, this result coincides with the standard Altshuler-Aronov correction to the 2D conductivity (Altshuler and Aronov, 1985; Zala *et al.*, 2001). This extra numerical factor is not accidental and reflects the essence of the drag measurement setup, where the current is allowed to flow in one part of the system only while the induced potential is measured in another part.

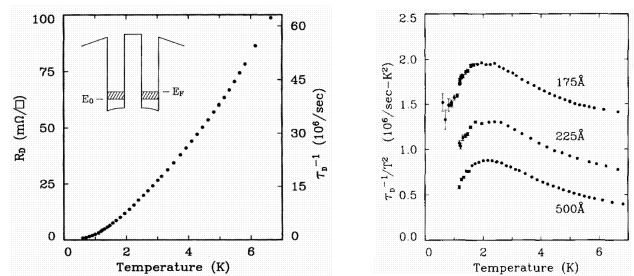


FIG. 9 Left panel: temperature dependence of the drag resistivity GaAs double-quantum-wells. The additional scale on the right provides the corresponding values of the momentum-transfer rate (see main text for more details). The inset shows an idealized energy diagram for a double-quantum-well structure indicating the ground subband energy E_0 and the Fermi energy E_F . [Reproduced from Gramila *et al.* (1991).] Right panel: Temperature dependence of the interlayer momentum transfer rate divided by T^2 . The three sets of data were measured in samples with interwell barrier widths of 175Å, 225Å, and 500Å. [Reproduced from Gramila *et al.* (1992).]

F. Comparison to experiment

The theory outlined in the preceding sections describes an idealized phenomenon of mutual friction between two two-dimensional electron systems. The electrons were assumed to belong to a parabolic band, with energy-independent impurity-scattering time and negligible intralayer correlations. Clearly, such assumptions can be realized in any experimental sample only approximately.

Coulomb drag between two two-dimensional electron gases was first observed by the group of J. Eisenstein (Eisenstein, 1992; Gramila *et al.*, 1991) in GaAs double-quantum-wells, see Fig. 9. Detailed comparison of the experimental data to the quantitative predictions of the Coulomb drag theory showed that the latter accounts for about 50% of the measured values¹⁰. This was judged as sufficient evidence of the relevance of the Coulomb mechanism of frictional drag. Also, the overall reduction of the drag resistance with the increase of the interwell barrier width (see Fig. 9) was in rough agreement with Eq. (21b). At the same time, the data (see the right panel in Fig. 9) show noticeable deviations from the T^2 behavior predicted by Eqs. (21) and (34), indicating that other scattering mechanisms might also be important.

One additional mechanism (Gramila *et al.*, 1991) is due to electron-phonon interaction. This suggestion was

¹⁰ The momentum relaxation time reported in Gramila *et al.* (1991) is twice smaller than Eq. (21b). In addition, the paper cited unpublished calculations of MacDonald, Gramila, and Eisenstein involving a more realistic modeling of finite-width quantum wells. In particular, these calculations were reported to include vertex corrections to the RPA interaction propagator (7). Hence, it is difficult to judge whether that factor of 2 has played any role in the actual analysis of Gramila *et al.* (1991).

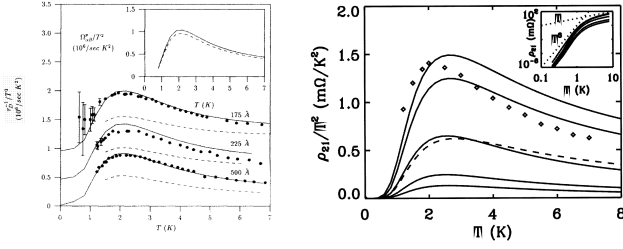


FIG. 10 Left panel: calculated τ_D^{-1}/T^2 (solid curves) compared to the data of Gramila *et al.* (1991). A less optimal choice of a fitting parameter yields results shown by the dashed curves. Inset: calculated contribution of virtual-phonon exchange processes to τ_D^{-1}/T^2 . [Reproduced from Tso *et al.* (1992).] Right panel: calculated ρ_D/T^2 for various values of the phonon mean free path and $d = 500\text{\AA}$ (solid curves). The dots show the data of Gramila *et al.* (1992). The dotted line represents the contribution of the modified plasmon pole. Inset: the crossover of the T^6 to T temperature dependence. [Reproduced from Bønsager *et al.* (1998a).]

developed theoretically in Badalyan and Rössler (1999); Bønsager *et al.* (1998a,b); and Tso *et al.* (1992) and experimentally in Jörger *et al.* (2000a); Noh *et al.* (1999); and Rubel *et al.* (1995), see Fig. 10.

Both the Coulomb and phonon drag mechanisms assume smallness of the transferred momentum q [see, e.g., Eq. (6)], which is fully justified for samples with the small screening length, $\kappa d \gg 1$. In addition, for low-density samples with closely spaced layers (i.e., for $k_F d \sim 1$) backward scattering processes with $q \sim 2k_F$ may become important (Kellogg *et al.*, 2002a). The contribution of such processes to drag shows the $T^2 \ln T$ temperature dependence [in contrast to Eq. (21)]. While such logarithmic correction is difficult to ascertain, the experiment (Kellogg *et al.*, 2002a) shows sizable deviations from Eq. (21) with the observed unusual density dependence of ρ_D suggesting the importance of the $2k_F$ scattering processes. Quantitative theoretical description of these results was later achieved in Asgari *et al.* (2008) and Yurtsever *et al.* (2003) using a numerical approach based on the effective interaction scheme developed in Kukkonen and Overhauser (1979) and Vignale and Singwi (1985).

Further corrections to the single-particle Coulomb mechanism are associated with the plasmon contribution. As shown in Flensberg and Hu (1994), plasmons are expected to be most important at intermediate temperatures, $T \sim 0.5T_F$. This prediction was tested experimentally in Hill *et al.* (1997), see the left panel in Fig. 11, and in Noh *et al.* (1998). While the theoretical results show qualitative agreement with the data, discrepancies persist. Taking into account many-body correlations [see, e.g., Swierkowski *et al.* (1995)] improves the agreement, but further advances in many-body theory are necessary before a more precise quantitative description of the correlation effects in double-layer structures is achieved.

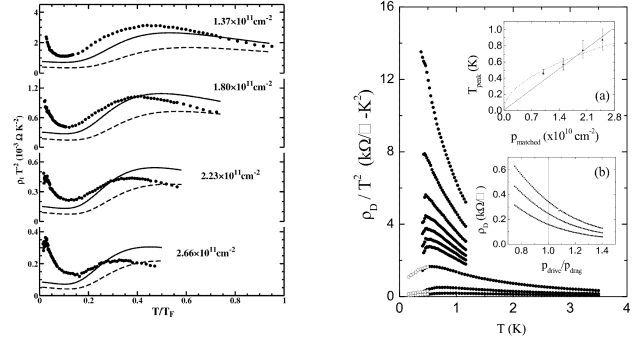


FIG. 11 Left panel: measured ρ_D/T^2 for various values of the carrier density, $n_1 = n_2$. Dashed lines represent the results of Flensberg and Hu (1994) adjusted for the sample parameters of the experiment. Solid lines show the results of additional calculations taking into account intralayer many-body correlations within the Hubbard approximation. [Reproduced from Hill *et al.* (1997).] Right panel: measured ρ_D/T^2 for different carrier densities. Inset: (a) peak position temperature vs matched layer density; (b) ρ_D vs density ratio for $T = 860, 730, \text{ and } 600\text{mK}$. [Reproduced from Pillarisetty *et al.* (2002).]

The discrepancies between the simple single-particle description and laboratory experiments are by no means universal, especially since many measurements were performed in very different systems. One of the first drag experiments (Solomon *et al.*, 1989) was performed on a hybrid 2D-3D system. This device showed considerable thermoelectric effects masking the purely Coulomb contribution to drag. Experiments on electron-hole systems (Sivan *et al.*, 1992) showed behavior that could not be accounted by neither the phonon, nor plasmon corrections. Instead, generalized RPA (taking into account exchange processes to all orders) (Tso *et al.*, 1993) appears to yield satisfactory agreement with observations of Sivan *et al.* (1992) at low temperatures. Apparently, the traditional RPA overestimates screening which results in the underestimated drag resistivity.

Experiments on dilute 2D hole systems (Pillarisetty *et al.*, 2002, 2004) show marked enhancement of the drag resistivity, along with the stronger temperature dependence (empirically, $\rho_D \propto T^{2.5}$ at low temperatures, followed by a crossover towards a sublinear temperature dependence at $T \simeq E_F$). These systems are characterized by rather high values of the dimensionless Wigner-Seitz radius¹¹ (Ando *et al.*, 1982; Giuliani and Vignale, 2005) $r_s \simeq 20\text{--}40$ and also exhibit signs of a metal-insulator transition in single-layer measurements (Pillarisetty *et al.*, 2005b). The data obtained in Pillarisetty

¹¹ Physically, the dimensionless Wigner-Seitz radius can be understood as the ratio of the average potential energy to the average kinetic energy of the electronic system. In 2D systems it can be estimated as $r_s = e^2 m^* / (\hbar^2 \epsilon \sqrt{\pi n}) = (\sqrt{2}/\epsilon) [e^2 / (\hbar v_F)]$, where m^* is the band mass and ϵ is the dielectric constant.

et al. (2002) are not explained by taking into account corrections due to phonons (Bønsager *et al.*, 1998a), plasmons (Flensberg and Hu, 1994), or many-body effects (Swierkowski *et al.*, 1995), as follows from the density dependence of the measured drag illustrated in the right panel of Fig. 11. The lack of adequate theoretical description of these experiments is not surprising, given that the regime of relatively high r_s remains an unsolved problem in single-layer (bulk) systems as well.

Croxall *et al.* (2008) and Das Gupta *et al.* (2008) report anomalous drag in electron-hole bilayers. Below $T = 1\text{K}$, the measured drag resistivity exhibits an upturn that may be followed by a downturn, although ρ_D does not seem to vanish for $T \rightarrow 0$. The observed upturn may indicate exciton formation (Hu, 2000b; Vignale and MacDonald, 1996), however neither the observed violation of Onsager reciprocity, nor the apparent downturn at lower temperatures are anticipated by the theory. The effect of density imbalance on the drag upturn was studied in Morath *et al.* (2009). The data were interpreted in terms of a pairing-fluctuations mechanism based on the theory of Hwang and Das Sarma (2008b). The theory accounts for most qualitative features of the effect, however the predicted peak in ρ_D at equal layer densities was not observed in experiment (Morath *et al.*, 2009).

Further experiments demonstrate interesting correlation effects such as Wigner crystallization in quantum wires (Yamamoto *et al.*, 2006, 2012), exciton formation in electron-hole bilayers (Seamons *et al.*, 2009), or quantum Hall effect (Girvin and MacDonald, 1997; Lilly *et al.*, 1998), see Sec. VII.A. Clearly these phenomena cannot be described by the simple theory presented in this Section. At the same time, single-particle effects are still important at relatively low temperatures ($T \lesssim 0.2T_F$) in traditional semiconductor heterostructures hosting two-dimensional electron systems and even more so in graphene (see Sec. IV), where interlayer separation can be as small as several interatomic distances (Gorbachev *et al.*, 2012).

1. Phonon effects

Electrical resistivity due to electron-phonon scattering is a standard topic in condensed matter physics (Ziman, 1965). At temperatures higher than the Debye frequency $T \gg \omega_D$, it exhibits linear behavior $\rho \propto T$, that is observed in a wide class of materials including high-mobility 2DEG (Stormer *et al.*, 1990) and graphene (Efetov and Kim, 2010). At low temperatures $T \ll \omega_D$ [in low density electron systems the crossover occurs at a lower scale, the so-called Bloch-Grüneisen temperature $T \ll T_{BG} < \omega_D$ (Stormer *et al.*, 1990)] the phonon contribution is rapidly decreasing as $\rho \propto T^5$ in metals (Bloch, 1930; Grüneisen, 1933) and heterostructures (Price, 1984; Stormer *et al.*,

1990) and as $\rho \propto T^4$ in graphene (Efetov and Kim, 2010; Hwang and Das Sarma, 2008a).

Qualitative physics of electron-phonon interaction in semiconductor double-quantum-well heterostructures is captured by the following interaction Hamiltonian

$$\mathcal{H}_{ep} = \frac{1}{\sqrt{V}} \sum_{\lambda, \lambda'; \mathbf{k}} \sum_{\mathbf{Q}; \eta} M_{\lambda, \lambda'}^{\eta}(\mathbf{Q}) F_{\lambda, \lambda'}(q_z) \times \left[\hat{b}_{\eta}^{\dagger}(-\mathbf{Q}) + \hat{b}_{\eta}(\mathbf{Q}) \right] \hat{c}_{\lambda}^{\dagger}(\mathbf{k}) \hat{c}_{\lambda'}(\mathbf{k} + \mathbf{q}). \quad (46)$$

Here $\mathbf{Q} = (\mathbf{q}, q_z)$ is the 3D wave vector of a phonon with polarization η , \mathbf{k} is the 2D electron wave vector, $M_{\lambda, \lambda'}^{\eta}$ is the bulk electron-phonon matrix element corrected by the subband form-factor

$$F_{\lambda, \lambda'}(q_z) = \int_{-\infty}^{\infty} dz \xi_{\lambda}(z) \xi_{\lambda'}^* e^{iq_z z}, \quad (47)$$

where $\xi_{\lambda}(z)$ is the bound state wave function associated with the quantized motion in the subband λ . This Hamiltonian was used to study effects of interaction between electrons and longitudinal optical phonons in Das Sarma and Mason (1985) and to calculate quasiparticle properties in weakly polar 2DEG in Jalabert and Das Sarma (1989). In double-layer systems, the Hamiltonian (46) was used to describe interlayer interaction mediated by acoustic phonons in Bønsager *et al.* (1998a) and Zhang and Takahashi (1993) and by optical phonons in Hu (1998).

Electrons experience the phonon-mediated interaction (46) alongside the Coulomb interaction. The propagator of the effective interlayer interaction can be obtained within the RPA (Bønsager *et al.*, 1998a; Jalabert and Das Sarma, 1989; Zhang and Takahashi, 1993) similarly to Eq. (7). The result can be represented in the form $\mathcal{D}_{12} = (V_{12} + D_{12})/\epsilon(\mathbf{q}, \omega)$, where D_{12} is the propagator of the phonon-mediated interaction and $\epsilon(\mathbf{q}, \omega)$ is the effective dielectric function for interlayer interactions that is also determined by the sum of the Coulomb interaction (5) and the phonon propagator. Thus the phonon and Coulomb mechanisms are generally not independent of each other. However, the Coulomb interaction contributes only to small momentum transfers (6), while the phonon contribution peaks at $q \sim 2k_F$ (Bønsager *et al.*, 1998a). Neglecting interference between the two, one can estimate the effect of phonon-mediated interaction by considering only the phonon part $\mathcal{D}_{12} \rightarrow D_{12}/\epsilon(\mathbf{q}, \omega)$.

A simple analytical estimate for the strength of the phonon-mediated interaction in GaAs/AlGaAs systems was suggested in Bønsager *et al.* (1998a). In this material, electron-phonon interaction is due to the deformation potential and piezoelectric effect. It turns out, that the deformation mechanism dominates (except for very low electron densities). Assuming infinite phonon mean free path, the corresponding (unscreened) effective

interaction has the form

$$\mathcal{D}_{12} = -\frac{C_{DP}\omega^2 e^{-d\sqrt{q^2 - \omega^2 c_l^{-2}}}}{\nu k_F c_l \sqrt{c_l^2 q^2 - \omega^2}}, \quad (48)$$

where c_l is the velocity of longitudinal acoustic phonons and $C_{DP} \approx 2.7 \times 10^{-3} k_F / (10^6 \text{cm}^{-1})$. The smallness of electron-phonon coupling constants implies weakness of the phonon-mediated interlayer interaction as compared to the Coulomb interaction. However, the effective interaction (48) diverges near $\omega \approx c_l q$ leading to a logarithmic divergence in the drag resistivity. Although this divergence is removed by either dynamic screening or phonon relaxation, the above argument illustrates the reason behind the relative strength of the phonon-mediated interlayer interaction.

Detailed calculations of the phonon-mediated drag resistivity have been performed numerically by several authors. Tso *et al.* (1992) showed that combining the phonon and Coulomb mechanisms of mutual friction accounts for the nonparabolic temperature dependence observed in GaAs/AlGaAs devices (Gramila *et al.*, 1991), see the left panel of Fig. 10. A refined discussion of the phonon mechanism was given in Bønsager *et al.* (1998a), see the right panel of Fig. 10. It was shown, that the temperature dependence of the phonon contribution to drag exhibits a crossover from linear to T^6 behavior around the Bloch-Grüneisen temperature (see the inset in Fig. 10), explaining the peak in the drag resistivity, Fig. 9. In addition, it was shown that there exists a collective mode that can be found setting $\epsilon(\mathbf{q}, \omega) = 0$. This mode is similar to the usual plasmon and results from coupling of the electrons from both layers to the phonons with $\omega \sim c_l q$. A similar mode resulting from interaction between electrons and optical phonons was discussed in Güven and Tanatar (1997a,b). A detailed analysis of the mutual friction due to optical phonons is given in Hu (1998).

2. Interlayer interaction beyond RPA

The expression (7) for the dynamically screened interlayer Coulomb interaction has been obtained within the RPA. While capturing the qualitative physics of the effect, this representation is by no means exact. In particular, RPA-based calculations seem to underestimate the value of ρ_D as compared to experimental data (Sivan *et al.*, 1992). A pedagogical discussion of the RPA and possible approaches to interacting many-body systems that go “beyond” the RPA can be found in Giuliani and Vignale (2005). Most of these approaches are not parametrically justified. The results of the calculations are typically compared to either experimental data or computer simulations.

Coulomb drag between electron and hole layers within the generalized RPA approach was considered in Tso

et al. (1993). The resulting ρ_D is about twice larger than that calculated within RPA, but still about twice smaller than the experimental data. Furthermore, it was understood in Swierkowski *et al.* (1995) that the true temperature dependence of ρ_D should exhibit a crossover from the T^2 dependence at low temperatures to a power-law at higher temperatures. However, the local field approach [or the Singwi-Tosi-Land-Sjölander method (Singwi *et al.*, 1968)] used in this work still fails to reproduce $\rho_D(T)$ measured in Sivan *et al.* (1992), although yields roughly the same magnitude of the effect (in contrast to the above RPA and generalized RPA calculations). This approach was further extended to drag between two 2DEG in Swierkowski *et al.* (1996, 1997). The results of that work suggest that many-body correlations enhance interlayer interaction and improve agreement with experiments. Nevertheless, experiments [see, e.g., Hill *et al.* (1997) and Fig. 11] show, that existing theoretical methods are still incapable of providing precise quantitative description of real systems.

A detailed consideration of Coulomb drag resistivity based on an extrapolation of Fermi-liquid-based formulas to the region where intralayer correlations are strong has been carried out by Hwang *et al.* (2003) in an attempt to address the striking data of Pillarisetty *et al.* (2002) in low density and high mobility hole bilayers. The observed drag was two to three orders of magnitude larger than previously reported values. The calculations of Hwang *et al.* (2003) were different from that leading to Eq. (21a) in several points, all of them leading to an increase of the drag resistivity: (i) Hubbard approximation was employed to obtain the polarization operator, which accounts for the exchange-driven local field corrections; (ii) experimentally measured dependence of conductivity on density was used to extract the electron-hole asymmetry factor; (iii) large-momentum transfer component was included to calculate drag; (iv) finite thickness of quantum wells was included to calculate form-factors of Coulomb matrix elements; (v) lastly, phonon contribution was added. Combining all these factors, Hwang *et al.* (2003) were able to account for most of the results of the measurements within a Fermi liquid approach.

G. Single-particle drag in magnetic field

The semiclassical Drude model described by Eqs.(2) predicts that the drag resistivity is independent of the magnetic field. Moreover, there is no “Hall drag”: the direction of the induced motion of charge carriers in the passive layer is expected to coincide with that of the driving current. These predictions contradict numerous experiments [see, e.g., Eisenstein and MacDonald (2004); Finck *et al.* (2010); Lilly *et al.* (1998); Muraki *et al.* (2004); Nandi *et al.* (2012); and Rubel *et al.* (1997b)] showing that Coulomb drag is not only sensitive to mag-

netic field, but in fact the drag resistivity can be greatly enhanced once the field is applied.

In single-layer measurements, magnetoresistance is usually associated with either (i) multi-band systems, or (ii) quantum effects. A close analog of the former can be found in graphene-based systems, see Gorbachev *et al.* (2012), Titov *et al.* (2013a) and Sec. IV. The latter effects are manifest in strong, quantizing magnetic fields leading to emergence of a qualitatively different behavior (Eisenstein and MacDonald, 2004; Girvin and MacDonald, 1997) discussed in Sec. VII.

The situation somewhat simplifies if the field is tuned close enough to the point where the Landau levels in the two layers are half-filled. In this case, the many-body state in each layer can be viewed as a Fermi liquid of composite fermions (Halperin *et al.*, 1993). Long range, interlayer interaction between these excitations can lead either to a “single-particle” drag effect (Kim and Millis, 1999; Sakhi, 1997; Ussishkin and Stern, 1997, 1998), or to novel correlated states, see Sec. VII. Alternative approaches include magnetodrag due to electron-phonon interaction (Badalyan and Kim, 2003), semiclassical theory (Brenner and Metzner, 2005), diagrammatic theory in high Landau levels (Bønsager *et al.*, 1996, 1997; Gornyi *et al.*, 2004; von Oppen *et al.*, 2001), self-consistent Hartree approximation (Tso *et al.*, 1998), and the effect of magnetoplasmons (Khaetskii and Nazarov, 1999; Manolescu and Tanatar, 2002).

1. Hall drag in weak (classical) magnetic field

Recall that the standard single-band Drude theory (2) does not allow for any dependence of the drag resistivity on the magnetic field and in particular predicts zero Hall drag, see Eq. (3d). The same conclusion can be reached using diagrammatic perturbation theory (Kamenev and Oreg, 1995). This result is justified by the assumption of energy-independent impurity scattering time τ . Lifting this assumption (Hu, 1997), one can show that a weak Hall drag signal may appear

$$\rho_D^H \propto sT^4, \quad s = \frac{\partial\tau(\epsilon)}{\partial\epsilon} \frac{E_F}{\tau(E_F)}. \quad (49)$$

As argued in Hu (1997), this effect is hard to observe in conventional semiconductor heterostructures where interlayer relaxation processes are dominated by electron-electron interaction: in this case the nonequilibrium distribution function quickly relaxes to a drifted Fermi-Dirac distribution and hence the impurity scattering time is effectively almost independent of energy, i.e. $s \ll 1$.

Hall drag in weak magnetic fields was studied in Patel *et al.* (1997). The experimental device comprised two 180Å-wide quantum wells separated by 100Å and exhibited measurable tunneling between the layers, contrary

to the assumptions of Hu (1997). Hall drag in graphene (Titov *et al.*, 2013a) was attributed to a different mechanism, see Sec. IV. Other observations of Hall drag were performed in the quantum Hall regime (see Sec. VII), where the effect is much stronger (von Oppen *et al.*, 2001) than Eq. (49).

2. Coulomb drag of composite fermions

All of the previous discussion was based on the underlying physical picture of weakly interacting fermions. Typically, this picture becomes invalid in a strong, quantizing magnetic field. The only exception to this statement is the peculiar state at the half-filled Landau level. This state can be described as a Fermi liquid of composite fermions (Halperin *et al.*, 1993). Each composite fermion is an electron with two attached flux quanta (Jain, 1989), that interacts with the others both electrostatically and by means of a Chern-Simons interaction.

Composite fermions can be characterized by linear response functions similar to those of electrons. In particular, their respective single-layer resistivities are related to each other by (Halperin *et al.*, 1993)

$$\hat{\rho}_{el} = \hat{\rho}_{cf} + \frac{2h}{e^2} \begin{pmatrix} 0 & 1 \\ -1 & 0 \end{pmatrix}. \quad (50)$$

If one is interested in the relation between conductivities of the electrons and composite fermions, then one has to invert the resistivity matrices in Eq. (50). Clearly, the electronic conductivity is not identical to that of the composite fermions.

Extending Eq. (50) to the case of a double-layer system, one obtains a similar relation for the 4×4 resistivity matrices (Ussishkin and Stern, 1997). If interlayer interaction is weak enough, so that composite fermions in a given layer are not sensitive to the Chern-Simons field of the other layer, then similarly to Eq. (50), longitudinal resistivities of the electrons and composite fermions are the same and hence

$$\rho_D^{el} = \rho_D^{cf}. \quad (51)$$

Again, conductivities (in particular, drag conductivities) of electrons and composite fermions are not equivalent.

The quantity measured in drag experiments is the electronic drag resistivity ρ_D^{el} , Eq. (13). Given the equality (51), one can calculate either ρ_D^{cf} or ρ_D^{el} . The former approach was developed in Kim and Millis (1999), while the latter was considered in Ussishkin and Stern (1997). Both calculations are based on the standard lowest-order perturbation theory and yield similar results (albeit with a rather different interpretation¹²). The calculation of

¹² The subquadratic temperature dependence (53) of the drag re-

Kim and Millis (1999) consists evaluating Eq. (15) for composite fermions and using the correspondence (51). Alternatively (Ussishkin and Stern, 1997), one can treat the problem in purely electronic terms assuming that interlayer interaction is dominated by the direct Coulomb coupling [the assumption which justifies Eq. (51)]. At the same time, single-layer electronic response functions (such as $\text{Im}\Pi^R$) can be calculated within the composite-fermion approach of Halperin *et al.* (1993).

Within RPA (including the response of composite fermions to the external, Coulomb, and Chern-Simons potentials) and in the limit $q \ll k_F$, $\omega \ll v_F q$, the electronic density-density response function (the polarization operator) is given by (Halperin *et al.*, 1993)

$$\Pi^R(\mathbf{q}, \omega) = \frac{dn}{d\mu} \frac{q^3}{q^3 - 8\pi i \omega k_F (dn/d\mu)}, \quad (52)$$

where $dn/d\mu$ is the thermodynamic compressibility of the $\nu = 1/2$ state. At large momenta, $\text{Im}\Pi^{-1} \propto q^{-3}$; consequently (Ussishkin and Stern, 1997), the momentum integration in Eq. (15) is dominated by the region $q \approx k_F (T/T_0)^{1/3}$ [i.e., determined by poles of the interlayer interaction, rather than Eq. (6)]. As a result, the temperature dependence of the drag resistivity is weaker than in the absence of magnetic field (Stern and Ussishkin, 1997; Ussishkin and Stern, 1997)

$$\rho_D = 0.825(h/e^2)(T/T_0)^{4/3}, \quad (53)$$

where the characteristic temperature depends on the carrier density n , interlayer spacing d , dielectric constant ϵ , and thermodynamic compressibility

$$T_0 = \frac{\pi e^2 n d}{\epsilon} \left[1 + \frac{\epsilon}{2\pi e^2 d} \left(\frac{dn}{d\mu} \right)^{-1} \right].$$

The same temperature dependence was reported in Kim and Millis (1999) and Sakhi (1997).

For realistic parameter values similar to those of the experiment of Lilly *et al.* (1998), the drag resistivity (53) is much larger than the zero-field result (21). This fact is associated with the smallness of the typical momenta involved in the interlayer scattering processes and slow relaxation of density fluctuations in the $\nu = 1/2$ state.

The effect of disorder on drag in the $\nu = 1/2$ state was considered in Stern and Ussishkin (1997). In the diffusive regime, the polarization operator is given by the standard form (30) and hence the drag resistivity is given by Eq. (34), albeit with a different diffusion coefficient than

sistivity at $\nu = 1/2$ was interpreted in Kim and Millis (1999) as a signature of the non-Fermi-Liquid nature of composite fermions. In particular it was related to the similar power law in the self-energy of the composite fermions leading to the $\omega \sim q^3$ scaling of the typical frequencies.

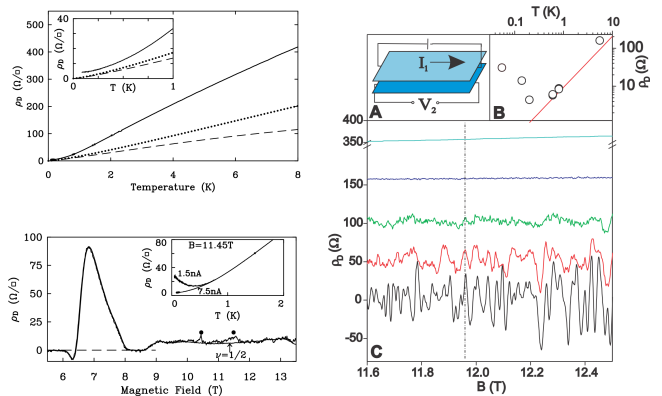


FIG. 12 (Color online) Coulomb drag measurements at $\nu = 1/2$. Left panel: the top plot shows the experimental $\rho_D(T)$ (solid line) compared to the theory of Stern and Ussishkin (1997); the bottom plot shows the field dependence. The inset shows ρ_D at $B = 11.45\text{T}$ for two values of the driving current. [Reproduced from Lilly *et al.* (1998).] Right panel: (A) circuit schematic; (B) $\rho_D(T)$ (dots) vs Eq. (53); (C) $\rho_D(B)$ for different temperatures, $T = 0.05 - 5.6\text{K}$. The vertical line corresponds to the B field at which the points plotted in panel (B) were measured. [Reproduced from Price *et al.* (2010).]

the same system would have in the absence of magnetic field. The result is much larger than at $B = 0$. In the diffusive regime, this follows from the observation that the longitudinal conductivity (or the diffusive constant, which encodes all microscopic details) at $\nu = 1/2$ is much smaller than at $B = 0$.

Although the above theory is qualitatively similar to the experimental observations (Lilly *et al.*, 1998) (e.g. drag at $\nu = 1/2$ is much larger than at $B = 0$; the temperature dependence in clean samples is subquadratic), theoretical calculations significantly underestimate the overall value of ρ_D as compared to the experiment of Lilly *et al.* (1998). Yang (1998) suggested, that the reason for the discrepancy is that the interlayer separation in the samples of Lilly *et al.* (1998) was close to the critical value, where the system forms an incompressible interlayer state (for a detailed discussion of correlated states see Sec. VII). An alternative suggestion by Ussishkin and Stern (1998) attributes the unexplained features of the experiment (including the extrapolated nonvanishing drag at $T = 0$) to pairing fluctuations of composite fermions. The two scenarios could be distinguished by measuring Hall drag, which vanishes in the latter theory. Finally, the anomalous temperature dependence shown in the inset of the lower left panel in Fig. 12 appears to be qualitatively similar to the effect of mesoscopic fluctuations of Coulomb drag, see Fig. 13. A later experiment (Price *et al.*, 2010) reported both the magnitude and temperature dependence of Eq. (53) to be in good agreement with the measured data.

III. MESOSCOPIC FLUCTUATIONS OF COULOMB DRAG

Universal conductance fluctuations (Altshuler *et al.*, 1991) is a quantum interference effect which is a manifestation of the wave nature of electrons. As the same electrons are responsible for Coulomb drag, it is natural to expect that the drag resistivity also exhibits mesoscopic fluctuations. The drag fluctuations were first studied theoretically in Narozhny and Aleiner (2000) and Mortensen *et al.* (2001, 2002a) and then observed experimentally (Kim *et al.*, 2011; Price *et al.*, 2008, 2007, 2010).

In a disordered system, it is impossible to track each individual impurity and one uses a statistical approach. Impurities are described by a distribution function and each physical quantity is treated as being random. Observables correspond to average values of the random physical quantities with respect to the distribution of impurities. If a system is large enough, it can be viewed as a combination of smaller parts, which become statistically independent if they are separated by distances larger than any relaxation length. Then instead of averaging over a statistical ensemble, one can average over the volume of one large system.

In the problem of electronic transport, averaging over the system volume can be understood as averaging over all possible paths that an electron can take moving between points A and B (Aleiner *et al.*, 1999; Altshuler and Aronov, 1985; Altshuler *et al.*, 1991). Such paths can cover all of the system volume and thus experience all possible local impurity configurations, making the average over the system equivalent to ensemble averaging.

Consider two paths between the points A and B. The total transmission probability is determined by the absolute value of the sum of the corresponding quantum amplitudes (Altshuler and Lee, 1988; Altshuler *et al.*, 1991):

$$W = |A_1 + A_2|^2 = |A_1|^2 + |A_2|^2 + 2|A_1||A_2|\cos(\varphi_1 - \varphi_2),$$

where $\varphi_{1(2)}$ are the quantum-mechanical phases that an electron accumulates along the paths. Typically, the phases $\varphi_{1(2)}$ are random (or incoherent). As a result, the interference term vanishes upon averaging over all possible paths (or impurity configurations), leading to the semiclassical sum of transition probabilities¹³

$$\langle \cos(\varphi_1 - \varphi_2) \rangle = 0 \Rightarrow W = W_1 + W_2, \quad W_{1(2)} = |A_{1(2)}|^2.$$

Random quantities can be characterized not only by their average value, but also by higher moments of their

statistical distribution, which may be sensitive to the interference term even if the phases $\varphi_{1(2)}$ are still random. Indeed, fluctuations of the transition probability

$$\langle [W - \langle W \rangle]^2 \rangle = 4W_1W_2\langle \cos^2(\varphi_1 - \varphi_2) \rangle = 2W_1W_2.$$

are completely determined by the interference term.

Fluctuations of the transmission probability result in fluctuations of transport coefficients. The effect of such fluctuations can be observed only in small enough samples (Altshuler *et al.*, 1991). Indeed, in order to justify the concept of the phase associated with a given electronic path, the length of the path should be less than a typical inelastic relaxation length L_φ , otherwise coherence would be lost before the electron reaches point B (Anderson *et al.*, 1979). At the same time, the path length should be larger than the mean free path in the system (otherwise electron motion along the path would be deterministic). Therefore, typical paths (and hence, the sample sizes) should be characterized by intermediate lengths L

$$\ell \ll L \ll L_\varphi.$$

Fluctuations observed at such length scales are known as “mesoscopic fluctuations” (Altshuler *et al.*, 1991).

A. Drag fluctuations in conventional diffusive samples

Mesoscopic fluctuations of the usual conductance (Altshuler *et al.*, 1991) are known as the “universal conductance fluctuations” (UCF). The universality is manifest when $T \ll E_T$, where E_T is the Thouless energy of the sample (i.e. in small samples or at low temperatures; in the diffusive regime, $E_T = D/L^2 = g/(2\pi\nu L^2)$, with g being the dimensionless conductance and ν – the DoS). Then the fluctuations are characterized by the universal value

$$\delta\sigma \simeq \frac{e^2}{h}, \quad \langle \delta G^2 \rangle \approx \frac{e^4}{h^2}, \quad \sqrt{\frac{\langle \delta G^2 \rangle}{\langle G \rangle^2}} \simeq \frac{1}{g(L)}, \quad (54)$$

where $G = ge^2/h$ is the conductance of the system. The latter equality emphasizes the fact that the dimensionless conductance is a function of the system size.

In larger samples, $\langle \delta G^2 \rangle$ is a function of temperature and the sample size. Arguments leading to Eq. (54) are valid only for coherent samples (Altshuler *et al.*, 1991). At larger length scales, $L \gg L_\varphi$ the coherence is lost, and the disorder averaging should be performed by dividing the sample into patches of the size L_φ . Individual self-coherent patches (54) can be combined as a network of random conductors. This yields (in dimension d)

$$\langle \delta G^2(L) \rangle \simeq \langle \delta G^2(L_\varphi) \rangle (L_\varphi/L)^d. \quad (55)$$

The patches of the size L_φ remain self-coherent as long as $T \ll E_T(L_\varphi)$. At higher temperatures, thermal averaging should be performed up to energies of order T ,

¹³ In special cases of coherent paths (for instance, time-reversed paths) the phase difference is exactly zero. Then the interference term does not vanish and leads to quantum corrections to semiclassical transport properties, such as the weak localization correction (Altshuler and Aronov, 1985; Altshuler *et al.*, 1991).

suppressing the conductance fluctuations

$$\langle \delta G^2(L_\varphi) \rangle \simeq (e^2/h)^2 E_T(L_\varphi)/T.$$

The conductance fluctuations of the sample become

$$\langle \delta G^2[L; T > E_T(L_\varphi)] \rangle \simeq (e^2/h)^2 (L_\varphi/L)^d \hbar / (T\tau_\varphi), \quad (56)$$

where $\tau_\varphi = E_T^{-1}(L_\varphi)$ is the dephasing time (Altshuler *et al.*, 1980).

The fluctuations (56) are only observable in mesoscopic samples. Assuming the samples to be “metallic”, $g \gg 1$, the UCF (54) yield only a small correction to the average value of conductance. For example, in the experiment of Price *et al.* (2007) the single-layer resistance fluctuates by about 200m Ω around the average of about 500 Ω .

Now, we apply the above arguments to Coulomb drag (Narozhny and Aleiner, 2000). The drag conductivity depends on (i) the phase space available to electron-hole excitations; (ii) matrix elements of the interlayer interaction; and (iii) electron-hole asymmetry, expressed through the energy dependence of the density of states (or, the density dependence of the single-layer Drude conductivity). This can be schematically summarized by

$$\sigma_D \simeq \frac{e^2}{\hbar} \left(\frac{\partial}{\partial \mu} \ln g \right)^2 \times \left(\frac{\text{phase}}{\text{volume}} \right) \times \left(\frac{\text{matrix}}{\text{element}} \right). \quad (57)$$

The average drag conductivity [cf. Eqs. (34) and (35)] can then be understood (up to the logarithmic factor) by estimating the phase volume by T^2 , the matrix element by $(\kappa d)^{-2}$ (coming from static screening), and the factor of the electron-hole asymmetry by E_F^{-2} .

Fluctuations of the drag conductivity can also be estimated with the help of Eq. (57). Consider first the lowest temperatures $T \ll E_T$, where the sample is effectively zero-dimensional (0D). The phase space is then only limited by temperature, yielding the usual factor of T^2 . The factor of the electron-hole asymmetry in Eq. (57) is a random quantity with the typical value $\sim E_T^{-2}$, since the Thouless energy is the typical scale of mesoscopic effects. Interaction matrix elements in 0D are independent of energy (Aleiner *et al.*, 1999); fluctuations are determined by off-diagonal elements that contain a small factor of g^{-2} . As a result, one finds the variance of the drag conductivity that strongly exceeds the average

$$\delta\sigma_D \sim \frac{e^2}{\hbar} \frac{T^2}{g^2 E_T^2}, \quad \frac{\sqrt{\langle \delta\sigma_D^2 \rangle}}{\langle \sigma_D \rangle} \simeq \frac{E_F^2}{g^2 E_T^2} \simeq \frac{L^4}{\ell^4} \gg 1. \quad (58)$$

The quadratic temperature dependence of the variance of the drag conductivity (Narozhny and Aleiner, 2000) for mesoscopic samples ($L \ll L_\varphi$, $T \ll E_T$) was also obtained in the context of quantum circuits [see Sec. V and Levchenko and Kamenev (2008a)] and within the random matrix theory (Mortensen *et al.*, 2001, 2002b).

In order to extend the 0D argument to larger samples, $L \gg L_\varphi$, we again divide the system into patches of the size L_φ . Since the patches are largely uncorrelated (due to the loss of phase coherence), they can be combined as a network of random conductors, see Eq. (55). Each patch can be analyzed similarly to the 0D case. However, now the interaction matrix elements become energy-dependent on the scales larger than E_T , decreasing with the transmitted energy ω as $|M|^2 \sim \omega^{-2}$. Thus the energy transfer is limited by the Thouless energy of the patch $\omega \sim E_T(L_\varphi) = \tau_\varphi^{-1}$, rather than temperature. As a result, the phase space is limited by $T\tau_\varphi^{-1}$, rather than the usual T^2 . The fluctuations of the density of states (which determine the factor of electron-hole asymmetry) should now be calculated on the scale of temperature rather than the Thouless energy. This suppresses the fluctuations in each layer by the factor of $\sqrt{E_T(L_\varphi)}/T$. Combining the above estimates, we find

$$\delta\sigma_D(L_\varphi) \sim \frac{e^2}{\hbar} \frac{T\tau_\varphi^{-1}}{g^2 E_T^2(L_\varphi)} \frac{E_T(L_\varphi)}{T} \sim \frac{e^2}{\hbar g^2}, \quad (59)$$

which is T -independent, in contrast to the 0D result (58).

Final the Coulomb drag fluctuations in 2D samples can be estimated by combining Eqs. (55) and (59):

$$\langle \delta\sigma_D^2(L) \rangle \sim \frac{e^4}{\hbar^2 g^4} \frac{L_\varphi^2}{L^2} \sim \frac{e^4}{\hbar^2 g^4} E_T(L) \tau_\varphi \propto \frac{1}{T}. \quad (60)$$

The temperature dependence of the fluctuations (60) is contained in the dephasing time $\tau_\varphi \sim g/T$ (Altshuler and Aronov, 1985). At high enough temperatures, $T \gg T^*$, the fluctuations are small [the average value of σ_D (35) is representative], but for $T \ll T^*$ fluctuations dominate, see Fig. 13. The crossover temperature T^* can be found by setting the relative fluctuation to unity

$$T^* \sim E_F (g^2 n L^2)^{-1/5}.$$

The fluctuation-dominated regime is characterized by typical values of σ_D determined by Eq. (60) rather than the average. In particular, the temperature dependence of the measured drag conductivity in this regime appears almost saturating as $\sigma_D \propto 1/\sqrt{T}$. The value of the prefactor in this expression is sample-dependent and has a random sign. If temperature is decreased further, then eventually (although probably only in theory) one may reach the regime where $T < E_T$. Then the sample will become effectively zero-dimensional and the quadratic temperature dependence $\sigma_D \propto T^2$ will be restored. In this regime of lowest temperatures, fluctuations greatly exceed the average [see Eq. (58)] and therefore the coefficient in the quadratic temperature dependence will be random (with random sign). The temperature dependence of a typical drag signal is sketched in the left panel of Fig. 13 (cf. the inset in the right panel of Fig. 13; see also the inset in the lower left panel of Fig. 12 and the discussion of the data of Lilly *et al.* (1998) in Sec. III.C).

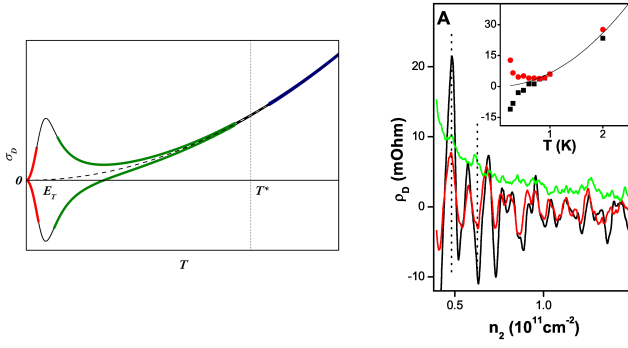


FIG. 13 (Color online) Left: Qualitative picture of the typical measured drag signal. At high enough temperatures $T > T^*$ the average drag conductivity (35) is representative, $\sigma_D \propto T^2$, with positive coefficient (blue curve). Below T^* (left of the dotted line), fluctuations dominate and the sign of the measured signal becomes random, i.e. dependent on a particular configuration of disorder. For $T < T^*$ the temperature dependence weakens to $\sigma_D \propto 1/\sqrt{T}$ (the corresponding transition region is shown in green). At very low (most likely, experimentally inaccessible) temperatures $T < E_T \ll T^*$, the quadratic temperature dependence is restored, but with a random coefficient (red curves), as fluctuations in the effectively 0D system are much stronger than the average, see Eq. (58). Right: Measured drag resistance as a function of carrier density in the passive layer for $T = 1, 0.4, 0.24\text{K}$ (from top to bottom). Inset: the temperature dependence of the same data for the two values of n_2 denoted by vertical dotted lines in the main plot. The line indicates the T^2 dependence. [From Price *et al.* (2007). Reprinted with permission from AAAS.]

The above qualitative picture is in full agreement with microscopic calculations (Narozhny and Aleiner, 2000). The average square of the drag conductivity has the form

$$\langle \sigma_D^{\alpha\beta} \sigma_D^{\alpha'\beta'} \rangle = \left(\delta^{\alpha\alpha'} \delta^{\beta\beta'} + \delta^{\alpha\beta'} \delta^{\alpha'\beta} \right) \langle \sigma_D^2 \rangle, \quad (61a)$$

$$\langle \sigma_D^2 \rangle = \frac{e^4}{\hbar^2} \frac{\gamma}{18\pi^3} \left(\frac{32 \ln 2 - 14}{3} \right) \frac{E_T \tau_\varphi \ln \varkappa d}{g^4 (\varkappa d)^3}, \quad (61b)$$

where $\gamma = 1.0086$. Comparing Eq. (61) with the average drag conductivity in the diffusive regime (35), one finds the cross-over temperature $T^* = E_F (16\pi g^2 n L^2)^{-1/5}$.

For heterostructures used in Gramila *et al.* (1991) and Lilly *et al.* (1998), the value of T^* can be estimated as $T^* \approx 0.2\text{K}$, which is below the temperature range of these experiments. Hence, the average drag coefficients (34) and (35) were sufficient to account for the observed effect with no trace of the random sign predicted by Eqs. (61).

More recently, drag fluctuations were observed in diffusive graphene-based double-layer samples (Kim *et al.*, 2011; Kim and Tutuc, 2012), see Fig. 14. The temperature dependence $\delta\sigma_D \propto T^{-1/2}$ [following from Eq. (61) and the assumption that the main phase-breaking mechanism in the device is electron-electron scattering (Altshuler and Aronov, 1985)] appears to be in agreement

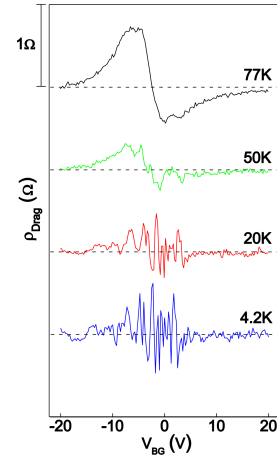


FIG. 14 (Color online) Mesoscopic fluctuations of Coulomb drag in graphene. At low temperatures the fluctuations fully obscure the average drag. The curves are shifted for clarity; the horizontal dashed lines indicate 0Ω for each curve. [Reproduced from Kim *et al.* (2011).]

with the experimental data. Other aspects of this experiments are specific to graphene. The fluctuations appear to be more pronounced in the vicinity of the charge neutrality point. However, at the time of writing, a theory of drag fluctuations in graphene has not been developed. There is also no explanation for the most puzzling feature of the data reported in Kim and Tutuc (2012) showing an apparent violation of Onsager reciprocity as the drag fluctuations depend only on the charge density in the passive layer and not in the active layer.

The result (61) is valid for homogeneous 2D diffusive samples in the absence of magnetic field. The randomness (i.e. the sample to sample variation) of the sign of the effect should be contrasted with the deterministic sign change of the drag resistivity suggested for bilayer systems with in-plane periodic potential modulation (Alkauskas *et al.*, 2002). Drag signals of both signs have been observed in vertically integrated 1D quantum wires (Laroche *et al.*, 2011). While the observed effect has been argued (Büttiker and Sánchez, 2011) to have a mesoscopic origin (Mortensen *et al.*, 2001) dominated by charge fluctuations (Levchenko and Kamenev, 2008a; Sánchez *et al.*, 2010), the data appear to be not random, but reproducible. Very similar data were obtained in the subsequent experiment (Laroche *et al.*, 2014) and interpreted with the help of the Luttinger Liquid theory (Pustilnik *et al.*, 2003) (see Sec. VI).

Closing this Section, we note that strong fluctuations of Coulomb drag ultimately follow from strong fluctuations of the nonlinear susceptibility. The fact that the fluctuations of the drag resistivity exceed the average is related to the overall smallness of the drag effect due to electron-hole symmetry. A related phenomenon is the fluctuations of the electro-acoustic current⁷ determined

by the same nonlinear susceptibility.

B. Giant fluctuations of Coulomb drag

The predictions of the fluctuation theory (Narozhny and Aleiner, 2000) were put to the test in the dedicated experiment (Price *et al.*, 2007). Both the UCF and drag fluctuations were measured in the same structure. The observed UCF have shown the usual behavior (Altshuler *et al.*, 1991). A direct comparison of the correlation fields for the UCF and drag fluctuations confirmed that both effects depend on the same coherence length L_φ (Aleiner *et al.*, 1999) and have the same quantum origin. Surprisingly, the observed giant drag fluctuations (Price *et al.*, 2007) greatly exceeded the original prediction (Narozhny and Aleiner, 2000). This discrepancy was attributed to the fact that the experiment was performed in the ballistic regime (Narozhny *et al.*, 2002; Zala *et al.*, 2001).

Let us remind the reader (see Sec. II) that the in drag measurements difference between “diffusive” and “ballistic” samples is in the relation between the mean-free path ℓ and interlayer separation d . The latter sets the upper limit for the interlayer momentum transfer due to the exponential decay of the Coulomb interaction (5). Thus, if the mean free path is small $\ell \ll d$, then $q \ll d^{-1} \ll \ell^{-1}$ and the effect is dominated by the diffusive motion of charge carriers. In “cleaner” samples with $\ell \gg d$, both small $q \ll \ell^{-1}$ and large $\ell^{-1} \ll q \ll d^{-1}$ momentum transfers are possible. The conventional statement, that in such samples Coulomb drag is dominated by ballistically moving carriers (Kamenev and Oreg, 1995), follows from observing that processes with large momentum transfers yield a much larger drag resistivity Eq. (21) compared with the diffusive result (34), see Eq. (36).

Coherence properties of electrons are also sensitive to the nature of their motion. The dephasing time τ_φ is a manifestation of inelastic electron-electron scattering (Aleiner *et al.*, 1999; Altshuler and Aronov, 1985). The conventional theory of interaction effects in electronic systems (Altshuler and Aronov, 1985) yields the following estimate for the dephasing time in diffusive systems

$$\tau_\varphi^{-1}(T\tau \ll 1) \sim (T \ln g)/g. \quad (62a)$$

At higher temperatures, transport is dominated by processes with one or few successive impurity scatterings. In this “ballistic” regime (Zala *et al.*, 2001), the dephasing time exhibits somewhat stronger temperature dependence (Narozhny *et al.*, 2002)

$$\tau_\varphi^{-1}(T\tau \gg 1) \sim (T^2/E_F) \ln(2E_F/T). \quad (62b)$$

In Eqs. (62a) and (62b) the parameter distinguishing the diffusive and ballistic regimes is $T\tau$ which is independent of the interlayer separation. This is to be expected since

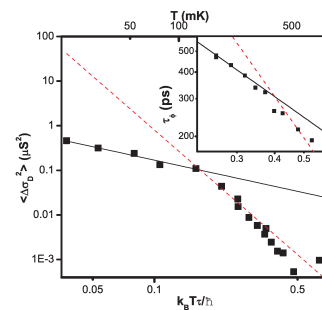


FIG. 15 Drag fluctuations in ballistic samples. The lines represent the asymptotic power laws, see Eq. (63). The inset shows the measured dephasing time. The lines in the inset represent the power laws from Eq. (62). [Adapted from Price *et al.* (2007). Reprinted with permission from AAAS.]

the theory leading to Eqs. (62a) and (62b) was devoted to two-dimensional systems and not bilayers.

The effect of the external magnetic field on the single-layer conductance fluctuations analyzed in Price *et al.* (2007) demonstrates the expected crossover between the ballistic and diffusive results :

$$\tau_\varphi^{-1} \propto \begin{cases} T, & T\tau \lesssim 1, \\ T^2, & T\tau \gtrsim 1. \end{cases} \quad (62c)$$

The same sample where Coulomb drag is dominated by the ballistic motion of electrons with large interlayer momentum transfers, $\ell^{-1} \ll q \ll d^{-1}$, may exhibit *both* the diffusive and ballistic behavior of single-layer transport properties, e.g. of the dephasing time (62).

Similar crossover was observed also in the drag fluctuations that exhibited strikingly different temperature dependence at large and small $T\tau$ (Price *et al.*, 2007):

$$\langle \delta\sigma_D^2 \rangle \propto \begin{cases} T^{-1}, & T\tau \lesssim 1, \\ T^{-4}, & T\tau \gtrsim 1. \end{cases} \quad (63)$$

The crossover temperature in Eq. (63) was found to be about the same as in Eq. (62). This coincidence raised the question of whether the large magnitude of the observed drag fluctuations and their unexpected temperature dependence (63) had the same origin that would involve large momentum transfers $\ell^{-1} \ll q \ll d^{-1}$ [given that the small momentum transfers lead to Eq. (61)].

Scattering processes characterized by large momentum transfers $q \gg 1/\ell$ involve two electrons at a distance that is smaller than the average impurity separation. Thus, the effect should be determined by *local* electron properties. Local properties, such as the local DoS, are known to exhibit mesoscopic fluctuations stronger than those of the global properties (responsible for drag fluctuations in the diffusive regime). In particular, fluctuations of the local DoS are given by (Lerner, 1988)

$$\delta\nu^2 \sim (\nu^2/g) \ln[\max(L_T, L_\varphi)/\ell], \quad (64)$$

where $L_T = \sqrt{D/T}$ is the thermal length.

Contribution of processes with large momentum transfers to drag fluctuations can be estimated using Eqs. (57) and (55). Electron-electron scattering can be described with the help of “ballistic” expressions discussed in Sec. II.B. As small angle scattering plays the dominant role, the matrix element of the interlayer interaction is proportional to the ratio of the mean-free path to the interlayer separation $|M|^2 \sim g^{-2}\ell^2/(\varkappa^2 d^4)$. As this interaction is static, the phase space is only limited by T . Assuming that the fluctuations of the nonlinear susceptibility are dominated by fluctuations of the local density of states (64), one finds (up to a logarithmic factor)

$$\delta\sigma_D(L_\varphi) \sim \frac{e^2}{\hbar} \frac{T}{gE_T(L_\varphi)} \frac{\ell^2}{\varkappa^2 d^4}, \quad (65)$$

where the thermal smearing was taken into account similarly to Eq. (59). This leads to the estimate for the drag fluctuations in the whole sample (Price *et al.*, 2007)

$$\langle \delta\sigma_D^2 \rangle \sim \frac{e^4}{\hbar^2} \frac{\ell^4}{g^2 \varkappa^4 d^8} \frac{T^2}{E_T^2(L_\varphi)} \frac{L_\varphi^2}{L^2} \propto T^2 \tau_\varphi^3. \quad (66)$$

The result (66) contains two falsifiable predictions: (i) the magnitude and (ii) the temperature dependence of the drag fluctuations. In comparison with Eq. (61), the prefactor in Eq. (65) contains the large factor ℓ^4/d^4 and moreover, g^2 instead of g^4 in the denominator. Consequently, the drag fluctuations (66) are much stronger than the diffusive prediction. At the same time, using the temperature dependence of the dephasing time (62), one immediately recovers the measured temperature dependence of the drag coefficient (63). The crossover between the two temperature regimes in Eqs. (63) and (66) is illustrated in Fig. 15.

C. Drag fluctuations at the half-filled Landau level

Mesoscopic fluctuations of Coulomb drag of composite fermions were studied theoretically in Narozhny *et al.* (2001) and experimentally in Price *et al.* (2010). Despite the significant increase in the magnitude of drag of composite fermions relative to that of normal electrons (Jörger *et al.*, 2000c; Lilly *et al.*, 1998; Muraki *et al.*, 2004; Zelakiewicz *et al.*, 2000) the fluctuations of the drag resistivity can still exceed the average, resulting in an alternating sign of the measured drag resistivity.

Qualitatively, one can estimate the fluctuation effects using Eq. (25). Similarly to the $B = 0$ case, drag fluctuations stem from the fluctuations of the nonlinear susceptibility. In the diffusive regime, $\langle \Gamma \rangle$ is given by Eq. (28) with the polarization operator having the standard form (30), although with a different diffusion constant (Stern and Ussishkin, 1997). In contrast to the $B = 0$ case, the $\nu = 1/2$ state is characterized by a large Hall conductivity. This leads to the nonlinear susceptibility being approximately orthogonal to the transferred momentum \mathbf{q} [unlike Eq. (31)].

Fluctuations of Γ (and thus of the drag resistivity) result from mesoscopic fluctuations of $\partial\sigma/\partial n$. Other parameters, such as the compressibility and the diffusion constant can be taken at their average values (their fluctuations are much smaller than the averages). To estimate fluctuations of $\partial\sigma/\partial n$, one can express the conductivity in terms of the response functions of composite fermions using Eq. (50). On average, the conductivity matrix of composite fermions is diagonal. Assuming the large dimensionless conductance of composite fermions, $g_{cf} \gg 1$, the electronic longitudinal conductivity is inversely proportional to g_{cf} , meaning *smallness* of the electronic dimensionless conductance

$$g \approx 1/(4g_{cf}) \ll 1. \quad (67)$$

This is the reason one needs to perform calculations in the composite-fermion basis: the $B = 0$ theory of Sec. III.A is justified by the small parameter $1/g$.

Adapting the $B = 0$ theory to the case of composite fermions, Narozhny *et al.* (2001) found the fluctuations of the nonlinear susceptibility (28) of a coherent sample of size L in the $\nu = 1/2$ state to be large

$$\delta\Gamma \sim iq \frac{e}{\hbar} \frac{L^2}{g_{cf}^2} \text{Im}\Pi^R, \quad \frac{\langle \delta\Gamma^2 \rangle}{\langle \Gamma \rangle^2} \sim \frac{k_F^4 L^4}{g_{cf}^4} \gg 1, \quad (68)$$

similarly to Eq. (58). This is already an observable conclusion: in a fully coherent sample in the diffusive regime, fluctuations of the acoustoelectric current (determined by the same nonlinear susceptibility) are much larger than its average. The result (68) is justified as long as the thermal $L_T^{cf} \equiv \sqrt{\hbar D^{cf}/T}$ and phase breaking L_φ^{cf} length scales of composite fermions are much larger than L .

For larger samples, the global phase coherence is lost and one has to employ the averaging procedure described in Sec. III.A. The system can be divided into $L^2/(L_\varphi^{cf})^2$ self-coherent patches of the size of the phase-breaking length of composite fermions L_φ^{cf} . Summing up contributions of all patches according to Eq. (55), one finds

$$\langle \rho_D^2 \rangle = \frac{\hbar^2}{e^4} \frac{1}{g_{cf}^4 (\kappa d)^2} \left(\frac{L_\varphi^{cf}}{L} \right)^2 \min \left[1, \alpha_1 \left(\frac{g_{cf}^2 T \tau_\varphi^{cf}}{\kappa d \hbar} \right)^2 \right] \min \left[\alpha_3, \alpha_2 (T \tau_\varphi^{cf} / \hbar)^2 \right], \quad (69)$$

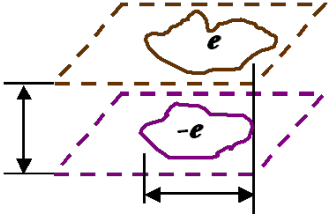


FIG. 16 (Color online) A cartoon illustration of the phase-breaking mechanism at $\nu = 1/2$. A random flux in the system can be generated by charge density fluctuations with the opposite signs of excess local charges in the two layers.

where $\alpha_3 \approx 0.2(32/9\pi) = 0.23$ and the coefficients $\alpha_{1,2}$ are of order unity (Narozhny *et al.*, 2001).

The magnitude of the mesoscopic fluctuations depends on the precise source of phase breaking, but their temperature dependence is robust: all generic models of phase breaking in two dimensions (Altshuler and Aronov, 1985) lead to $1/\tau_\varphi \propto T$ in the diffusive regime. In the $\nu = 1/2$ state phase breaking comes from the *quasi-elastic* scattering of composite fermions off the thermal quasi-static fluctuations of the Chern-Simons magnetic field. This mechanism can be illustrated using a cartoon shown in Fig. 16. Consider a density fluctuation where the excess charges in the two layers have opposite signs. Such a fluctuation is accompanied by a random flux that interacts with the composite fermions leading to the loss of coherence. The energy of this fluctuation is of order T . It can also be estimated as the energy of a simple capacitor, $2\pi e^2 d / [\varepsilon (L_\varphi^{cf})^2] \simeq T$, where ε is the bulk dielectric constant and L_φ^{cf} is the typical size of the density fluctuation with the electron number of the order of unity creating the random flux of approximately Φ_0 . As a result,

$$1/\tau_\varphi^{cf} \simeq g_{cf} T / (\varkappa d). \quad (70)$$

Substituting the above estimate into Eq. (69), one finds (assuming $g^{cf} \gg \varkappa d$)

$$\langle \rho_D^2 \rangle \simeq \frac{\hbar^2}{e^4} \frac{2\pi e^2 d}{T \varepsilon L^2 g_{cf}^6}.$$

Using realistic parameters (Lilly *et al.*, 1998) (i.e. $L \simeq 100\mu\text{m}$; $d = 300\text{\AA}$; $T = 0.6\text{K}$; $R = 3k\Omega/\square$ leading to $g_{cf} \approx 8$; and $\langle \rho_D \rangle = 15\Omega/\square$), the magnitude of the drag fluctuations can be estimated as $\delta\rho_D \approx 0.3\Omega$, which is much smaller than the experimental data of Lilly *et al.* (1998), see the lower left panel of Fig. 12. That experiment remains poorly understood. For lower temperatures and smaller samples, the theory predicts stronger fluctuations (i.e. exceeding the average). Such strong fluctuations were observed in Price *et al.* (2010), albeit again with a substantially larger magnitude that follows from the above estimate, see Fig. 17.

The dephasing time due to above mechanism of quasi-elastic scattering of composite fermions on thermal fluctuations

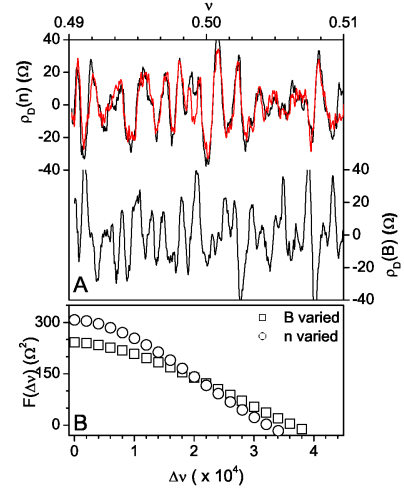


FIG. 17 (Color online) Mesoscopic fluctuations of Coulomb drag at $\nu = 1/2$, $T = 50\text{mK}$. Upper panel: comparison of $\delta\rho_D$ as a function of the filling fraction ν obtained by varying either the carrier density or magnetic field. The red curve shows a different measurement run demonstrating the reproducibility of the fluctuations. Similarity of the periods of $\rho_D(n)$ and $\rho_D(B)$ is the proof of composite-fermion drag. Lower panel: autocorrelation function of the fluctuations shown in the upper panel. Squares represent $\rho_D(B)$ and circles - $\rho_D(n)$. [Reproduced from Price *et al.* (2010).]

tuations of the Chern-Simons field appears to be shorter than the temperature scale $T\tau_\varphi^{cf} \ll 1$. This does not create any additional complication since most of the phase breaking results from scattering off the Chern-Simons field fluctuations whose dynamics (with characteristic frequency T/g_{cf}) is very slow compared to τ_φ^{cf} , but fast compared to the time of the experiment. Field fluctuations which are static on the scale of the experiment time affect the mesoscopic fluctuations only by affecting g_{cf} . Field fluctuations that are faster than that scale make the potential landscape seen by the composite fermions time dependent, and lead to a suppression of the mesoscopic fluctuations by partial ensemble averaging.

Consider the correlation function

$$\langle \rho_D(B)\rho_D(B+\delta B) \rangle - \langle \rho_D(B) \rangle \langle \rho_D(B+\delta B) \rangle = F_1 \left(\frac{\delta B}{B^*} \right),$$

with the field B near the $\nu = 1/2$ value. An experimental study of the decay of this correlation function is a way to measure L_φ^{cf} : the characteristic magnetic field of the decay is $B^* \sim (L_\varphi^{cf})^{-2} \Phi_0$. The decay of this correlator as a function of density

$$\langle \rho_D(n)\rho_D(n+\delta n) \rangle - \langle \rho_D(n) \rangle \langle \rho_D(n+\delta n) \rangle = F_2 \left(\frac{\delta n}{n^*} \right).$$

also yields L_φ^{cf} : the characteristic density change n^* at which it decays is expected to correspond to half of an

electron in a phase coherent region, i.e. $n^* = (L_\varphi^{cf})^{-2} / 2$. This statement holds as long as the composite fermion cyclotron radius is much larger than its mean free path, i.e., for $|\nu - 1/2| < (2g_{cf})^{-1}$.

The ratio of the above characteristic field B^* to the characteristic density n^* yields two flux quanta

$$\frac{B^*}{n^*} \simeq 2\Phi_0. \quad (71)$$

This should be contrasted to the zero field case, where

$$B^* \rightarrow \frac{\Phi_0}{L_\varphi^2}, \quad n^* \rightarrow \frac{k_F \ell}{L_\varphi^2} \Rightarrow \frac{B^*}{n^*} \simeq \frac{\Phi_0}{g}.$$

At $B = 0$ the electrons do not carry any attached flux. Therefore the characteristic density n^* corresponds to a change in the chemical potential of order τ_φ^{-1} . Consequently, observation of the ratio (71) in a laboratory experiment serves as a verification of the concept of the flux attachment and the fact that charge carriers in the system are indeed composite fermions.

In single-layer measurements of mesoscopic fluctuations, the ratio (71) has been reported in Kvon *et al.* (1997). In double-layer systems, mesoscopic fluctuations of Coulomb drag were investigated in Price *et al.* (2010), where it was shown, that the fluctuations of drag resistivity obtained either by varying of the magnetic field (with $n = \text{const}$) or by varying the carrier density (holding B constant) exhibit the same characteristic scale (or a “period”), if plotted as a function of the filling factor $\nu = nh/eB$, see Fig. 17. The similarity of the two “periods” is equivalent to the ratio (71).

IV. DRAG IN GRAPHENE-BASED DOUBLE-LAYER DEVICES

The physical picture of frictional drag outlined in the preceding Sections is based on the following assumptions: (i) each of the layers is in a Fermi-liquid state, which at the very least means $\mu_{1(2)} \gg T$; (ii) electron-electron interaction does not contribute to the intralayer transport scattering time; (iii) the interlayer Coulomb interaction is assumed to be weak enough, $\alpha = e^2/v_F \ll 1$, such that ρ_D is determined by the lowest-order perturbation theory (Flensberg and Hu, 1994; Flensberg *et al.*, 1995; Jauho and Smith, 1993; Kamenev and Oreg, 1995; Zheng and MacDonald, 1993) leading to Eq. (15). Most of the experiments in semiconductor devices (Eisenstein, 1992; Rojo, 1999) were performed on samples with high carrier density, where $\mu_{1(2)} \gg T$ [with the notable exception of Pillarisetty *et al.* (2002)].

Lifting one or more of the above assumptions leads to significant changes in the drag effect. Recently drag measurements were performed in a system of two parallel graphene sheets (Gorbachev *et al.*, 2012; Kim *et al.*, 2011; Kim and Tutuc, 2012; Titov *et al.*, 2013a). This system

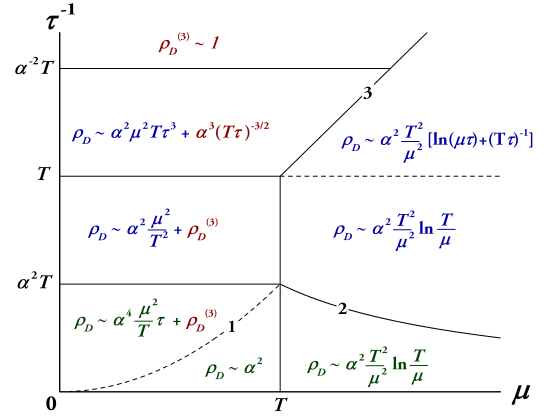


FIG. 18 (Color online) Summary of the parameter regimes and the resulting drag coefficient in graphene for identical layers, $\mu \ll \min(T/\alpha, v/d)$, and uncorrelated disorder. Bottom row (below the curve 2, $\tau^{-1} \ll \alpha^2 T^2/\mu$): solutions to the quantum kinetic equation, see Sec. IV.B. Curve 1 ($\tau^{-1} = \alpha^2 \mu^2/T$) separates the two regimes in Eq. (104). Middle row ($\alpha^2 T \ll \tau^{-1} \ll T$): the region where the QKE approach overlaps with the perturbation theory (Narozhny *et al.*, 2012). The third-order contribution $\rho_D^{(3)} = \mathcal{O}(\alpha^3)$ yielding nonzero drag at $\mu = 0$ is shown in red. Upper row ($\tau^{-1} \gg T$): the diffusive regime, where $\rho_D^{(3)}$ saturates for $\tau^{-1} \gg T/\alpha^2$. [Reproduced from Schütt *et al.* (2013).]

offers much greater flexibility compared to prior experiments in semiconductor heterostructures. The graphene-based system allows one to scan a wide range of chemical potentials (by electrostatically controlling carrier density) from the Fermi-liquid regime to the charge neutrality (or Dirac) point $\mu_i = 0$. Moreover, using hexagonal boron nitride as a substrate (Ponomarenko *et al.*, 2011; Titov *et al.*, 2013a), one can decrease disorder strength in the system and reach the regime, where transport properties of the two layers are dominated by electron-electron interaction, $\tau \gg \tau_{ee}$. In addition, modern technology allows for a controlled growth of boron nitride yielding devices with a relatively wide range of the interlayer separations, which can be as low as $d = 1\text{nm}$ (corresponding to only three atomic layers!). While the experiments (Gorbachev *et al.*, 2012; Kim *et al.*, 2011; Kim and Tutuc, 2012; Titov *et al.*, 2013a) were performed at relatively low temperatures $T < v_g/d$ (v_g is the quasiparticle velocity in graphene), the range of temperatures available for these measurements (typically, 4 – 240K) is much wider than in earlier studies. In a parallel development, Coulomb drag measurements in graphene double ribbon structures were reported in Chen and Appenzeller (2013).

In graphene one can reach parameter regimes, which were inaccessible in semiconductor samples, see Fig. 18: (i) near charge neutrality, the chemical potential may become smaller than temperature, $\mu_{1(2)} \ll T$; the electronic system becomes nondegenerate; (ii) low-energy excita-

tions in graphene are characterized by the linear Dirac-like dispersion; there is no Galilean invariance in the system and transport properties are strongly affected by electron-electron interaction (Katsnelson, 2012; Schütt *et al.*, 2011). Moreover, electrons interact by means of 3D nonrelativistic Coulomb interaction, which breaks the Lorenz invariance of the Dirac Hamiltonian.

Nondegenerate systems were considered in three early work on frictional drag (Boiko and Sirenko, 1988; Jacoboni and Price, 1988; Pogrebinskii, 1977; Price, 1983) in the context of semiconductors, where elementary excitations are typically modeled by quasiparticles with parabolic dispersion. In that case, electron-electron interaction plays a subleading role in single-layer transport (due to Galilean invariance). In contrast, in ultra-clean graphene near the Dirac point single-layer transport is dominated by electron-electron interaction (Narozhny *et al.*, 2012; Schütt *et al.*, 2011).

The low-temperature degenerate regime $T \ll \mu$ can be achieved by, e. g., electrostatically tuning the carrier density away from charge neutrality. In this case the system is expected to exhibit the same qualitative behavior as the semiconductor devices. Indeed, in ballistic samples and under the additional assumption of the small screening length $\kappa d \gg 1$, one recovers (Narozhny *et al.*, 2012; Tse *et al.*, 2007) the standard expression for the drag resistivity (21), albeit with an extra factor $N = 4$ reflecting higher degeneracy of the single-particle spectrum in graphene. However, this regime might be outside of the experimentally accessible parameter range of drag measurements in graphene-based samples (Gorbachev *et al.*, 2012; Kim *et al.*, 2011; Kim and Tutuc, 2012; Titov *et al.*, 2013a).

For weaker doping, the assumption of the small screening length is invalid and the standard result (21) has to be modified (Narozhny *et al.*, 2012). A perturbative treatment can still be developed as long as the transport properties of both layers are dominated by disorder (i.e., $\tau_{ee} \gg \tau$). If electron-electron interaction is weak enough

$$\alpha^2 T \tau \min(1, T/\mu_i) \ll 1, \quad (72)$$

then the drag conductivity is given by the standard expression (25). Close to the Dirac point ($\mu_i \ll T$), this yields $\rho_D \propto \mu_1 \mu_2$. At intermediate densities ($\mu \sim T$), the drag coefficient reaches a maximum and then decays to-

wards the asymptotic limit (21). This decay is characterized by a long crossover from the logarithmic behavior at $\mu_i > T$ to the standard result (21) that is only achieved for small screening lengths, $\kappa d \gg 1$. As a result, the density dependence of $\rho_D(\mu_i \gtrsim v_g/d)$ cannot be described by a power law. Partially due to this fact, several conflicting results for ρ_D have been reported in literature (Amorim and Peres, 2012; Carrega *et al.*, 2012; Hwang *et al.*, 2011; Katsnelson, 2011; Lux and Fritz, 2012; Peres *et al.*, 2011; Song and Levitov, 2012, 2013; Tse *et al.*, 2007).

A. Perturbative regime in ballistic samples

The perturbation theory is valid when transport properties of the sample are dominated by potential disorder, such that $\tau \ll \tau_{ee}$, see Eq. (72). In ballistic samples the mean-free path is large compared to the interlayer separation $\ell \gg d$. For experimentally relevant temperature range $T < v_g/d$, the latter condition is compatible with the more standard condition for ballistic transport in disordered systems $T\tau \gg 1$. The resulting parameter range occupies the middle row of the “phase diagram” shown in Fig. 18 between the line $T\tau \simeq 1$ and curve 2.

Perturbative calculations in the ballistic regime can be performed using either the diagrammatic (see Fig. 2), or kinetic-equation approach (see Sec. II.B). In both cases, one arrives at the expression similar to (15), where the nonlinear susceptibility and screened interlayer interaction (and hence the polarization operator) have to be specified for Dirac fermions in graphene.

1. Nonlinear susceptibility in graphene

In contrast to the theory reviewed in Sec. II, here we are interested in a wide range of chemical potentials including the Dirac point $\mu = 0$. The nonlinear susceptibility and polarization operator in graphene for arbitrary μ and T were derived in Narozhny *et al.* (2012). Assuming the long, energy-independent impurity scattering time τ and neglecting intralayer interaction, the nonlinear susceptibility has the form

$$\Gamma(\omega, \mathbf{q}) = -2 \frac{e\tau \mathbf{q}}{\pi} g\left(\frac{\omega}{2T}, \frac{v_g \mathbf{q}}{2T}; \frac{\mu}{T}\right), \quad (73)$$

where [with $W = \omega/(2T)$, $Q = v_g q/(2T)$, and $x = \mu/T$]

$$g(W, Q; x) = \begin{cases} \sqrt{\frac{W^2}{Q^2} - 1} \int_0^1 dz \frac{z\sqrt{1-z^2}}{z^2 - W^2/Q^2} I(z; W, Q; x), & |W| > Q \\ -\sqrt{1 - \frac{W^2}{Q^2}} \int_1^\infty dz \frac{z\sqrt{z^2-1}}{z^2 - W^2/Q^2} I(z; W, Q; x), & |W| < Q \end{cases}. \quad (74)$$

$$I(z; W, Q; x) = \tanh \frac{zQ + W + x}{2} - \tanh \frac{zQ + W - x}{2} + \tanh \frac{zQ - W - x}{2} - \tanh \frac{zQ - W + x}{2}. \quad (75)$$

Under the same assumptions, the polarization operator is given by

$$\begin{aligned} \Pi^R = \frac{q}{4\pi^2 v_g} \int_0^1 \int_0^1 \frac{dz_1 dz_2}{z_1 \sqrt{(1-z_1^2)(1-z_2^2)}} & \left[(z_1^{-2} - 1) \left(\frac{Q}{z_2 Q + W + i\eta} + \frac{Q}{z_2 Q - W - i\eta} \right) J_1(z_1^{-1}, z_2, x) \right. \\ & \left. + (1 - z_2^2) \left(\frac{Q}{z_1^{-1} Q + W + i\eta} + \frac{Q}{z_1^{-1} Q - W - i\eta} \right) J_2(z_1^{-1}, z_2, x) \right], \end{aligned} \quad (76a)$$

where

$$J_{1(2)}(z_1, z_2, x) = \tanh \frac{(z_1 + z_2)Q + x}{2} + \tanh \frac{(z_1 + z_2)Q - x}{2} \mp \tanh \frac{(z_1 - z_2)Q + x}{2} \mp \tanh \frac{(z_1 - z_2)Q - x}{2}. \quad (76b)$$

The perturbative calculation amounts to using the polarization operator (76) to determine the effective interlayer interaction (7) and then evaluating the drag conductivity [cf. Eqs. (15) and (25)] (Tse *et al.*, 2007)

$$\sigma_D^{\alpha\beta} = \frac{1}{16\pi T} \sum_{\mathbf{q}} \int d\omega \frac{|\mathcal{D}_{12}^R|^2}{\sinh^2 \frac{\omega}{2T}} \Gamma_1^\beta(\omega, \mathbf{q}) \Gamma_2^\alpha(\omega, \mathbf{q}), \quad (77)$$

using the nonlinear susceptibility (73). The drag resistivity is then given by Eq. (13). For arbitrary μ and T this calculation has to be performed numerically (Lux and Fritz, 2012; Peres *et al.*, 2011). At the same time, all qualitative features of the drag effect can be elucidated by using simple limiting values.

The nonlinear susceptibility (73) decays exponentially for $q \gg \max(\mu, T)$. In the vicinity of the Dirac point, $T \gg \mu$, the integral that determines the function $g(W, Q, x)$ cannot be evaluated in terms of elementary functions. It can be shown, however, that in this case the nonlinear susceptibility is proportional to μ/T (Narozhny *et al.*, 2012)

$$g(x \ll 1) \propto \mu/T, \quad (78)$$

which could be expected since drag is supposed to vanish – or, more precisely, to change sign – at the Dirac point.

In the degenerate limit $T \ll \mu$, the dimensionless function $g(W, Q, x)$ may be approximated by

$$g(x \gg 1, |W| < Q) \approx \frac{4W}{Q} \sqrt{1 - \frac{W^2}{Q^2}} \frac{\sinh x}{\cosh Q + \cosh x}. \quad (79)$$

Furthermore, for $\mu \gg v_F q \gg \omega \sim T$ (or $Q \gg W$) the nonlinear susceptibility becomes similar to the standard (Kamenev and Oreg, 1995) ‘‘Fermi-liquid’’ expression for the ballistic regime (17)

$$g(x \gg 1, |W| \ll Q) \approx 4\omega/(v_g q), \quad (80)$$

where the extra factor of 4 corresponds to extra degeneracy of Dirac fermions in graphene (Amorim and Peres, 2012; Tse *et al.*, 2007).

The relation (18) between $\mathbf{\Gamma}$ and $\text{Im}\Pi$ is not satisfied in graphene. This follows from a direct comparison between their respective integral representations. In particular, the nonlinear susceptibility (73) vanishes at the Dirac point due to exact electron-hole symmetry, $\mathbf{\Gamma}(\mu = 0) = 0$ (Tse *et al.*, 2007), while the polarization operator (76) remains finite, $\text{Im}\Pi(\mu = 0) \neq 0$ (Schütt *et al.*, 2011).

Similarly to the usual Lindhard function (Giuliani and Vignale, 2005; Lindhard, 1954), the polarization operator in doped graphene has the simple static limit

$$\Pi^R(\omega = T = 0) = 2k_F/(\pi v_g). \quad (81)$$

At the Dirac point, the result is somewhat different

$$\Pi^R(\mu = \omega = 0) = \begin{cases} q/(4v_g), & T \ll v_g q, \\ 4T \ln 2/(\pi v_g^2), & T \gg v_g q. \end{cases} \quad (82)$$

2. Lowest-order perturbation theory

We now use the above approximations to find the limiting expressions for the drag resistivity in the perturbative regime (Narozhny *et al.*, 2012).

In the simplest limit $N\alpha\mu \ll T$, the perturbative approach is justified automatically. In this case, the single-layer conductivity is determined by weak impurity scattering and has the form

$$\sigma_0 = e^2 T \tau h_0(\mu/T), \quad (83a)$$

where

$$h_0(x) = \frac{2}{\pi} \int_{-\infty}^{\infty} \frac{dz|z|}{\cosh^2(z + \frac{x}{2})} = \frac{2}{\pi} \begin{cases} x, & x \gg 1, \\ 2 \ln 2, & x \ll 1. \end{cases} \quad (83b)$$

In this limit screening is ineffective and for $\mu_i, T \ll v_g/d$ the interlayer spacing drops out of the problem. Then we may use the ‘‘bare’’ Coulomb potential (5), while the

frequency and momentum integration in Eq. (77) are determined by the nonlinear susceptibility (73).

Close to the double Dirac point, $\mu_i \ll T$, the nonlinear susceptibility can be approximated by Eq. (78), while the remaining integration is dominated by frequencies and momenta of order temperature, $\omega, v_g q \sim T$, yielding a dimensionless coefficient. The resulting drag resistivity is given by

$$\rho_D(\mu_i \ll T) \approx 1.41\alpha^2(\hbar/e^2)(\mu_1\mu_2/T^2). \quad (84a)$$

If only one of the layers is tuned close to the Dirac point, $\mu_1 \ll T \ll \mu_2$, the drag conductivity (77) is independent of the properties of the second layer, as the integration in Eq. (77) is still determined by the region $\omega, v_g q \sim T$. The single-layer conductivity in the second layer is still determined by μ_2 , see Eq. (83). As a result,

$$\rho_D(\mu_1 \ll T \ll \mu_2) \approx 5.8\alpha^2(\hbar/e^2)(\mu_1/\mu_2). \quad (84b)$$

In the opposite limit $\mu_i \gg T$, the nonlinear susceptibility is given by Eq. (79). Now the momentum integral in Eq. (77) is logarithmic and is dominated by large values of momentum $Q \gg W$. The ratio of the hyperbolic functions in Eq. (79) is similar to the step function: it's equal to unity for $Q \ll x$ and vanishes at larger values of momentum $Q \gg x$. Therefore x effectively acts as the upper cut-off and the momentum integral can be approximated by a logarithm

$$\int_W^\infty \frac{dQ}{Q} \frac{\sinh^2 x}{(\cosh Q + \cosh x)^2} \approx \ln \frac{x}{W}. \quad (84c)$$

Consequently the drag coefficient is similar to the standard results of Sec. II

$$\rho_D(\mu_2 > \mu_1 \gg T) \approx \alpha^2 \frac{\hbar}{e^2} \frac{8\pi^2}{3} \frac{T^2}{\mu_1\mu_2} \ln \frac{\mu_1}{T}. \quad (84d)$$

This is to be expected, since at low temperatures $T \ll \mu_i$ the phase-space argument yielding the T^2 dependence is justified and the electron-hole asymmetry determines the dependence on the chemical potential. The logarithmic factor is beyond such qualitative estimates (the result (84d) was calculated with logarithmic accuracy).

a. Static screening for vanishing interaction strength

For slightly stronger interaction (i.e. smaller dielectric permittivity of the insulating substrate) or slightly larger interlayer spacing the condition $N\alpha\mu_i \ll T, \mu_i \ll v_g/d$ breaks down and one needs to take into account static screening. Static screening corresponds to the approximation (81) to the polarization operator. If the interaction strength is still small $\alpha \rightarrow 0$, then the interaction can be described by

$$\mathcal{D}_{12}^R = -\frac{2\pi\alpha v_g^2}{v_g q + 2N\alpha\mu} e^{-qd}, \quad (85)$$

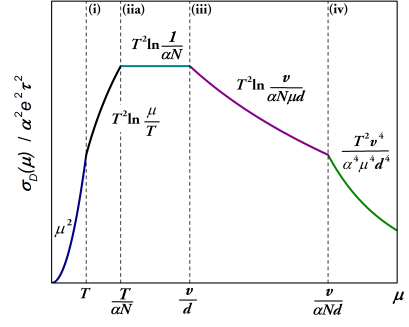


FIG. 19 (Color online) Sketch of the drag conductivity (in the units of $\alpha^2 e^2 \tau^2$; identical layers) as a function of the chemical potential illustrating the results (86). The blue line shows the quadratic dependence (84a) in the vicinity of the Dirac point. If $T \gg N\alpha v_g/d$, then the region (iia) should be replaced by (ii): the logarithmic dependence $T^2 \ln(1/\alpha)$ should be replaced by $T^2 \ln[v_g/(Td)]$, and the limits v_g/d and $T/(N\alpha)$ should be exchanged. [Reproduced from Narozhny *et al.* (2012).]

where $N = 4$ is due to spin and valley degeneracy. The additional constant in the denominator affects the logarithmic integral (84c). As the chemical potential is being increased away from the Dirac point, the following regimes may be gradually achieved [here we discuss these regimes for the case of identical layers; generalization to the case of two inequivalent layers is straightforward]:

(i) $N\alpha\mu \ll T \ll \mu \ll v_g/d$. This regime is identical to the above arguments leading to Eq. (84d).

(ii) $N\alpha\mu \ll T \ll v_g/d \ll \mu$. If the chemical potential is increased beyond the inverse interlayer spacing, then the momentum integration in Eq. (84c) is cut off by v_g/d instead of μ . The logarithmic behavior of the drag conductivity will be modified and σ_D no longer depends on the chemical potential

$$\sigma_D \sim \alpha^2 e^2 T^2 \tau^2 \ln[v_g/(Td)]. \quad (86a)$$

(iia) $T \ll N\alpha\mu \ll \mu \ll v_g/d$. In this case one finds instead of Eq. (86a)

$$\sigma_D \sim \alpha^2 e^2 T^2 \tau^2 \ln[1/(N\alpha)]. \quad (86b)$$

(iii) $T \ll N\alpha\mu \ll v_g/d \ll \mu$. Increasing the chemical potential further leads to the regime where the static screening can no longer be neglected. Now the lower integration limit in Eq. (84c) is effectively given by the inverse screening length rather than the frequency. The upper limit is still determined by the interlayer spacing. Therefore the drag conductivity again depends logarithmically on the chemical potential (Katsnelson, 2011)

$$\sigma_D \sim \alpha^2 e^2 T^2 \tau^2 \ln[v_g/(N\alpha\mu d)], \quad (86c)$$

but now this is a *decreasing* function, indicating the existence of the absolute maximum of the drag conductivity as a function of the chemical potential.

(iv) $T \ll v_g/d \ll N\alpha\mu \ll \mu$. Finally, if the chemical potential is so large that the screening length becomes smaller than the interlayer spacing the momentum integral in Eq. (84c) is no longer logarithmic. As the integration is now dominated by momenta large compared to T , the nonlinear susceptibility may be approximated by Eq. (80), leading to the standard Fermi-liquid result

$$\sigma_D = \frac{\zeta(3)}{4} \frac{e^2 \tau^2 T^2}{(k_F d)^2 (\varkappa d)^2}, \quad \varkappa = 4\alpha k_F, \quad (86d)$$

which differs from that of Kamenev and Oreg (1995) [see Eq. (21)] only by the factor reflecting valley degeneracy in graphene (Amorim and Peres, 2012; Katsnelson, 2011; Tse *et al.*, 2007). The above results are illustrated in Fig 19.

b. Static screening for intermediate interaction strength

The results (84) and (86) rely on the interaction weakness. For stronger interaction, $N\alpha > 1$, (i) the approxi-

mation (85) might be unjustified and the full expression (7) for the interaction propagator should be used; (ii) the four regimes (86) may not exist, since it might happen that $T/(N\alpha) \ll T < v_g/(N\alpha d) \ll v_g/d$. In this case, perturbative analysis can still be justified in the degenerate regime, $\mu \gg T$, where there are two distinct regimes, (a) $\mu \ll v_g/d$, and (b) $\mu \gg v_g/d$ (Narozhny *et al.*, 2012); the latter regime is usually identified with the Fermi-liquid result (86d). As the single-layer conductivity is still large and dominated by disorder, the condition (72) can be somewhat relaxed:

$$\tau_{ee} \gg \tau \Rightarrow \tau^{-1} \gg \alpha^2 T^2 / \mu \Rightarrow \alpha^2 T \tau \ll \mu / T. \quad (87)$$

Proceeding under the assumptions of static screening and the ballistic regime (i.e., the dominant contribution to the effect comes from large momenta $v_g q > \omega$), the result of momentum integration is determined by the upper limit and can be assumed independent of ω . The frequency and momentum integrals factorize and neglecting W/Q under the square root in Eq. (79) one finds

$$\sigma_D = \alpha^2 e^2 T^2 \tau^2 f_0 \left(\frac{\mu}{T}; \alpha; \frac{Td}{v_g} \right), \quad f_0(x; \alpha; \lambda) \approx \frac{32}{3} \int_1^\infty \frac{dQ Q^3 e^{-4\lambda Q}}{[(Q + \tilde{\alpha}(x))^2 - \tilde{\alpha}(x)^2 e^{-4\lambda Q}]^2} \frac{\sinh^2 x}{(\cosh Q + \cosh x)^2}, \quad (88)$$

where

$$\tilde{\alpha}(x) = N\alpha x/2. \quad (89)$$

The results for weaker interaction, Eqs. (86), can be recovered from Eq. (88) by neglecting terms proportional to $\tilde{\alpha}^2$ in the denominator [which corresponds to approximating the interlayer interaction (7) by Eq. (85)]. In the limit $\mu \gg v_g/d$, the function f_0 depends on a single parameter

$$f_0(x\lambda \gg 1) \approx \tilde{f}_0(4\lambda\tilde{\alpha}), \quad (90a)$$

parameter region	drag coefficient
$\mu \ll T$	$\rho_D \sim nT^{-2}$
$T \ll \mu \ll v_g/d$	$\rho_D \sim T^2 n^{-1} \ln(\alpha N n^{1/2} d/v_g)$
$\mu \gg v_g/d$	$\rho_D = \rho_D^{FL} \sim T^2 n^{-3} d^{-4}$

TABLE I Asymptotic expressions for the drag coefficient to the leading order of perturbation theory assuming “realistic” interaction strength $\alpha N \gtrsim 1$, identical layers $n_1 = n_2 = n$, and the experimentally relevant situation $T < v_g/d$. In the opposite regime $T \gg v_g/d$ all results for ρ_D should be divided by Td/v_g (Lux and Fritz, 2012; Narozhny *et al.*, 2012).

where

$$\tilde{f}_0(y) = \frac{32}{3} \int_0^\infty \frac{dZ Z^3 e^{-Z}}{[(Z+y)^2 - y^2 e^{-Z}]^2}. \quad (90b)$$

The function (90b) describes the crossover between the regimes (iii) and (iv) of Eqs. (86) (see Fig. 19). This can be seen by evaluating the integral in the two limits (here $\gamma_0 \approx 0.577216$ is the Euler’s constant)

$$\tilde{f}_0(y \ll 1) \approx -32/3 (\ln y + \gamma_0 + 11/6), \quad (91a)$$

$$\tilde{f}_0(y \gg 1) \approx 64\zeta(3)y^{-4}. \quad (91b)$$

Numerically, this crossover spans a large interval of values of the chemical potential such that the Fermi-liquid result (86d) is practically unattainable in graphene-based drag measurements (Tutuc *et al.*, 2009), see Fig. 20.

In experiment one typically measures carrier density rather than the chemical potential (Gorbachev *et al.*, 2012; Kim *et al.*, 2011; Kim and Tutuc, 2012; Titov *et al.*, 2013a). In graphene, the electron density is given by

$$n = \int_{-\infty}^{\infty} \frac{d\epsilon |\epsilon|}{\pi v_g^2} \left[\tanh \frac{\epsilon}{2T} - \tanh \frac{\epsilon - \mu}{2T} \right]. \quad (92a)$$

Using the asymptotic expressions

$$n = \frac{1}{\pi v_g^2} \begin{cases} \mu^2, & \mu \gg T, \\ (4 \ln 2)\mu T, & \mu \ll T, \end{cases} \quad (92b)$$

one can obtain the qualitative dependence of ρ_D on n , see Table I.

The strongly doped, Fermi-liquid regime has attracted the most attention in literature. Most authors report the standard $\rho_D \sim T^2 n^{-3} d^{-4}$ behavior (Amorim and Peres, 2012; Carrega *et al.*, 2012; Hwang *et al.*, 2011; Katsnelson, 2011; Narozhny *et al.*, 2012; Tse *et al.*, 2007) assuming the energy-independent impurity scattering time.

3. Energy-dependent scattering time

In graphene, the impurity scattering time strongly depends on the type of disorder and on energy (Katsnelson, 2012). In particular, for Coulomb scatterers (Ando, 2006; Cheianov and Fal'ko, 2006; Nomura and MacDonald, 2006, 2007) or strong short-range impurities (Ostrovsky *et al.*, 2006)

$$\tau(\epsilon) = \tau_0^2 |\epsilon|. \quad (93a)$$

For weak short-ranged disorder (Shon and Ando, 1998)

$$\tau(\epsilon) = \gamma/|\epsilon|. \quad (93b)$$

Moreover, quenched disorder in graphene experiences logarithmic renormalization (Aleiner and Efetov, 2006).

Drag in the presence of Coulomb impurities was first considered in Hwang *et al.* (2011) and Peres *et al.* (2011). Both papers reported a stronger dependence of the drag coefficient on the carrier density and interlayer separation, $\rho_D \sim T^2 n^{-4} d^{-6}$. This result was later disputed in Amorim *et al.* (2012); Carrega *et al.* (2012); and Narozhny *et al.* (2012). These authors showed that the energy (or momentum) dependence of τ is qualitatively irrelevant for the asymptotic behavior of ρ_D . In the degenerate limit, microscopic calculations lead to the same results with $\tau(\mu)$ substituted in place of τ . Close to the neutrality point, the drag coefficient acquires an additional logarithmic factor

$$\rho_D(\mu_i \ll T) \sim \alpha^2 (\hbar/e^2) (\mu_1 \mu_2 / T^2) \ln T \tau(T). \quad (94)$$

4. Plasmon contribution

The dynamically screened interaction propagator contains plasmon poles, that may (see Section II.B) affect the resulting drag resistivity. Theoretically, plasmons were studied in graphene monolayers (at $T = 0$) in Hwang and Das Sarma (2007); Schütt *et al.* (2011);

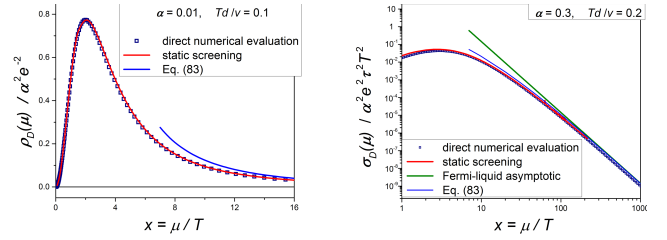


FIG. 20 (Color online) Results of the numerical evaluation of the drag coefficient in the case of identical layers. The squares represent the calculation of Eq. (25) with the only approximation that the polarization operator in the screened interlayer interaction (7) was evaluated in the absence of disorder. The red line corresponds to the same calculation, with the polarization operator replaced by Eq. (81). The blue line was calculated with the approximate expression (90b), valid for $\mu \gg v_g/d$. Left panel: $\alpha = 0.01$, $Td/v_g = 0.1$. Right panel: $\alpha = 0.3$ and $Td/v_g = 0.2$; log-log scale. The straight green line represents the Fermi-liquid result (86d). [Reproduced from Narozhny *et al.* (2012).]

and Wunsch *et al.* (2006) and in double-layer graphene systems in Badalyan and Peeters (2012); Profumo *et al.* (2012); and Stauber and Gómez-Santos (2012). Renormalization of the plasmon spectrum due to electron-electron interaction was considered in Abedinpour *et al.* (2011). Experimentally, plasmons were observed in graphene on SiO₂ substrate (Fei *et al.*, 2011, 2012), graphene-insulator stacks (Yan *et al.*, 2012a), and in graphene micro-ribbon arrays (Ju *et al.*, 2011). Bound states of plasmons with charge carriers, the so-called “plasmareons” were observed in Bostwick *et al.* (2010) and Walter *et al.* (2011). Plasmons subjected to high magnetic field were studied in Yan *et al.* (2012b). For reviews of graphene plasmonics see Grigorenko *et al.* (2012) and Luo *et al.* (2013). More recently, plasmonic excitations in Coulomb coupled N -layer graphene structures were studied in Zhu *et al.* (2013).

Within the above perturbative approach, i.e., Eq. (72), and for low enough temperatures, $\mu, T \ll v_g/d$, the plasmon contribution to drag is subleading (Narozhny *et al.*, 2012). The plasmon pole appears in the region $\omega > v_g q$. Similarly to the situation in semiconductor devices (Sec. II.B), double-layer graphene systems admit an acoustic ($\omega \sim q$) and an optical ($\omega \sim \sqrt{q}$) plasmon modes (Das Sarma and Madhukar, 1981; Principi *et al.*, 2012). In the case where the plasmon decay rate is small (as determined by either weak Coulomb interaction or weak disorder), one can use the δ -function approximation to the interlayer interaction propagator (Flensberg and Hu, 1995). The corresponding contribution to the drag conductivity contains a small factor $g^2 |D|^2 \sim \alpha^3$ for small momenta $v_g q \sim \alpha T$ (or α^4 for $v_g q \sim T$). If the energy dependence of the scattering time is taken into account, the small parameter is $\alpha^2 T \tau$, see Eq. (72).

The above conclusion is illustrated in Figs. 20 show-

ing a comparison between the full numerical evaluation of the perturbative drag coefficient using Eqs. (7), (73), (76), and (77) and the same calculation within the approximation of static screening (85). Numerical modeling of experimental samples, see Figs. 21 and 22 below, includes the contribution was automatically by using the dynamically screened interaction propagator (7).

At the same time, quantitative description of experiments, especially in devices with wider interlayer spacing, might be significantly affected by such aspects as inhomogeneous dielectric background (Badalyan and Peeters, 2012; Carrega *et al.*, 2012) and hybridization between phonon and plasmon modes (Amorim *et al.*, 2012). Plasmon-mediated drag between graphene wave-guides was suggested in Shylau and Jauho (2014).

5. Drag between massless and massive fermions

Graphene-based double-layer devices can be used to observe Coulomb drag between massless and massive particles by coupling Dirac fermions in monolayer graphene to quasiparticles with parabolic dispersion in either bilayer graphene (Scharf and Matos-Abiague, 2012) or a usual 2DEG (Principi *et al.*, 2012; Scharf and Matos-Abiague, 2012). Experimental realizations were reported in Fisichella *et al.* (2014) and Gamucci *et al.* (2014).

Theoretical analysis of Principi *et al.* (2012) and Scharf and Matos-Abiague (2012) is based on the standard expression (77). Both works focus on the low-temperature, degenerate regime $T \ll \mu$. As expected, in the case of strong screening $\kappa d \gg 1$, both works reproduce the standard result (21). For $\kappa d \ll 1$, the resulting drag coefficient is still quadratic in temperature, but contains also a logarithmic factor reminiscent of Eqs. (86). Principi *et al.* (2012) report a d -independent drag in the special case $k_g = k_{2D}$ (which implies a density mismatch between the layers due to the difference in the degeneracies of single-particle states). In the low-density limit $n \rightarrow 0$ this yields $\rho_D \propto n^{-1}$, similarly to the results of Carrega *et al.* (2012), see also Table I. On the other hand, Scharf and Matos-Abiague (2012) report $\rho_D \propto n^{-2}$ in the limit $d \rightarrow 0$ and for $n_g = 2n_{2D}$. Such discrepancies in the asymptotic behavior of ρ_D may appear due to the complicated structure of the nonlinear susceptibility in graphene, see Eqs. (86) and Fig. 19.

The predicted T^2 dependence is observed in experiment (Gamucci *et al.*, 2014) in the $10\text{K} < T < 40\text{K}$ range, although with the smaller magnitude. At higher temperatures, a violation of Onsager reciprocity was observed. This was attributed to the interlayer current. Most interestingly, at lower temperatures $T < 10\text{K}$, the measured drag shows a marked upturn that may indicate a phase transition at $T_c \sim 10 - 100\text{mK}$, see Sec. VII.B.

The system of coupled Dirac and Schrödinger quasipar-

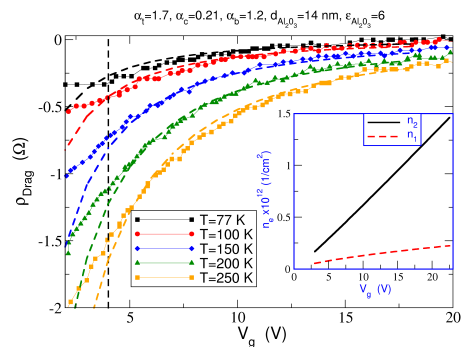


FIG. 21 (Color online) Results of the numerical evaluation (lines) of the drag coefficient and comparison with the data (symbols) of Kim *et al.* (2011). The interlayer spacing ($d = 14\text{nm}$) and dielectric constants of the insulating material were chosen to represent the experimental device. Inset: the relation of the carrier densities and gate voltage, obtained from the electrostatic model of the sample. [Reproduced from Peres *et al.* (2011).]

ticles was also considered in Balram *et al.* (2014), where it was found that interspecies interaction plays a significant role in determining collective (plasmon) modes.

6. Numerical evaluation of the drag coefficient

The above discussion demonstrates that already at the perturbative level, the drag conductivity (77) exhibits multiple asymptotic dependencies. Consequently, virtually every paper on the subject presents results of numerical evaluation of Eq. (77). In contrast to the earlier work on semiconductor devices (see Sec. II), most authors focus on the density (or chemical potential) dependence rather than on the T -dependence. The overall shape of $\rho_D(n)$ curves is qualitatively the same in all calculations. At the Dirac point, drag vanishes, $\rho_D(n = 0) = 0$ (this conclusion does not agree with the experiments of Gorbachev *et al.* (2012) and Titov *et al.* (2013a), see below). Deep in the degenerate (or low-temperature) regime, $T \ll \mu$, $\kappa d \gg 1$, the drag coefficient reaches the standard decaying result (21). Therefore, for intermediate densities there has to be a maximum, roughly at $\mu \sim T$. The corresponding shape is shown in Fig. 20.

Peres *et al.* (2011) presented detailed numerical calculations aimed at describing the experimental findings of Kim *et al.* (2011), see Fig. 21. This calculation included electrostatic modeling of the device (which included two insulators, SiO_2 and Al_2O_3), dynamically screened (within RPA) electron-electron interaction, and the realistic model of Coulomb impurities. For doped graphene layers, the results of the calculation show excellent agreement with the data.

Theoretical modeling of ultra-clean graphene double-

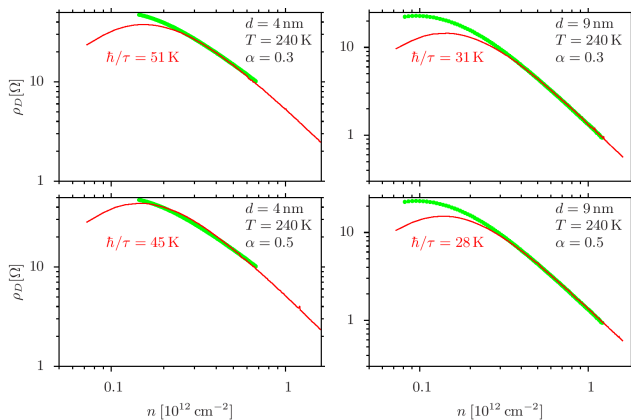


FIG. 22 (Color online) Results of the numerical evaluation (Titov *et al.*, 2013b) of the drag coefficient (red line) and the experimental data (green dots) (Ponomarenko, 2013) in the case of identical layers. The values of $T = 240\text{K}$ and d are taken from the experiment. The only fitting parameter is the energy-independent impurity scattering time (once the value of α_g is chosen). The polarization operator was calculated at $T = 240\text{K}$ and in the presence of disorder (in the ballistic regime).

layers (using boron nitride as a substrate as well as insulating spacer) based the theory of Narozhny *et al.* (2012) was performed by Titov *et al.* (2013b), see Fig. 22. In this calculation, the polarization operator was calculated at the experimental temperature in the presence of disorder, in contrast to the $T = 0$, free-electron expression (76). The use of full, dynamically screened Coulomb interaction ensured that all plasmon-related features were taken into account automatically. Choosing realistic values (Kozikov *et al.*, 2010; Peres *et al.*, 2011) for the effective coupling constant, the only fitting parameter in this calculation was the impurity scattering time τ , which was taken to be energy-independent similarly to the above discussion. Such calculation was also able to reproduce the data (Ponomarenko, 2013) in the doped regime.

The results shown in Figs. 21 and 22 confirm the applicability of the perturbative approach to Coulomb drag in doped graphene. In contrast to similar calculations aimed at semiconductor devices (see Sec. II), these theories are able to reach quantitative agreement with the experimental data with the minimum of fitting parameters. This implies that frictional drag in graphene is dominated by Coulomb interaction, with phonons playing only a subleading role. The latter conclusion can be expected, given that electrons in graphene are physically confined to move in a two-dimensional plane and the rigidity of the crystal lattice (Katsnelson, 2012).

B. Hydrodynamic regime

The perturbation theory outlined in Sec. IV.A can be justified either in the case of weak interaction $\alpha \ll 1$ or in the degenerate regime $\mu \gg T$, see Eq. (72). At the same time, the applicability condition (72) involves the impurity scattering time τ : the perturbation theory fails if the system is “too clean”, or in other words, if electronic transport is dominated not by disorder, but rather by electron-electron interaction. The latter affects transport properties of graphene due to the absence of Galilean invariance: the velocity of Dirac fermions $\mathbf{v} = v_g^2 \mathbf{p} / \epsilon$ is independent of the absolute value of the momentum and therefore total momentum conservation does not prevent velocity (or current) relaxation. As a result, electron-electron scattering is characterized by its own transport relaxation time, which may become smaller than the scattering time due to potential disorder, $\tau_{ee} \ll \tau$.

“Ultra-clean” graphene double-layers were discussed in Narozhny *et al.* (2015); Schütt *et al.* (2013); and Titov *et al.* (2013a) within the framework of the quantum kinetic equation. In principle, solving the kinetic equation in a strongly interacting system is a formidable problem, that cannot be solved in general terms using presently available analytic methods. However in graphene, one can take advantage of the kinematic peculiarity specific to Dirac fermions. Indeed, scattering of particles with almost collinear momenta is enhanced since the momentum and energy conservation laws coincide. This restricts kinematics of the Dirac fermions (Fritz *et al.*, 2008; Kashuba, 2008; Schütt *et al.*, 2011) and leads to the singularity in the collision integral. This singularity leads to the fast thermalization of particles within a given direction and allows one to derive macroscopic - or hydrodynamic - equations that generalize Eq. (2) for interacting Dirac fermions. In monolayer graphene, this approach was discussed in Foster and Aleiner (2009); Fritz *et al.* (2008); Kashuba (2008); Müller and Sachdev (2008); and Svintsov *et al.* (2012). An alternative macroscopic approach to Coulomb drag in graphene¹⁴ has been suggested in Song *et al.* (2013); Song and Levitov (2012, 2013).

1. Collinear scattering singularity

Singular behavior of the collision integrals in the case of collinear scattering of the Dirac fermions (Arnold *et al.*, 2000; Fritz *et al.*, 2008; Kashuba, 2008; Müller *et al.*,

¹⁴ The theory of Song *et al.* (2013); Song and Levitov (2012, 2013) relies on correlations of the disorder potential in the two layers, see Sec. IV.F.

2009; Schütt *et al.*, 2013) is central to the hydrodynamic approach to transport in graphene.

The general form of the kinetic equation in layer i is given by Eq. (9) with the addition of the intralayer collision integral. If the system is weakly perturbed from

$$\mathcal{I}_{ij} = \sum_{1,1',2'} w_{12,1'2'} f_{j,1}^{(0)} f_{i,2}^{(0)} \left[1 - f_{j,1'}^{(0)}\right] \left[1 - f_{i,2'}^{(0)}\right] [h_{j,1'} + h_{i,2'} - h_{j,1} - h_{i,2}], \quad (95a)$$

where the function

$$w_{1,2;1',2'} = |\langle 1, 2|U|1', 2'\rangle|^2 (2\pi)^3 \delta(\epsilon_1 + \epsilon_2 - \epsilon_{1'} - \epsilon_{2'}) \delta(\mathbf{k}_1 + \mathbf{k}_2 - \mathbf{k}'_1 - \mathbf{k}'_2), \quad (95b)$$

determines the probability of scattering from states $1', 2'$ into states $1, 2$ (within the Fermi Golden Rule approximation). Here $\langle 1, 2|U|1', 2'\rangle$ is the interaction matrix element. The indices $i, j = 1, 2$ denote the two layers¹⁵.

In graphene, the interaction matrix elements are most conveniently expressed in the basis of the eigenstates of the Dirac Hamiltonian $|\epsilon, \mathbf{e}_v\rangle$ labeled by their energy ϵ and the unit vector $\mathbf{e}_v = \mathbf{v}/v_g$ pointing in the direction of velocity (for a given spin and valley projection):

$$|\langle 1, 2|U|1', 2'\rangle|^2 = |U(\mathbf{q})|^2 \frac{1 + \mathbf{e}_v^{(1)} \cdot \mathbf{e}_v^{(1')}}{2} \frac{1 + \mathbf{e}_v^{(2)} \cdot \mathbf{e}_v^{(2')}}{2}. \quad (96)$$

Here $\mathbf{q} = \mathbf{k}_1 - \mathbf{k}'_1$ is the transferred momentum and the two fractions are the ‘‘Dirac factors’’ (Katsnelson, 2012). Now one can separate quantities related to the initial and final states in the function $w_{12,1'2'}$ by using the identities

$$\delta(\epsilon_1 + \epsilon_2 - \epsilon'_1 - \epsilon'_2) = \int d\omega \delta(\epsilon_1 - \epsilon'_1 + \omega) \delta(\epsilon_2 - \epsilon'_2 - \omega),$$

$$\delta(\mathbf{k}_1 + \mathbf{k}_2 - \mathbf{k}'_1 - \mathbf{k}'_2) = \int d^2q \delta(\mathbf{k}_1 - \mathbf{k}'_1 + \mathbf{q}) \delta(\mathbf{k}_2 - \mathbf{k}'_2 - \mathbf{q}).$$

The δ -functions yield $\epsilon'_1 = v_g |\mathbf{k}_1 + \mathbf{q}|$ and hence allow one to sum over the states $1'$ and $2'$ in the collision integral (95). Each of these sums result in a diverging factor¹⁶.

$$\sum_{1'} \propto \frac{1}{\sqrt{v_g^2 q^2 - \omega^2}}. \quad (97)$$

¹⁵ In the perturbative approach of Sec. II.B, the kinetic equation (9) contained only the interlayer collision integral. Therefore, one could associate the states 1 and 2 with the active and passive layers and avoid extra layer indices.

¹⁶ In Sec. IV.A, the nonlinear susceptibility (73) did not exhibit this divergence due to an accidental cancellation that is specific to the particular case of energy-independent impurity scattering time. In a more general situation the cancellation does not occur and as a result the rate τ_D^{-1} contains an extra logarithmic factor, see Eq. (94).

equilibrium, then the distribution function can be written in the form (10). Weak deviations from equilibrium are associated with the smallness of the nonequilibrium correction h , allowing one to linearize the collision integrals (Lifshitz and Pitaevskii, 1981). The linearized form of the collision integrals is given by

One can see that the divergence corresponds to collinear scattering by examining the angle $\varphi_{\mathbf{k}_1 \mathbf{q}}$ at the light cone:

$$\cos \varphi_{\mathbf{k}_1 \mathbf{q}} (\omega = v_g q) = 1 \quad \Rightarrow \quad \varphi_{\mathbf{k}_1 \mathbf{q}} = 0 \quad (\text{or } \pi).$$

Hence, the argument of one of the above δ -functions vanishes: $\epsilon'_1 = \epsilon_1 + \omega$. Similar conclusion follows for the momentum \mathbf{k}_2 . Thus, all momenta are collinear.

Physically, the divergence (97) represents the fact that for the linear spectrum the energy and momentum conservation laws coincide. Consequently, any relaxation rate obtained by integrating the collision integral (95) over the state 2 will be logarithmically divergent. In order to regularize this divergence, one has to go beyond the Golden-Rule approximation and take into account renormalization of the spectrum (Abrikosov and Beneslavskii, 1971; González *et al.*, 1999; Son, 2007). This leads (Arnold *et al.*, 2000; Fritz *et al.*, 2008) to the appearance of a large factor $|\ln(\alpha)| \gg 1$ in generic relaxation rates in graphene. In disordered graphene, this singularity is also cut off by disorder-induced broadening of the momentum-conservation delta-function (Narozhny *et al.*, 2012).

2. Macroscopic linear-response theory in graphene

The collinear scattering singularity (97) allows for an approximate, yet nonperturbative solution of the kinetic equation in graphene (Fritz *et al.*, 2008; Kashuba, 2008; Narozhny *et al.*, 2015; Schütt *et al.*, 2013). The idea is to find zero modes of the collision integral and build macroscopic equations for the corresponding currents.

The standard perturbative description of Coulomb drag is based on the energy-independent approximation for the nonequilibrium distribution function (10). This constant solution of the kinetic equation describes the single zero mode of the intralayer collision integral corresponding to conservation of the electric charge (or the

number of particles). Macroscopic charge flow is described by the electric current (12). Integrating the kinetic equation, one finds the macroscopic equation for \mathbf{j} equivalent to the Drude theory, see Eqs. (2). Such solution is justified by the condition (72), which means that the collision integral in the kinetic equation is dominated by disorder.

In contrast, in “ultra-clean” graphene the collision integral is dominated by Coulomb interaction. Using the collinear scattering singularity (i.e., for $|\ln(\alpha)| \gg 1$), one can neglect all but the zero modes of \mathcal{I} [treated as an integral operator acting on $h_i(\epsilon)$]. In practice, this means retaining only those terms in the power series of the distribution function h_i which correspond to either zero modes of the collision integral, or to its eigenmodes with nondivergent eigenvalues. Fritz *et al.* (2008); Kashuba (2008); and Schütt *et al.* (2013) have developed the following *two-mode approximation*

$$h_i = \left(\mathbf{a}_0^{(i)} + \mathbf{a}_1^{(i)} \epsilon \right) \mathbf{v}. \quad (98)$$

The vectors \mathbf{a}_i can be expressed in terms of the two macroscopic currents in graphene, the electric current (12) and the energy current

$$\mathbf{Q}_i = \sum \epsilon \mathbf{v} \delta f_i. \quad (99)$$

The appearance of inequivalent currents is the essential feature of graphene physics. In general, the collision integral has three nondecaying eigenmodes; hence Narozhny *et al.* (2015) have used the *three-mode approximation*:

$$h_i = \left(\mathbf{a}_0^{(i)} + \mathbf{a}_s^{(i)} \text{sign}(\epsilon) + \mathbf{a}_1^{(i)} \epsilon \right) \mathbf{v}. \quad (100)$$

The $\text{sign}(\epsilon)$ mode is described by the imbalance current (Foster and Aleiner, 2009)

$$\mathbf{P}_i = \sum \text{sign}(\epsilon) \mathbf{v} \delta f_i. \quad (101)$$

Integrating the kinetic equation with the help of either of the above approximations for the nonequilibrium distribution function, one obtains macroscopic equations for the currents \mathbf{j} , \mathbf{Q} , and \mathbf{P} , that generalize the Ohm’s law for graphene¹⁷. Solutions of these equations yield linear response transport coefficients. Note, that this approach does not rely on the Kubo formula. In particular, the drag coefficient can be obtained without the use of the perturbative expressions (15) or (77).

The simplest macroscopic equation describes the energy current. In an infinite sample, where all quantities are homogeneous, the equation reads (Schütt *et al.*, 2013)

$$e v_g^2 n \mathbf{E} + (v_g^2/c) [\mathbf{j} \times \mathbf{B}] = \mathbf{Q}/\tau, \quad (102)$$

where n is the carrier density in graphene (92). The collision integral does not contribute to Eq. (102) due to energy conservation. In the limit $\mu \gg T$, all currents are equivalent, such that $\mathbf{j}(\mu \gg T) \approx (e/\mu) \mathbf{Q}(\mu \gg T)$, and Eq. (102) becomes equivalent to the Ohm’s law (26). In this limit, the Galilean invariance is restored, all relaxation rates due to electron-electron interaction vanish, and all three macroscopic equations become equivalent.

At the charge neutrality point $n = 0$, the equation (102) yields $(v_g^2/c) [\mathbf{j} \times \mathbf{B}] = \mathbf{Q}/\tau$. This simple-looking relation illustrates all the essential qualitative features of linear response transport in graphene. Firstly, in the absence of disorder, $\tau \rightarrow \infty$, the equation becomes senseless, at least when the system is subjected to external magnetic field. Physically, this means that in the absence of disorder the assumption of the steady state in an infinite system becomes invalid: under external bias, the energy current increases indefinitely. Secondly, if the system is stabilized by disorder, but $\mathbf{B} = 0$, then one finds $\mathbf{Q} = 0$. Finally, if the system is subjected to external magnetic field, the electric and energy currents are orthogonal, $\mathbf{j} \perp \mathbf{Q}$. This leads to appearance of *classical, positive magnetoresistance* (Müller and Sachdev, 2008; Narozhny *et al.*, 2015)

$$\delta R(B; \mu = 0) \propto (v_g^4 \tau / c^2) (B^2 / T^3), \quad (103)$$

as well as magnetodrag in graphene, see Sec. IV.D below. These results are in sharp contrast with the standard Drude theory, see Eqs. (3).

3. Coulomb drag in weakly disordered graphene.

Close to charge neutrality and in the presence of weak, uncorrelated disorder $\alpha^2 T \tau \gg 1$ (i.e. $\tau^{-1} \ll \tau_{ee}^{-1}$), the drag resistivity in the absence of magnetic field was found in Schütt *et al.* (2013) and has the form

$$\rho_D(\mu_i \ll T) \approx 2.87 \frac{h}{e^2} \frac{\alpha^2 \mu_1 \mu_2}{\mu_1^2 + \mu_2^2 + 0.49 T / (\alpha^2 \tau)}. \quad (104)$$

As long as any (even infinitesimal) disorder is present, ρ_D vanishes at the double Dirac point $\rho_D(\mu_1 = \mu_2 = 0) = 0$, and grows sharply in its immediate vicinity, see Fig. 23. If only one of the layers is tuned to the Dirac point (median lines in Fig. 23), the drag resistivity always vanishes

$$\rho_D(\mu_1 = 0, \mu_2 \neq 0) = \rho_D(\mu_1 \neq 0, \mu_2 = 0) = 0.$$

If one varies the carrier density in one of the layers through the Dirac point, then the drag resistivity changes sign. In the color maps in Fig. 23 this is represented by the color change between neighboring quadrants. The same sign pattern of the drag resistivity (in zero magnetic field) were observed in experiments of Gorbachev *et al.* (2012); Kim *et al.* (2011); and Kim and Tutuc (2012).

¹⁷ The full three-mode equations are too cumbersome to reproduce here, the interested reader is referred to Narozhny *et al.* (2015).

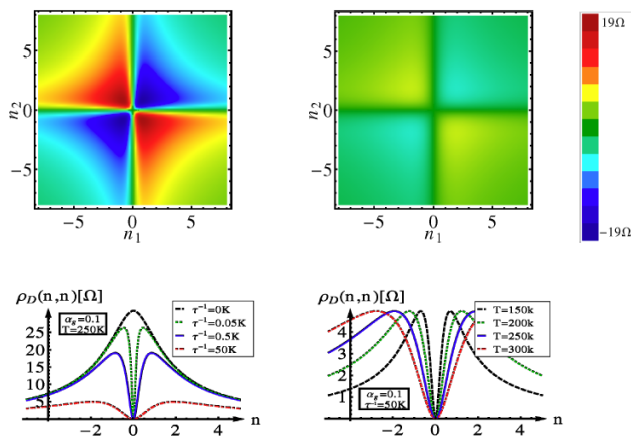


FIG. 23 (Color online) Leading-order drag coefficient in the ballistic regime as a function of carrier densities (in units of 10^{11}cm^{-2}) for $d = 9\text{nm}$. Left: ρ_D at $T = 250\text{K}$; the upper panel refers to ultra-clean graphene $\tau^{-1} = 0.5\text{K}$; the lower left panel shows the evolution of ρ_D with increasing disorder from $\tau^{-1} = 0$ to $\tau^{-1} = 50\text{K}$. Right: ρ_D for $\tau^{-1} = 50\text{K}$; the lower panel shows ρ_D for $T = 150, 200, 250,$ and 300K . [Reproduced from Schütt *et al.* (2013).]

At the double Dirac point in the absence of disorder, one finds (for $\mathbf{B} = 0$) $\rho_D(\mu_1 = \mu_2 = 0) \sim \alpha_g^2 h/e^2$. This peculiar feature is shown in Fig. 23 by the black curve in the lower left panel. It is however unlikely that this result is relevant to the nonzero drag resistivity at the Dirac point observed in Gorbachev *et al.* (2012). A possible explanation for this observation is provided by the higher-order effects (Schütt *et al.*, 2013).

For intermediate disorder strength, $\alpha^2 T \ll \tau^{-1} \ll T$, the applicability region of the hydrodynamic approach overlaps with that of the conventional perturbation theory reviewed in Sec. IV.A and one recovers perturbative results, see Fig. 18.

Finally, let us stress the novel qualitative feature of the hydrodynamic approach: the electron-hole asymmetry does not play a definitive role in the drag effect. Indeed, the “drag rate” τ_D^{-1} dominates the observable effect only under the standard assumptions of the Fermi-liquid behavior in the two layers. On the contrary, in the vicinity of the Dirac point in graphene, another scattering process, the interplay of fast interlayer energy and current relaxation which is insensitive to the electron-hole asymmetry, becomes important. Further examples to such novel behavior are presented in Section IV.D.

C. Diffusive regime

In strongly disordered graphene samples or, equivalently, at the lowest temperatures, $T\tau \ll 1$, the electron motion becomes diffusive. In this regime, the standard perturbative approach based on Eq. (77) is applicable. In particular, the polarization operator has the standard

form (30). The nonlinear susceptibility can be found using the argument leading to Eq. (28). In graphene close to the Dirac point, $\mu \ll T \ll \tau^{-1}$, the derivative of the longitudinal conductivity with respect to the carrier density is independent of the precise nature of disorder and is given by (Schütt *et al.*, 2013)

$$\partial\sigma/\partial n \sim nv^4\tau^4.$$

In contrast to the theory reviewed in Sec. II, in graphene the Thomas-Fermi screening length is much longer than the interlayer spacing $\kappa d \ll 1$; hence one finds the following expression for the drag resistivity

$$\rho_D(\mu_i \ll T \ll \tau^{-1}) \sim (h/e^2)\alpha^2\mu_1\mu_2T\tau^3, \quad (105)$$

vanishing at $\mu_i = 0$ due to the electron-hole symmetry.

In the degenerate regime, $\mu \gg T$, one recovers the usual quadratic temperature dependence of the drag resistivity. The behavior of ρ_D in the diffusive regime is summarized in Fig. 18 (the upper row). The “Fermi-liquid” result (34) is only recovered in the academic limit of strong screening $\kappa d \gg 1$. This regime is not shown in Fig. 18 since in graphene it can be reached only at the extreme values of the chemical potential, see Fig. 20.

Calculations of the lowest-order drag resistivity in the diffusive regime are essentially the same in any system, see Sec. II.C. As shown in Fig. 18, the behavior of ρ_D at the lowest temperatures may be dominated by higher-order drag effects.

D. Giant magneto-drag in graphene

Although the effect of classical magnetoresistance in multi-band systems is well known in semiconductor physics (Seeger, 2002), the equivalent effect in Coulomb drag was only recently observed in graphene-based devices (Gorbachev *et al.*, 2012; Titov *et al.*, 2013a). One of the reasons is that the majority of earlier drag measurements were performed in double-well semiconductor heterostructures. Then each of the layers is represented by a two-dimensional electron gas that is formed by electrons occupying the lowest level in the quantum well at the interface between two semiconductors in the device. In contrast in graphene, the conduction and valence bands touch at the Dirac point and as a result, both electrons and holes participate in transport phenomena at low doping.

The experimental data on magnetodrag in graphene (Gorbachev *et al.*, 2012) is shown in Fig. 24¹⁸. There

¹⁸ Notice, that Gorbachev *et al.* (2012) adopted an alternative definition of the drag resistivity $\rho_{xx}^D = E_{2x}/j_{1x}$. Therefore in this Section we will discuss the off-diagonal resistivity $\rho_{xx}^{12} = E_{2x}/j_{1x}$ rather than ρ_D that is defined in the rest of the paper with the opposite sign.

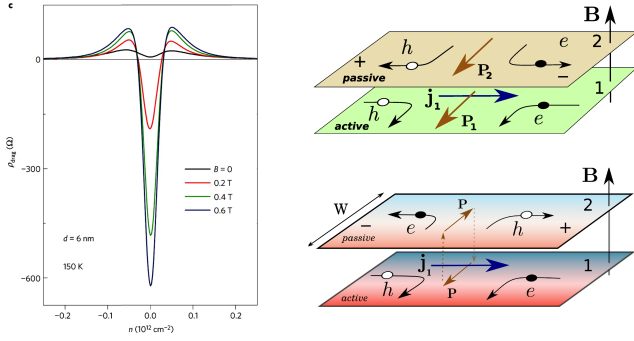


FIG. 24 (Color online) Left: Off-diagonal resistivity ρ_{xx}^{12} in magnetic field, measured in a graphene-based double-layer device. The two graphene sheets are kept at “opposite” carrier densities $n_1 = -n_2 = n$ and $T = 150\text{K}$. [Reprinted by permission from Macmillan Publishers Ltd: Nature Physics, Gorbachev *et al.* (2012)] Right: Mechanism of magnetodrag at charge neutrality. Upper panel: in an infinite system quasi-particle currents in the two layers (denoted by \mathbf{P}_i) flow in the same direction, leading to positive ρ_{xx}^{12} . Lower panel: in a thermally isolated system no net quasiparticle flow is possible; the quasiparticle currents in the two layers have opposite directions yielding negative ρ_{xx}^{12} . [Reproduced from Titov *et al.* (2013a).]

are two outstanding features in Fig. 24. At high carrier densities (or in the degenerate regime), the effect of the magnetic field is relatively weak. This observation is consistent with the expectation, that transport properties of doped graphene are dominated by one of the two bands (the contribution of the other being exponentially suppressed). In the vicinity of the Dirac point both types of carriers contribute to transport. Moreover, the leading contribution to drag at zero field vanishes right at the neutrality point due to exact electron-hole symmetry of the Dirac spectrum. Once the magnetic field is applied, the system develops a drag signal which is no longer determined by electron-hole asymmetry. As a result, the drag resistivity near the Dirac point in the presence of weak magnetic field is much higher than the maximum value in zero field, see e.g. Fig. 22.

The classical, two-band mechanism of magnetodrag in graphene at charge neutrality can be readily illustrated in the case, where the system size is much larger than any characteristic length scale, such that the two graphene sheets may be considered effectively infinite. In this case (see Fig. 24), the driving current in the active layer, \mathbf{j}_1 , corresponds to the counter-propagating flow of electrons and holes with zero total momentum (due to the exact electron-hole symmetry). Once the weak magnetic field is applied, electrons and holes are deflected by the Lorentz force and drift in the same direction. The resulting quasi-particle flow, \mathbf{P}_1 , carries a nonzero net momentum in the direction perpendicular to \mathbf{j}_1 . This momentum can be transferred to the passive layer by the interlayer Coulomb

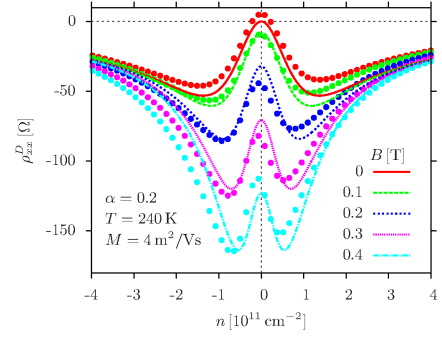


FIG. 25 (Color online) Off-diagonal resistivity ρ_{xx}^{12} in magnetic field, measured in a graphene-based double-layer device. Both graphene sheets are kept at the same carrier density $n_1 = n_2 = n$ and at $T = 240\text{K}$. Solid symbols represent the experimental data. [Reproduced from Titov *et al.* (2013a).]

interaction inducing the quasi-particle current, \mathbf{P}_2 , in the same direction as \mathbf{P}_1 . The Lorentz forces acting on both types of carriers in the passive layer drive the charge flow in the direction opposite to \mathbf{j}_1 . If the passive circuit is open, this current is compensated by a finite drag voltage, yielding a positive drag resistivity (Titov *et al.*, 2013a).

This mechanism of magnetodrag at charge neutrality is closely related to the anomalous Nernst effect in single-layer graphene (Müller and Sachdev, 2008; Wei *et al.*, 2009; Zuev *et al.*, 2009). Indeed, the quasi-particle current is proportional to the heat current at the Dirac point. The fact that the Lorentz force in the electron and hole bands has the opposite sign is also the reason for the vanishing Hall effect at charge neutrality.

Despite being qualitatively clear, the above description of magnetodrag yields the induced drag voltage which has the sign opposite to that observed in experiment (Gorbachev *et al.*, 2012; Titov *et al.*, 2013a), see Fig. 24. In fact, the *negative* drag in Fig. 24 can only appear if the quasiparticles currents in the two layers \mathbf{P}_1 and \mathbf{P}_2 have opposite directions. According to Narozhny *et al.* (2015) and Titov *et al.* (2013a), this is what happens in small, mesoscopic samples used in experiment.

Consider the continuity equation for the quasiparticle current \mathbf{P}_1 , including relaxation by electron-hole recombination (Foster and Aleiner, 2009; Titov *et al.*, 2013a)

$$\nabla \mathbf{P}_1 = -(\rho_1 - \rho_0)/\tau_{ph} - (\rho_1 - \rho_2)/(2\tau_Q), \quad (106)$$

where ρ_i are the quasiparticle densities in the two layers, $\rho_0 = \pi T^2/(3v_g^2)$ is the equilibrium quasiparticle density at the Dirac point, τ_{ph} describes the energy loss from the system dominated by phonon scattering, and τ_Q characterizes quasiparticle imbalance relaxation due to inter-layer Coulomb interaction. The equation for the passive layer can be obtained by interchanging layer indices. In the absence of quasiparticle recombination, hard-wall boundary conditions at the sample boundaries allow only

for the trivial solution. In contrast, taking into account inelastic processes, one finds the nontrivial solution illustrated in Fig. 24: $\mathbf{P}_1 = -\mathbf{P}_2$.

Combining the continuity equation (106) with the hydrodynamic description of linear response transport in graphene (with the additional gradient terms that account for inhomogeneity of physical quantities in finite-size systems), one can describe the negative drag observed in experiment (Narozhny *et al.*, 2015; Titov *et al.*, 2013a), see Fig. 25. The exponential collapse of theoretical curves at high carrier density is an artifact of the two-mode approximation adopted in Titov *et al.* (2013a). The more accurate three-mode approximation (Narozhny *et al.*, 2015) includes thermoelectric effects formulated in terms of energy currents; the corresponding hydrodynamic description yields only the power-law decay of the magnetodrag at $\mu_i \gg T$, in contrast to the exponential collapse shown in Fig. 25. As compared to lower-temperature data (see Fig. 24), the results shown in Fig. 25 exhibit qualitatively new features which can be attributed to higher efficiency of relaxation processes at higher temperature.

E. Hall drag in graphene

Hall drag measurements in graphene were reported in Titov *et al.* (2013a). These experiments were performed at relatively high temperatures $T = 160 - 240\text{K}$, where macroscopic coherence is not expected to exist. While disorder effects in graphene are often attributed to Coulomb scatterers characterized by mean free time that is linear in energy, the measured Hall drag resistivity is not small as would follow from a mechanism similar to that suggested in Hu (1997) and von Oppen *et al.* (2001).

Instead, double-layer graphene samples demonstrate a much simpler, yet still strong effect based on the coexistence of electron and hole liquids in each layer (Foster and Aleiner, 2009). Consequently, the observed Hall drag resistance, Fig. 26, is large when one of the layers is close to the neutrality point and vanishes if two layers have the same charge densities with opposite signs (a white line running from the top left to bottom right corner in the left panel Fig. 26).

Hall drag effect in graphene can be understood with the help of the hydrodynamic theory (Narozhny *et al.*, 2015; Titov *et al.*, 2013a). Indeed, given the presence of two noncollinear currents in the model, it is not surprising to see the nonzero Hall drag away from the Dirac point, where both the conventional Hall effect and Hall drag change sign together with the carrier density and thus have to vanish¹⁹. Hall drag also has to vanish in the

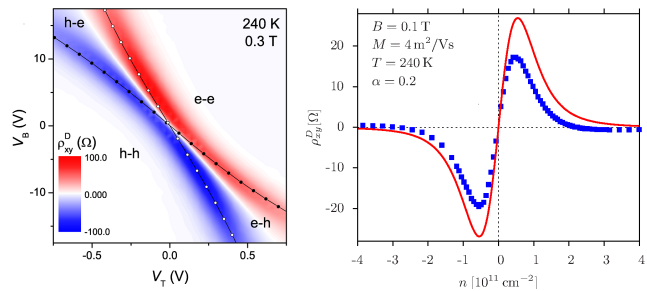


FIG. 26 (Color online) Left panel: Hall drag resistivity in graphene as a function of gate voltages controlling carrier densities in the two layers. White diagonal area corresponds to vanishing Hall drag for $n_1 = -n_2$. Lines track positions of maxima in single-layer resistivity in top (open symbols) and bottom (solid symbols) layers. Right panel: Hall drag resistivity as a function of carrier density for $n_1 = n_2 = n$. Blue squares represent the experimental data. The red curve represents the theoretical prediction. [Reproduced from Titov *et al.* (2013a).]

degenerate regime where only one band contributes to transport and the standard single-band theory (2) holds. However, this regime lies outside of the parameter range of the experiment (Titov *et al.*, 2013a). Thus, some Hall drag signal is observed at all densities, but ρ_{xy}^D decays to rather small values as the density increases beyond $n \simeq 1 \times 10^{11}\text{cm}^{-2}$. Interestingly enough, the data show a sign change of ρ_{xy}^D at $n \approx \pm 2 \times 10^{11}\text{cm}^{-2}$. This rather weak effect requires a more accurate consideration.

The right panel of Fig. 26 shows the results of the hydrodynamic theory alongside experimental data. This calculation was performed without any fitting (Titov *et al.*, 2013a). The value of impurity scattering time τ was determined from the measured single-layer resistivity. The effective interaction parameter was estimated by the most plausible value for graphene on hBN, $\alpha_g \approx 0.2$ [see e.g. Kozikov *et al.* (2010) and Reed *et al.* (2010) for general considerations and the experimental evidence for possible values of α_g].

F. Higher-order effects in graphene

All theories of Coulomb drag in graphene discussed so far were concerned with the leading-order contribution of the interlayer interaction. Indeed, even the nonperturbative results of the hydrodynamic approach were obtained by solving the kinetic equation with the collision integral (95), where the transition probability was estimated using the Fermi Golden Rule. All such theories predict

plain Hall drag in terms of the “energy-driven drag mechanism”. Indeed, if one omits the interlayer frictional force, one would still find nonzero Hall drag due to the interlayer energy relaxation.

¹⁹ A similar two-fluid model was used in Song *et al.* (2013) to ex-

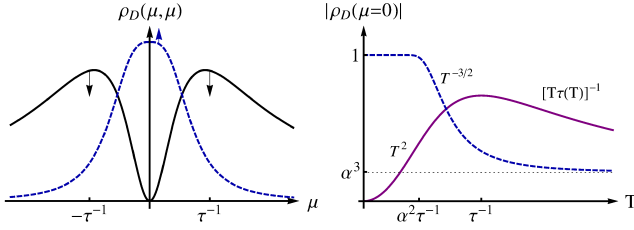


FIG. 27 (Color online) Schematic view of the drag resistivity at low temperatures. The dashed line illustrates the third-order drag effect. Left panel: The black solid line represents the lowest order contribution to drag. The arrows indicate the tendency of the two terms with the decrease of temperature $T \rightarrow 0$. Right panel: The purple solid line represents the contribution of correlated disorder. [Reproduced from Schütt *et al.* (2013).]

vanishing drag at the point of exact electron-hole symmetry [with the exception of the academic case of pure graphene, see Eq. (104) and Fig. 23].

However, measurements (Gorbachev *et al.*, 2012; Titov *et al.*, 2013a) reveal nonzero drag at the double Dirac point, see Fig. 24. At the time of writing, there is no consensus in the community regarding the origin of this effect. At the same time, higher-order processes (see Sec. II.D) are known to be insensitive to the electron-hole symmetry and thus may provide a plausible explanation (Titov *et al.*, 2013a).

1. Third-order drag in graphene

The third-order drag effect in graphene was considered in Schütt *et al.* (2013). The principle results are shown in Fig. 18 in red. A schematic illustration of the relative strength of the second- and third-order contributions is given in the left panel in Fig. 27.

The third-order drag resistivity in the diffusive regime can be found similarly to the conventional case, see Sec. II.D. All microscopic details are masked by the diffusive nature of electronic motion. However, due to the relatively weak screening and the possibility to tune the carrier density to the Dirac point, one finds a richer physical picture with multiple parameter regimes.

The standard “Fermi-liquid” regime (Levchenko and Kamenev, 2008b) corresponds to the condition

$$N\kappa \gg \max \left\{ d^{-1}, \sqrt{T/D} \right\},$$

where $N = 4$ describes spin and valley degeneracy of quasiparticle states in graphene. Here the temperature-independent result (40) is reproduced, although with the extra factors of N

$$\rho_D^{(3)} \sim (h/e^2) N^{-5} g^{-3} (\kappa d)^{-2}. \quad (107)$$

At higher temperatures, one can achieve a different, high-temperature regime with

$$d^{-1} \ll N\kappa \ll \sqrt{T/D}.$$

In this case, the resulting drag resistivity decays rapidly

$$\rho_D^{(3)} \sim \frac{h}{e^2} \frac{1}{g^3} \frac{1}{(N\kappa d)^2} \left(\frac{D\kappa^2}{T} \right)^{3/2}. \quad (108)$$

The experiment of Gorbachev *et al.* (2012) was performed on samples with the small interlayer spacing. In the limit $\kappa d \ll 1$, one finds three different temperature regimes.

Close to the Dirac point and at lowest temperatures, the drag resistivity is temperature-independent:

$$\rho_D^{(3)}(\mu \ll T; T\tau \ll \alpha^2) \sim h/e^2. \quad (109)$$

Note, that this result is also independent of the strength of the Coulomb interaction α !

At somewhat higher temperatures (or, equivalently, for slightly weaker disorder strength), the third-order contribution decays as function of temperature

$$\rho_D^{(3)}(\mu \ll T \ll \tau^{-1} \ll \alpha^{-2}T) \sim (h/e^2)(\alpha^2 T\tau)^{-3/2}. \quad (110)$$

These results are illustrated in the right panel in Fig. 27.

Away from the Dirac point, the third-order contribution decays as a function of the chemical potential (or equivalently, carrier density) and quickly becomes sub-leading, see the left panel in Fig. 27:

$$\rho_D^{(3)}(\mu\tau \gg \max[1, \alpha^{-1}(T\tau)^{1/2}]) \sim \frac{h}{e^2} \frac{1}{(\mu\tau)^3}. \quad (111)$$

As a result, $\rho_D^{(3)}$ may only be detectable at low temperatures and in vicinity of the Dirac point.

While estimating $\rho_D^{(3)}(\mu = 0)$, the single-layer conductivity was assumed to be of the order of the quantum conductance $\sigma \sim e^2/h$, i.e. discarding localization effects. Indeed, single-layer measurements on high-quality samples show temperature-independent conductivity down to 30mK (Tan *et al.*, 2007) [possibly due to the specific character of impurities in graphene (Ostrovsky *et al.*, 2007)].

For weak disorder or higher temperature the diffusive approximation fails. Drag in vicinity of the Dirac point can then be described by the quantum kinetic equation approach. The previously reviewed results, e.g., Eq. (104) were obtained by approximating the collision integrals with the help of the Fermi Golden Rule, see Eq. (95b). However, taking into account next-order matrix elements yields a nonzero contribution, similar to the above third-order result $\rho_D^{(3)}$.

Taking into account the second-order matrix element, one can generalize the Golden Rule expression (96) by using the combination

$$|U_{12}^{(1)} + U_{12}^{(2)}|^2 \simeq |U_{12}^{(1)}|^2 + 2\text{Re}\{U_{12}^{(1)}[U_{12}^{(2)}]^*\}. \quad (112)$$

Since $U_{12}^{(1)} \propto \alpha$ and $U_{12}^{(2)} \propto \alpha^2$, all relaxation rates will now get an additional contribution of the order of α^3 . In particular, the “drag rate” τ_D^{-1} gets a contribution that is independent of the carrier density

$$\tau_D^{-1} \sim \alpha^2 N(\mu/T)^2 + \alpha^3 NT, \quad (113)$$

which dominates near the Dirac point. In this case, one may neglect the conventional, second-order drag contribution; the result is (Schütt *et al.*, 2013)

$$\rho_D \sim \frac{\hbar}{e^2} \frac{\alpha^3 T + \alpha^4 \mu^2 \tau N}{T + \alpha^2 \mu^2 \tau N}, \quad \mu \ll \alpha^{1/2} T, \quad T\tau \gg 1.$$

Exactly at the Dirac point this yields

$$\rho_D \sim (\hbar/e^2)\alpha^3. \quad (114)$$

This result is illustrated in the right panel of Fig 27 by the horizontal asymptote at $T\tau \gg 1$.

2. Interlayer disorder correlations

Within the conventional theory, charge carriers in each layer scatter off an independent disorder potential. This picture is clearly applicable to the cases where impurities are mostly concentrated in the substrate insulator sandwiching the double-layer structure. In the case of the standard double-well heterostructures (Eisenstein, 1992; Gramila *et al.*, 1991; Hill *et al.*, 1997; Lilly *et al.*, 1998; Solomon *et al.*, 1989), the random potential originates in the delta-doped layers providing charge carriers. These layers are typically located on the outer sides of the double-well structure. In graphene, disorder potential is often attributed to the insulating substrate, in particular to SiO_2 . Indeed, in graphene-based samples of Kim *et al.* (2011) and Kim and Tutuc (2012), graphene monolayers are exfoliated onto a thick SiO_2 dielectric, while the interlayer spacer consists of 14nm-thick Al_2O_3 . In such a structure, the impurity potential created by the silicon oxide is likely to affect only the nearest monolayer.

In contrast, the samples of Gorbachev *et al.* (2012) consist of graphene–hexagonal-boron-nitride heterostructures, where the interlayer spacer contains only few atomic layers of the same insulator (boron nitride) that is used as a substrate. In this case, impurity potential originating from the interlayer spacer would be equally felt by carriers in both graphene layers. Another scenario for disorder correlation (Gorbachev *et al.*, 2012; Song and Levitov, 2012) involves interactions between charge-density inhomogeneities forming due to impurity potential in the two layers.

The effect of the correlated disorder in the drag measurements is insensitive to the electron-hole symmetry

(Gornyi *et al.*, 1999; Hu, 2000a), and thus may also provide an explanation (Schütt *et al.*, 2013; Song and Levitov, 2012) for the observed nonzero drag in graphene at the Dirac point (Gorbachev *et al.*, 2012).

At high temperatures, $T\tau \gg 1$, the effect of the correlated disorder can be described by the skeleton diagram similar to the third-order drag contribution, see the right panel of Fig. 7. Interlayer disorder correlations can be incorporated into the scattering amplitude, but now instead of the second-order matrix element in Eq. (112), one has to introduce an interlayer disorder scattering rate $1/(T\tau_{12})$. The resulting “drag rate” τ_D^{-1} is given by

$$1/\tau_D^{\text{corr}} \sim \alpha^2 T/(T\tau_{12}) = \alpha^2/\tau_{12},$$

corresponding to the drag resistivity

$$\rho_D^{\text{corr}} \sim \alpha^2/(T\tau_{12}),$$

which overcomes the third-order drag contribution $\rho_D^{(3)} \sim \alpha^3$ at $1/\tau_{12} > \alpha T$. This happens in the perturbative regime ($1/\tau > \alpha^2 T$ for moderately correlated disorder, $\tau_{12} \sim \tau$), where the correlated-disorder contribution can be calculated diagrammatically.

Macroscopic inhomogeneities can be described in terms of macroscopic spatial fluctuations $\delta\mu_i$ in chemical potentials of the two layers (Song and Levitov, 2012), characterized by the correlation function

$$F_{ij}^{(\mu)}(\mathbf{r} - \mathbf{r}') = \langle \delta\mu_i(\mathbf{r})\delta\mu_j(\mathbf{r}') \rangle \neq 0. \quad (115)$$

Assuming the spatial scale of the fluctuations to be much larger than all characteristic scales related to the particle scattering, one can solve the hydrodynamic equations locally, yielding the local drag rate

$$1/\tau_D(\mathbf{r}) \sim \alpha^2 N\mu_1(\mathbf{r})\mu_2(\mathbf{r})/T. \quad (116)$$

Averaging over the small fluctuations of the correlated chemical potentials, one arrives (Schütt *et al.*, 2013) at the correction to the universal third-order result (114),

$$\Delta\rho_D(\mu = 0) \sim \frac{\hbar}{e^2} \frac{\alpha^2 F_{12}^{(\mu)}(0)}{T^2} (1 + \alpha^2 NT\tau). \quad (117)$$

Finally, in the ultraclean limit

$$1/\tau \ll \alpha^2 N F_{ii}^{(0)}/T, \quad (118)$$

one can approximate the local drag resistivity by an analog of Eq. (104):

$$\Delta\rho_D(\mathbf{r}; \mu = 0) \sim \frac{\hbar}{e^2} \alpha^2 \frac{\delta\mu_1 \delta\mu_2}{\delta\mu_1 \delta\mu_1 + \delta\mu_2 \delta\mu_2}. \quad (119)$$

In particular, for perfectly correlated chemical potentials, $\delta\mu_1(\mathbf{r}) = \delta\mu_2(\mathbf{r})$, the fluctuations drops out from Eq. (119) and the local resistivity turns out to be independent of \mathbf{r} . In a more general case, the averaging over fluctuations becomes nontrivial, but this can only affect

the numerical prefactor in the final result. Thus, the correlated large-scale fluctuations of the chemical potentials in the layers in effect shift the curve 1 in Fig. 18 upwards, extending the validity of the fully equilibrated result,

$$\rho_D \sim (h/e^2)\alpha^2, \quad (120)$$

to the case of finite disorder, Eq. (118), at the Dirac point. This implies that in the case of correlated inhomogeneities the disorder-induced dip in the lower left panel of Fig. 23 develops only for sufficiently strong disorder.

V. COULOMB DRAG AT THE NANOSCALE

The effects of Coulomb interaction are especially pronounced at the nanoscale. In quantum dot devices one can utilize the Coulomb-modified Fano resonance to detect the electric charge (Johnson *et al.*, 2004). Two-level pulse technique was used to detect individual electron spin (Elzerman *et al.*, 2004). Quantum dots were also used as high-frequency noise detectors (Onac *et al.*, 2006). Transport measurements on adjacent but electrically isolated quantum point contacts (QPCs) exhibit a counterflow of electrons [i.e. detector current flowing in the direction opposite to the driving current (Khrapai *et al.*, 2007)]. In nanosize CdSe-CdS semiconductor tetrapods (Mausser *et al.*, 2010), Coulomb drag-like effects lead to photoluminescent emission.

Theoretically, Coulomb drag in a system of two electrically isolated QPCs was considered in (Levchenko and Kamenev, 2008a). Within the linear response the drag mechanism was found to be similar to that in the bulk 2D electron systems. Remarkably, already for seemingly modest drive voltages (much smaller than temperature) the system crosses over to the nonlinear regime, where the effect is dominated by the excess shot noise of the drive circuit. Nonlinear transport was also found to be crucial for drag effects in a system of parallel quantum dots (Moldoveanu and Tanatar, 2009). An exciting new development is the proposal to use the drag effects to study transport properties of polaritons in optical cavities and, in particular, their superfluidity (Berman *et al.*, 2010a,b).

A. Quantum dots and quantum point contacts

Interactively coupled mesoscopic and nanoscale circuits, such as quantum wires (Debray *et al.*, 2000, 2001; Laroche *et al.*, 2011; Morimoto *et al.*, 2003; Yamamoto *et al.*, 2006), quantum dots (Aguado and Kouwenhoven, 2000; Onac *et al.*, 2006) or point contacts (Khrapai *et al.*, 2006, 2007), provided new fruitful ways of studying Coulomb drag phenomena and revealed a plethora of interesting physics. These devices typically have dimensions smaller than the temperature length $L_T = v_F/T$

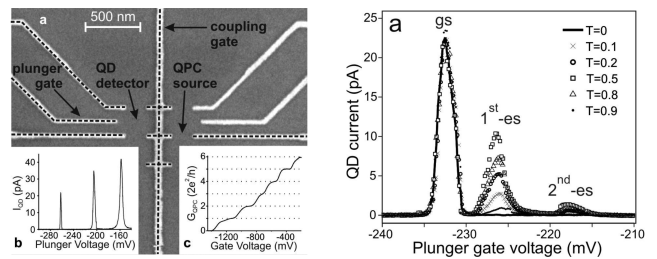


FIG. 28 Left panel inset-(a) represents scanning electron micrograph of the gate structure defined on top of the semiconductor heterostructure. The gates highlighted by dashed lines are used to define a quantum dot (QD) on the left and a quantum point contact (QPC) on the right. Inset-(b) shows current I_{QD} versus plunger gate voltage whereas inset-(c) displays QPC conductance G_{QPC} as a function of the gate voltage. In such device the QPC is used as a noise generator and the QD as a detector. Right panel shows current through the QD, as a function of the plunger gate voltage, under the influence of shot noise generated by the QPC with characteristic peaks. [Reproduced from Onac *et al.* (2006).]

and voltage-related length scale $L_V = v_F/(eV)$, and differ substantially from their two-dimensional quantum-well counterparts in several important ways. (i) The strength of Coulomb interaction is naturally enhanced by reducing system size that should lead to more profound dragging effect. (ii) Transmission across the device in the drag (drive) circuit or both can be efficiently controlled by the gate voltages that allows to open quantum conduction channels one by one. (iii) The electron-hole symmetry in such devices is broken much stronger than in bulk systems. In mesoscopic devices this is due to a random configurations of impurities, while in the quantum nanocircuits the effect is due to the energy dependence of transmission coefficients in Landauer picture of transport (Büttiker *et al.*, 1985; Landauer, 1957, 1970). (iv) Because of the above reasons, the quantum circuits may be easily driven out of the linear response domain and corresponding voltage scale is parametrically smaller than the temperature. (v) Ultimately, the mere mechanism of drag in the nonlinear regime is different and governed by the quantum noise fluctuations.

The most peculiar feature of the observed Coulomb drag in such systems was that the drag current exhibited maxima for specific values of the gate voltage, where the drive circuit was tuned to an opening of another conductance channel, see Fig. 28 for the illustration. This hinted the importance of the electron shot noise in the drive circuit, which was known to exhibit a qualitatively similar behavior (Lesovik, 1989; Reznikov *et al.*, 1995). Indeed, electron current shot noise power is proportional to the product of the transmission and reflection coefficients that is peaked between the conductance plateaus. It was argued early on that drag may be interpreted as a rectification of nearly equilibrium classical thermal fluctuations.

tuations in the drive circuit (Kamenev and Oreg, 1995). The extension of this idea to rectification of the quantum shot noise was plausible and happened to be correct in a certain regime. The subtlety of this picture was that such a rectification is only possible due to electron-hole asymmetry in both circuits, otherwise drag currents of electrons and holes cancel each other. The mismatch between transmission probabilities of electron and hole excitations is maximal at the verge of an opening of the new conduction channel, which implies that spikes of drag conductance may originate from the asymmetry alone rather than shot noise.

In order to get an insight into these delicate details consider the linear response regime when drag conductance g_D can be expressed as follows (Levchenko and Kamenev, 2008a)

$$g_D = \int \frac{d\omega}{8\pi T} \frac{|Z_{12}(\omega)|^2}{\omega^2} \frac{\Gamma_1(\omega)\Gamma_2(\omega)}{\sinh^2(\omega/2T)}. \quad (121)$$

Here $Z_{12}(\omega)$ is the interactively-induced trans-impedance relating local fluctuating currents and voltages between the circuits (Geigenmüller and Nazarov, 1991). The corresponding rectification coefficients are given explicitly by

$$\Gamma_i(\omega) = \frac{2e}{R_Q} \sum_n \int d\epsilon [f(\epsilon_-) - f(\epsilon_+)] [|\mathbf{t}_{in}(\epsilon_+)|^2 - |\mathbf{t}_{in}(\epsilon_-)|^2] \quad (122)$$

where $R_Q = 2\pi\hbar/e^2$ is the quantum of resistance, $\epsilon_{\pm} = \epsilon \pm \omega/2$, $f(\epsilon)$ is the Fermi distribution function, and $|\mathbf{t}_{in}|^2$ is the energy dependent transmission coefficient in the transversal channel n of the circuit $i = 1, 2$. This expression admits a transparent interpretation: potential fluctuations with frequency ω , say on the left of the quantum point contact, create electron-hole pairs with energies ϵ_{\pm} on the branch of right moving particles. Consequently the electrons can pass through the quantum point contact with the probability $|\mathbf{t}_{in}(\epsilon_+)|^2$, while the holes with the probability $|\mathbf{t}_{in}(\epsilon_-)|^2$. The difference between the two gives the net current flowing across the contact while the Fermi functions in Eq. (122) take care of the statistical occupation of participating scattering states. Notice that unlike in the Landauer formula for conductance of a single quantum point contact where transmissions can be treated as being energy independent, the energy dependence of these probabilities in the drag formula is crucial in order to have the asymmetry between electrons and holes, and thus nonzero rectification $\Gamma_i(\omega)$. A particular functional dependence of Γ on frequency depends on a model and details of device circuitry. It is instructive to focus on a limit of a single partially open channel in a smooth adiabatic quantum point contact. One may think then of the potential scattering barrier across it as being practically parabolic. In such a case its transmission probability is given by

$$|\mathbf{t}_{in}(\epsilon)|^2 = [\exp[(eV_{gi} - \epsilon)/\Delta_i] + 1]^{-1} \quad (123)$$

where Δ_i is an energy scale associated with the curvature of the parabolic barrier in the point contact i , while gate voltages V_{gi} move the top of the barrier relative to the Fermi energy within each of the point contact. This form of transmission was used to explain quantum point contact conductance quantization (Glazman *et al.*, 1988) and it turns out to be useful in application to the Coulomb drag problem. For the low temperature limit $T \ll \Delta_i$ using Eq. (123) in Eq. (122) and carrying out energy integration yields

$$\Gamma_i(\omega) = \frac{2e\Delta_i}{R_Q} \ln \left[\frac{\cosh(eV_{gi}/\Delta_i) + \cosh(\omega/\Delta_i)}{\cosh(eV_{gi}/\Delta_i) + 1} \right]. \quad (124)$$

In the opposite limit when $T \gg \Delta_i$ one should replace $\Delta_i \rightarrow T$. One should notice that for small frequency $\Gamma_i \propto \omega^2$ whereas trans-impedance $Z_{12}(\omega)$ is practically independent of frequency in this limit since its characteristic scale is typically set by the inverse RC -time of circuits. Assuming that $T \ll \max\{\Delta_i, \tau_{RC}^{-1}\}$ one arrives at

$$\frac{g_D}{g_Q} = \frac{\pi^2 u^2}{6} \frac{T^2}{\Delta_1 \Delta_2} \frac{1}{\cosh^2(eV_{g1}/\Delta_1) \cosh^2(eV_{g2}/\Delta_2)}, \quad (125)$$

where $u = Z_{12}(0)/R_Q$. The resulting expression for the drag conductance exhibits peaks as a function of gate voltage in drag or drive quantum point contact. Yet at this level it has nothing to do with the shot noise peaks, but rather reflects rectification of near-equilibrium thermal fluctuations (hence proportionality to T^2) along with the electron-hole asymmetry (hence a nonmonotonic dependence on V_{gi}). However, one should realize that the crossover to the nonlinear regime of transport in such devices can occur at rather low voltages $eV^* \sim T^2/\Delta_i$ such that Eq. (121) becomes inapplicable already at $V > V^*$. More general considerations by (Chudnovskiy, 2009; Levchenko and Kamenev, 2008a; Sánchez *et al.*, 2010) revealed that for the out of equilibrium nonlinear regime the drag current is due to the rectification of the quantum shot noise and hence proportional to the Fano factor $\sum_n |\mathbf{t}_{ni}|^2 [1 - |\mathbf{t}_{ni}|^2]$. It again exhibits a generic nonmonotonic behavior of drag with multiple peaks but for the entirely different reason independent of asymmetry factor. Nonlinear transport was also found to be crucial for drag effects in a system of parallel quantum dots (Moldoveanu and Tanatar, 2009).

Drag phenomena in quantum circuits can be naturally connected to our earlier discussion of drag in mesoscopic systems in Sec. III. Indeed, one or both circuits may be represented by a multichannel quasi-one-dimensional (or two-dimensional) mesoscopic sample. In this case $\sum_n |\mathbf{t}_n(\epsilon)|^2 = g(\epsilon)$ is a dimensionless (in units R_Q^{-1}) conductance of the sample as a function of its Fermi energy. As discussed above, such conductance exhibits universal fluctuations, that is $g(\epsilon) = g + \delta g(\epsilon)$, where $g \gg 1$ is an average conductance and $\delta g(\epsilon) \sim 1$ is a sample and

energy-dependent fluctuating part. Since the characteristic scale of the energy dependence of the fluctuating part is the Thouless energy E_T one naturally finds from Eq. (122) that corresponding mesoscopic fluctuations of the rectification coefficient are of the order

$$\Gamma(\omega) \sim \pm \frac{e}{R_Q} \frac{\omega^2}{E_T} \quad (126)$$

This result ultimately leads to the an estimate of the variance of drag in the form of Eq. (58)

Quantum Coulomb drag circuits provide a rich platform to explore nanoscale transport far beyond ideas of using them for high-frequency noise sensing. In particular, a different drag effect may also be observed in the absence of any drive current if one nanocircuit is made hotter than the other - the cold circuit is expected to rectify the thermal charge fluctuations of the hot circuit (Sothmann *et al.*, 2012). Furthermore, interactively coupled devices provide unique tools to test nonlinear fluctuation-dissipation relations and its closely related Onsager symmetry relations in the far from equilibrium conditions when detailed balance is explicitly broken (Bulnes Cuetara *et al.*, 2013; Sánchez *et al.*, 2010).

Other intriguing examples include nanosize CdSe-CdS semiconductor tetrapods (Mauser *et al.*, 2010) where Coulomb drag-like effects lead to photoluminescent emission. As an alternative to optical probes, electrical read-out of a single electron spin becomes possible in a Coulomb drag-like devices of interactively coupled QPC and QD (Elzerman *et al.*, 2004).

B. Optical cavities

Coulomb interaction is not exclusive to electrons and can couple any charges. Moreover, even neutral, composite objects may interact with charges by means of an effective “polarization” or “charge-dipole” interaction (Margenau and Kestner, 1969), which ultimately stems from the Coulomb interaction between an external charge and individual charged constituents of the composite object. In particular, long-ranged interactions between spatially separated electrons and polaritons may lead to interesting drag effects (Berman *et al.*, 2010a,b; Kulakovskii and Lozovik, 2004) that can be used, e.g., for designing electrically controlled optical switches (Berman *et al.*, 2014).

Two-dimensional excitonic polaritons have been a subject of intensive research (Amo *et al.*, 2009; Balili *et al.*, 2007; Kasprzak *et al.*, 2006; Snoke, 2008). These excitations appear as a result of resonant exciton-photon interaction in a system consisting of an optical microcavity and a quantum well embedded within the cavity. The lower polariton branch is characterized by extremely small effective mass raising the possibility of achieving

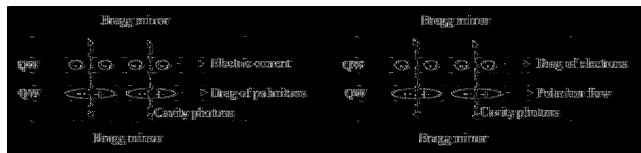


FIG. 29 Left: quasiparticle flow in the cavity polariton subsystem induced by the electric current in the 2DEG at low temperatures. Right: electric current in the 2DEG induced by the optically excited flow in the polariton subsystem. [Reproduced from Berman *et al.* (2010b).]

the Bose-Einstein condensation and superfluidity at relatively high temperatures (Balili *et al.*, 2007; Littlewood, 2007).

The optically excited excitons in microcavities should not be confused with the spontaneously formed excitons in double quantum wells discussed in Sec. VII.A. In particular, these excitons can be excited by laser pumping in the single quantum well embedded within the cavity. Now, if a second quantum well is added to the device (Berman *et al.*, 2010a), then Coulomb interaction binding electrons and holes into excitons can be screened (Finkelstein *et al.*, 1995; Gubarev *et al.*, 2000) by a 2DEG populating the second well. As a result, the excitonic binding energy is reduced and as the density of the 2DEG approaches a certain critical value, the excitons may disappear altogether. The excitonic collapse manifests itself through disappearance of the corresponding line in the photoluminescence spectrum.

Keeping the electron density below the above critical value, one obtains a system containing coexisting, spatially separated excitons and electrons. The effective interaction between electrons and excitons was considered in Lozovik and Nikitkov (1999). This interaction leads to mutual friction between the two systems that can be observed by selectively exciting one of them by external probes.

By focusing laser pumping on a particular region within the cavity, one can generate a gradient of exciton and polariton densities. These gradients induce a flow of both polaritons and excitons. The long-range interaction between the excitons (or the exciton component of the polaritons) may transfer energy and momentum to the electronic system in the second quantum well, generating an electric current or inducing voltage, similarly to the standard drag effect discussed in Sec. II.

Alternatively, one can drive a current through the 2DEG. In this case, the mutual friction will lead to the appearance of the exciton flow. These excitons are entangled with cavity photons and their flow will create a flow of polaritons. In other words, the long-ranged electron-exciton interaction allows one to effectively “move” the cavity photons by applying electric current to the 2DEG (Berman *et al.*, 2010a,b). The drag effects in microcavi-

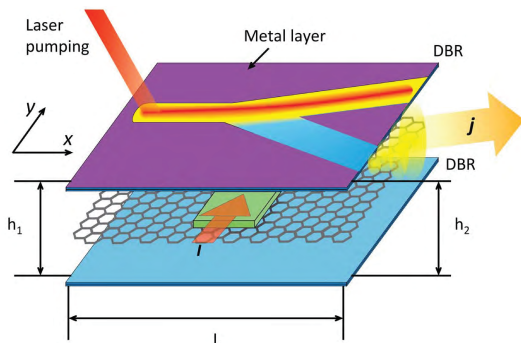


FIG. 30 (Color online) Schematic of the wedge-shaped microcavity formed by two distributed Bragg reflectors (DBR) that encompasses the embedded quantum wells. The excitons are located in the quantum well (gray) between the reflectors. A metal layer deposited on the upper DBR creates a Y-shaped potential energy landscape for the polaritons. The driving current runs perpendicularly to the stem of the channel in the quantum well (green). Reprinted with permission from Berman *et al.* (2014). Copyright (2014) American Chemical Society.]

ties are schematically illustrated in Fig. 29.

Recently, Berman *et al.* (2014) have proposed to use the drag effect in optical cavities for building an electrically controlled optical switch, see Fig. 30. The polaritons are assumed to be created at a constant rate by external laser pumping. The wedge-like shape of the microcavity is chosen in order to create a force driving the polaritons along the cavity towards the Y-junction. Without the drag effect, the polariton flux is distributed equally between the two branches of the junction. Driving an electric current through a second quantum well (shown in green in Fig. 30) results in a drag force in the junction region that effectively redistributes the polaritons flux between the branches. Berman *et al.* (2014) find that for realistic parameters of the device one can achieve 90% accuracy of the switching of the polariton flow.

VI. COULOMB DRAG BETWEEN PARALLEL NANOWIRES

It is well-known that physics of electrons confined to one spatial dimension (1D) is dominated by interactions. Coulomb drag between two closely spaced but electrically isolated quantum wires was used to observe Wigner crystallization (Yamamoto *et al.*, 2002, 2006, 2012) and Luttinger-liquid effects (Debray *et al.*, 2001; Laroche *et al.*, 2008, 2014). The effect was also used to study 1D sub-bands in quasi-1D wires (Debray *et al.*, 2000; Laroche *et al.*, 2011).

Early theoretical work on drag between 1D systems (Gurevich and Muradov, 2000, 2005; Gurevich *et al.*,

1998; Hu and Flensberg, 1996; Raichev and Vasilopoulos, 2000a,b, 1999) was based on the Fermi-liquid approach and targeted multiple-channel wires at high enough temperatures, where electron correlation effects (other than screening) are not important. Tanatar (1998) considered the role of disorder. It is however well-known, that the Fermi-liquid theory fails for purely 1D systems, i.e. single-channel wires (Giamarchi, 2004), quasi-1D wires with single 1D subband occupancy (Laroche *et al.*, 2014), and systems comprising a small number of coupled 1D channels. Coulomb drag between two Luttinger liquids with point-like interaction region was discussed in Flensberg (1998) and Komnik and Egger (2001). Nazarov and Averin (1998) considered two independent Luttinger liquids coupled by interwire backscattering. Schlottmann (2004a,b) used Bethe-Ansatz methods to solve the problem of two wires coupled by a particular δ -function potential. Especially interesting is the prediction of the Mott-insulator-type state corresponding to formation of two interlocked charge density waves (CDW) in quantum wires (Fuchs *et al.*, 2005; Klesse and Stern, 2000) [see also a recent preprint (Furuya *et al.*, 2015)].

A theory of Coulomb drag based on the Tomonaga-Luttinger liquid (TLL) theory (Haldane, 1981a,b; Luttinger, 1963; Tomonaga, 1950) predicts a behavior that qualitatively deviates from that in higher dimensions. Below a certain crossover scale T^* , the drag resistivity between *infinitely long quantum wires of equal electron density* is predicted to increase exponentially with decreasing temperature (Klesse and Stern, 2000)

$$\rho_D \sim \rho_T \exp(\Delta/T). \quad (127)$$

The energy gap Δ and crossover temperature T^* are complicated functions of the interwire distance d , width of wires w , effective Bohr radius a_B of the host material, and electron density n . For widely separated wires ($k_F d \gg 1$) they are exponentially suppressed

$$\Delta \sim T^* \sim E_F \exp[-k_F d/(1-K)], \quad (128)$$

and the drag resistivity exhibits the high-temperature power-law behavior²⁰

$$\rho_D \sim (h/e^2) k_F \lambda^2 (T/E_F)^{4K-3}, \quad (129)$$

for all practically relevant scales. Here K is the TLL interaction parameter in the relative charge sector determined by the difference of the small-momentum intra- and interwire couplings and λ is dimensionless interwire backscattering potential strength.

The physical picture behind Eq. (127) is that at low temperatures $T < T^*$ the electrons in both wires form

²⁰ In 1D, $\rho_D = -\lim_{I_1 \rightarrow 0} (1/L)(dV_2/dI_1)$, is the drag resistivity per unit length (Klesse and Stern, 2000; Pustilnik *et al.*, 2003).

zigzag-ordered interlocked charge density wave (CDW). Then a relative charge displacement can be created only by overcoming a potential barrier, which ultimately translates into transport via activation, and consequently into Arrhenius-like behavior of drag.

For short wires, Klesse and Stern (2000) report a qualitatively different behavior. Here the CDW in one wire may slip as a whole relative to the CDW in the other wire. These instantaneous slips may stem from either thermal fluctuations or tunneling events. The latter leads to the drag resistance that tends to a finite, but exponentially large (in the wire length L) value as $T \rightarrow 0$. In contrast, Ponomarenko and Averin (2000) find a vanishing drag resistance, $\rho_D \sim T^2$, regardless of whether the CDW is formed or not.

For wires with different electron densities, Fuchs *et al.* (2005) find that the drag resistance (127) is suppressed by an additional exponential factor $\exp(-|\delta\mu|/T)$, where $\delta\mu = \mu_1 - \mu_2$ is the difference between the chemical potentials μ_i in the two wires. The high-temperature result (129) also becomes exponentially suppressed as soon as $|\delta\mu|$ exceeds the temperature.

Allowing for a spin degree of freedom adds extra complexity to the problem, since the system might be unstable towards gap opening in the spin sectors²¹. If this does not happen (or at temperatures exceeding the spin gaps), the system shows the same qualitative behavior as above, but the exponent in Eq. (129) changes to $2K - 1$. However, if the single wires develop spin gaps, the drag resistivity vanishes at $T = 0$ (Klesse and Stern, 2000).

At temperatures above T^* , the charge sector is gapless and the system can be described as two coupled wires in the TLL phase. For quasiparticles with linear dispersion the only process contributing to drag is the interwire backscattering characterized by large momentum transfers $q \sim 2k_F$. This process can be described by the usual drag formula (15), where one typically assumes the nonlinear susceptibility to be proportional to the imaginary part of the polarization operator (Fiete *et al.*, 2006; Pustilnik *et al.*, 2003):

$$\rho_D = \frac{h}{e^2} \int \frac{dq d\omega}{4\pi^3} \frac{q^2 V_q^2}{n^2 T} \frac{[\text{Im}\Pi(q, \omega)]^2}{\sinh^2(\omega/2T)}, \quad (130)$$

where V_q describes the interwire interaction. In the limit $qd \gg 1$, the asymptotic form of V_q is given by $V_q = (e^2/\epsilon)\sqrt{2\pi/(qd)} \exp(-qd)$. The polarization operator for the TLL model is known (Giamarchi, 2004). For spinless fermions, the spectral weight of $2k_F$ density fluctuations

is given by

$$\begin{aligned} \text{Im}\Pi(q_{\pm}, \omega) &= -\frac{\sin \pi K}{4\pi^2 u} \left(\frac{2\pi\alpha T}{u} \right)^{2K-2} \\ &\times B\left(\frac{K}{2} - \frac{i(\omega - uq_{\pm})}{4\pi T}, 1 - K\right) \\ &\times B\left(\frac{K}{2} - \frac{i(\omega + uq_{\pm})}{4\pi T}, 1 - K\right), \end{aligned} \quad (131)$$

where $\alpha \sim k_F^{-1}$ is the short-distance cut-off of the TLL theory, $q_{\pm} = q \pm 2k_F$, u is the renormalized Fermi velocity, and $B(x, y)$ is the Euler beta-function. Using Eq. (131) in the expression (130) one recovers Eq. (129), which was obtained by Klesse and Stern (2000) by means of a renormalization group analysis. In the perturbative approach, the interaction parameter λ in Eq. (129) is given by $\lambda = V_{2k_F}/v_F$. This leads to the exponential dependence of ρ_D on distance separating the wires [since $V_{2k_F} \propto \exp(-2k_F d)$]. The regime of spin-incoherent Luttinger liquid and effect of disorder modify temperature dependence of Eq. (129) (Fiete *et al.*, 2006). In the weakly interacting limit ($K \simeq 1$) the drag resistivity is expected to grow linearly with temperature (Gurevich *et al.*, 1998; Hu and Flensberg, 1996).

In recent years, a lot of the attention was devoted to 1D liquids with nonlinear dispersion [for reviews on this topic see Deshpande *et al.* (2010); Imambekov *et al.* (2012); and Matveev (2013)]. In the TLL theory, the curvature of the quasiparticle spectrum is described by an irrelevant operator (in the renormalization group sense). However, at high enough temperatures it might lead to important effects and even mask the pure Luttinger behavior. In the context of Coulomb drag (Aristov, 2007; Dmitriev *et al.*, 2012; Pereira and Sela, 2010; Pustilnik *et al.*, 2003; Rozhkov, 2008, 2009), this is particularly important since nonlinearity of the band kinematically allows drag with small momentum transfer, $q \sim T/v_F \ll k_F$.

Analytic calculation of the dynamical structure factor $\text{Im}\Pi(q, \omega)$ for arbitrary interactions and nonlinear dispersion is a major challenge. However, such calculation is readily available in the case of weakly interacting electrons. At finite temperatures, but with the accuracy of the order $T \ll mv_F^2$, the one-loop diagram yields

$$\text{Im}\Pi(q, \omega) = \frac{m}{4k} \frac{\sinh(\omega/2T)}{\cosh(qv_F\xi_+/2T) \cosh(qv_F\xi_-/2T)}, \quad (132)$$

where $\xi_{\pm} = 2m(\omega - v_F q)/q^2 \pm 1$. It is now tempting to follow the conventional path and use this result for $\text{Im}\Pi$ in the expression for the drag (130) to obtain

$$\rho_D \simeq (hk_F/e^2)(V_0/v_F)^2(T/E_F)^2, \quad (133)$$

with the conclusion that curvature effects restore the Fermi-liquid behavior of drag in 1D wires; furthermore, the contribution (133) would dominate over the

²¹ For a comprehensive discussion of ground state properties of capacitively coupled 1D systems see Carr *et al.* (2013) and Giamarchi (2004).

backscattering component (129) already at temperatures above $T > E_F e^{-4k_F d}$ [in Eq. (133) V_0 should be understood as $V_{q \sim T/v_F}$]. At even higher temperatures, $(v/d) < T < E_F$, the same approach yields a saturating drag resistivity, $\rho_D \sim (\hbar k_F/e^2)(V_0/v_F)^2(v/dE_F)^2$, followed by a falloff $\rho_D \propto 1/T^{3/2}$ at $T > E_F$. For non-identical wires there appears an additional energy scale, $T_\delta = k_F|\delta v|$ describing splitting between symmetric and antisymmetric plasmons modes in the double-wire system, which is determined by the difference between Fermi velocities in the wires $\delta v = v_{F1} - v_{F2}$. Assuming that $T_\delta \ll T_d$, Eq. (133) holds only for $T_\delta < T < T_d$, whereas below T_δ drag resistivity due to forward scattering decreases as $\rho_D \propto T^5$ with lowering temperature.

However, as shown by Dmitriev *et al.* (2012) the above conclusions about the forward scattering contribution to drag may be premature. The reason is subtle: the expression (130) was derived under the tacit assumption that the intralayer relaxation processes due to electron-electron interaction are faster than the interwire momentum transfer. Now, in purely 1D systems relaxation is determined by three-body collisions (Levchenko *et al.*, 2011; Lunde *et al.*, 2007; Micklitz *et al.*, 2010; Rieder *et al.*, 2014) as inelastic two-body interaction is forbidden by energy and momentum conservation. Same kinematic restrictions require that intrawire backscattering responsible for equilibration involves states deep at the bottom of the band. Because of the Pauli statistics, the probability to find such a state unoccupied is exponentially small. Consequently, the equilibration rate τ_{eq}^{-1} in 1D is exponentially suppressed, $\tau_{eq}^{-1} \propto e^{-E_F/T}$, and the expressions (130) and (133) are difficult to justify.

At the same time, interwire backscattering with small momentum transfer $q \sim T/V_F \ll k_F$ is also allowed in 1D systems with nonlinear spectrum. This process involves a pair of scattering states: one near the Fermi level and another at the bottom of the band. Dmitriev *et al.* (2012) found a solution of two coupled kinetic equations [cf. Eqs. (9)] yielding the drag resistivity in the form

$$\rho_D \simeq \frac{\hbar k_F}{e^2} \left(\frac{V_0}{v_F} \right)^2 \frac{1}{k_F d} \frac{T_d}{T} \sqrt{\frac{E_F}{T}} e^{-2E_F/T}. \quad (134)$$

By comparing the exponential factors in Eqs. (134) and (129), one can see that backscattering-induced drag friction due to soft collision (namely collisions with small momentum transfer) dominate over direct backscattering with $2k_F$ momentum transfer at temperatures $T > T_d$. This is despite the fact that the contribution of soft collisions being strongly suppressed compared to Eq. (133).

At even higher temperatures there exists delicate interplay between the relaxation rates of two-particle interwire backscattering with small momentum transfer and triple-body intrawire chirality changing soft collisions that determine behavior of $\rho_D(T)$. Each of these scattering processes can be described by respective functions $\mathcal{D}_2(T)$ and $\mathcal{D}_3(T)$, which physically correspond to

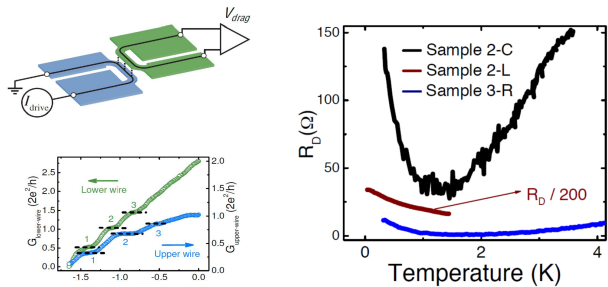


FIG. 31 (Color online) Left: measurement schematic (top) and single-wire conductance quantization (bottom). Right: temperature dependence of the drag signal for three different samples (the magnitude of ρ_D in sample 2-L is divided by 200 for visibility). For samples 2-L and 2-C, the temperature dependence was taken with no more than one 1D subband occupancy in each wire, whereas the number of 1D subband occupied in sample 3-R is known to be bounded by $0 < N_{drive} \leq 2$ and $0 < N_{drag} \leq 3$. [From Laroche *et al.* (2014). Reprinted with permission from AAAS.]

diffusion coefficients in momentum space. Their functional form is not universal and determined by the interaction model considered. Three-particle collisions dominate provided that $\mathcal{D}_3 > \mathcal{D}_2 e^{-E_F/T}$. This condition implicitly defines new crossover temperature scale $T_c > T_d$ at which Eq. (134) crosses over to (Dmitriev *et al.*, 2012)

$$\rho_D \simeq \frac{\hbar}{e^2} \frac{\mathcal{D}_3}{k_F E_F} \left(\frac{E_F}{T} \right)^{3/2} e^{-E_F/T}. \quad (135)$$

Notice that in this transport regime ρ_D is suppressed only by a single exponential factor. In the case of short-ranged interaction $\mathcal{D}_3 \propto T^2$ whereas \mathcal{D}_2 is temperature independent so that the pre-exponential factor in Eq. (135) scales with T as $T^{1/2}$. In the case of Coulomb interaction this scaling is different since $\mathcal{D}_3 \propto T^5$.

Coulomb drag between true 1D systems was recently observed by Laroche *et al.* (2014) in a system of vertically integrated quantum wires where each wire has less than one 1D subband occupied. The most striking theoretical prediction, i.e., the upturn in the temperature dependence was revealed below the crossover temperature $T^* \sim 1.6\text{K}$, see Fig. 31. However, a quantitative comparison between the data and above theoretical results proved to be difficult. Using the experimental estimates for the carrier density $n_{1D} = \sqrt{n_{2D}}$ and interwire distance $d \simeq 40\text{nm}$, one arrives at $k_F d \sim 2$. Then, from Eq. (128) one finds the values for the Luttinger parameter $K \simeq 0.1 - 0.2$ (for samples 3-R and 2-C) corresponding to very strong interaction that is beyond the applicability of the bosonization theory of Klesse and Stern (2000). On the other hand, fitting the high-temperature data to the power-law behavior (129) yields $K \simeq 1.5$. This estimate, however, should be approached with caution, since Eq. (129) was derived for identical wires which is not the case in experiment, where electronic densities in the par-

ent 2D layers differ by about 20%. In that case one expects (Fuchs *et al.*, 2005) an exponential suppression of ρ_D . All these issues remain to be clarified both theoretically and experimentally.

VII. NOVEL MANY-BODY STATES IN DOUBLE-LAYER SYSTEMS

When a double-layer system is subjected to a strong magnetic field, the standard theoretical description of Coulomb drag (Jauho and Smith, 1993; Kamenev and Oreg, 1995; Zheng and MacDonald, 1993) fails: in contrast to naive expectations, numerous experiments (Feng *et al.*, 1998; Hill *et al.*, 1996, 1998; Jörger *et al.*, 2000c; Lok *et al.*, 2001a,b; Patel *et al.*, 1997; Pillarisetty *et al.*, 2003; Rubel *et al.*, 1997a, 1998, 1997b) show significant dependence of the measured drag resistivity ρ_D on the applied field, especially in the extreme quantum regime (Lilly *et al.*, 1998; Murphy *et al.*, 1994; Nandi *et al.*, 2012).

Further experiments revealed the existence of novel quantum Hall states that are specific to bilayer systems and have no analog in single-layer samples. Early work in this direction was reviewed in Eisenstein (1992, 1997). Remarkably, the bilayer many-body states exhibiting the quantum Hall effect (Murphy *et al.*, 1994) may at the same time support a condensate of indirect (or interlayer) excitons (Finck *et al.*, 2010; Nandi *et al.*, 2012; Wiersma *et al.*, 2007). An interlayer exciton is a bound pair of an electron from one layer and a hole from another layer of the device. The exciton carries no electric charge. Nevertheless, exciton transport (especially in the superfluid state) leads to interesting electrical effects. The experimental situation in the field is reviewed in Eisenstein (2014) and Eisenstein and MacDonald (2004). Here we focus on the manifestations of this exciting new physics in the drag measurements.

A. Quantum Hall Effect in double-layer systems

In a seminal paper, Halperin (1983) has suggested a generalization of the Laughlin wave function for the analysis of multi-component systems. The simplest example of an extra degree of freedom that can be accounted for using this approach is the electron spin. A double-layer system provides another example, which is similar to the spin-1/2 in some respects and is significantly different in other. The two possible values of the layer index can be represented by the two orientations of a pseudo-spin (Stern *et al.*, 2000; Yang *et al.*, 1994). However, unlike the real spin, the double-layer system does not possess the $SU(2)$ symmetry due to the difference between the intra- and interlayer matrix elements of the Coulomb interaction. Consequently, in the double-layer system the

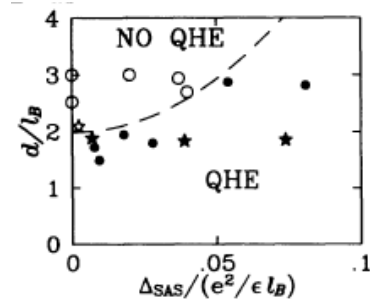


FIG. 32 Phase diagram of the quantum Hall effect at $\nu_T = 1$ in double-layer systems. Δ_{SAS} is the tunnel splitting and $e^2/(\epsilon\ell)$ is the Coulomb energy. Each symbol corresponds to a particular double-layer sample. Only the samples represented by solid symbols exhibit a quantized Hall plateau at $\nu_T = 1$. The interlayer quantum Hall state exists also in the absence of tunneling. [Reproduced from Murphy *et al.* (1994).]

energy eigenstates do not have to be eigenstates of the total spin operator \hat{S}_T (Girvin and MacDonald, 1997). As a result, states described by Halperin's wave functions that are not eigenstates of \hat{S}_T may be realized in double-layers (Eisenstein *et al.*, 1992; Suen *et al.*, 1992).

In this review we are mostly interested in double-layer systems where tunneling between the two layers is negligible. Such systems support novel many-body quantum Hall states, that are specific to bilayers and arise due to interlayer Coulomb interaction (Chakraborty and Pietiläinen, 1987; Haldane and Rezayi, 1987). Yoshioka *et al.* (1989) investigated a wide class of such states using Halperin's two-component wave functions (Halperin, 1983). The ground state of the system crucially depends on the ratio of the interlayer separation and magnetic length d/ℓ_0 . For a given filling factor, the magnetic length ℓ_0 is proportional to the average separation between electrons in one layer. Therefore, the ratio d/ℓ_0 parametrizes the relative strength of intra- and interlayer Coulomb interaction. Assuming truly two-dimensional layers (i.e., setting aside complications that arise due to the finite width of the quantum wells in GaAs samples), one finds that the interlayer many-body states are stable for $d/\ell_0 \sim 1$. At large d , the interlayer Coulomb interaction is inefficient and then the system behaves as if one connects two quantum Hall samples in parallel (Eisenstein, 1997). This observation can be illustrated with the help of the typical phase diagram shown in Fig. 32 for the case of the total filling factor $\nu_T = 1$ (Murphy *et al.*, 1994). In the opposite limit, $d/\ell_0 \rightarrow 0$, the system approaches the $SU(2)$ -symmetric point, and thus the Halperin states that are not eigenstates of \hat{S}_T are expected to collapse (Eisenstein, 1997).

Double-layers at the total filling factor $\nu_T = 1$ and with large interlayer separation (experimentally, $d/\ell_0 \sim 2 - 4$) behave as two weakly coupled systems of composite fermions (i.e. each layer is at $\nu = 1/2$) while exhibit-

ing strongly enhanced drag as compared to the zero-field case, see Sec. II.G. As the ratio d/ℓ_0 is decreased, experiments (Kellogg *et al.*, 2003, 2002b) show a gradual development of the Hall drag signal and a non-monotonic behavior of the longitudinal drag resistivity ρ_D . As d/ℓ_0 approaches the transition into the strongly correlated, many-body state ²², ρ_D shows strong enhancement, followed by a decrease. In the strongly coupled interlayer $\nu_T = 1$ state ρ_D practically vanishes. At the same time, the Hall drag resistance develops a quantized plateau, see Fig. 33. Similar behavior was observed in Tutuc *et al.* (2009, 2004); and Wiersma *et al.* (2004)

Early theoretical work on drag in quantum Hall states was focused on the non-dissipative drag (Duan, 1995; Renn, 1992; Yang, 1998; Yang and MacDonald, 2001). In contrast to the case of weak magnetic field (see Sec. II.G), a strong, quantized Hall drag has been identified as a signature of the interlayer correlated states. The 2×2 Hall resistivity matrix (for the two layers) has been shown (Renn, 1992; Yang, 1998) to be proportional to the Gram matrix (Conway and Sloane, 1988; Read, 1990) describing topological order in the quantum Hall state (Wen, 1995):

$$\rho_{ij}^{xy} = (h/e^2)K_{ij} \Rightarrow \rho_{12}^{xy} = nh/e^2, \quad n > 0. \quad (136)$$

Similar conclusion was reached in Yang and MacDonald (2001) on general topological grounds.

Kim *et al.* (2001) have suggested to use the drag resistivity to distinguish between various quantum Hall states in double-layer systems at $\nu_T = 1$. For the compressible (weak-coupling) state at large interlayer separation, the Hall drag resistivity vanishes, while the longitudinal drag is determined by gauge-field fluctuations and is given by Eq. (53). The compressible state exhibits a strong pairing instability (Bonesteel, 1993; Greiter *et al.*, 1991). If Landau-level mixing is substantial (as it often is in experimental samples), the paired state may be described by the $(3, 3, -1)$ Halperin wave function. This state resembles a $p_x + ip_y$ superconductor of composite fermions. As a result, it is expected to exhibit the quantized Hall drag resistivity (136) with $n = -1$.

For smaller interlayer separation ($d \simeq \ell_0$) the system undergoes a transition into an incompressible, correlated “quantum Hall ferromagnet” state described by the $(1, 1, 1)$ Halperin wave function. This state possesses a gapless neutral mode and is characterized by the Hall resistivity (136) with $n = 1$.

The nature of the transition between the compressible, weak coupling state at large interlayer separation

and the incompressible, strong coupling state at $d \simeq \ell_0$ is not completely understood (Eisenstein, 2014; Finck *et al.*, 2010). Numerical evidence (Burkov *et al.*, 2002; Schliemann *et al.*, 2001) suggests a first order transition at $T = 0$, which contradicts the experimental observation of gradual development of the quantized Hall drag (Kellogg *et al.*, 2003, 2002b), see Fig. 33. Stern and Halperin (2002) suggested a phenomenological description of the drag resistivity in the transition region. Postulating that in the transition region the system is split into regions of the strong-coupling $(1, 1, 1)$ phase and regions of the weak-coupling compressible phase, they describe the transition as the point where the fraction f of the sample occupied by the $(1, 1, 1)$ phase reaches the percolation threshold $f_c = 1/2$.

In a system of identical layers, the linear response theory can be formulated in terms of symmetric and antisymmetric states. Denoting the 2×2 resistivity matrices corresponding to symmetric and antisymmetric currents by ρ^s and ρ^a , one finds the drag resistivity as $\rho^D = (\rho^a - \rho^s)/2$.

In the weak-coupling phase at $d \gg \ell_0$, the drag resistivity is very small, $\rho^D \ll \rho^{a(s)}$. Neglecting ρ^D , one may approximate the resistivities as (in units of h/e^2)

$$\rho^a(d \gg \ell_0) = \rho^s(d \gg \ell_0) = \begin{pmatrix} \epsilon & 2 \\ -2 & \epsilon \end{pmatrix}, \quad (137)$$

where $\epsilon = 1/(k_F \ell_{tr}) \ll 1$ (within the composite fermion model), $k_F = 4\pi n$ is the Fermi wave vector, n is the electronic density, and ℓ_{tr} is the transport mean free path. For $T < 1\text{K}$, the experimentally measured values of ρ^D are almost two orders of magnitude less than ϵ .

The strong-coupling $(1, 1, 1)$ phase exhibits features of the quantum Hall state for the symmetric currents

$$\rho_0^s(d \lesssim \ell_0) = \begin{pmatrix} 0 & 2 \\ -2 & 0 \end{pmatrix}, \quad (138)$$

while for the antisymmetric currents it is a superfluid (Stern and Halperin, 2002) $\rho_0^a(d \lesssim \ell_0) = 0$.

Analyzing the system close to the transition as a composite system comprising regions of both phases, Stern and Halperin (2002) have found a phenomenological expression for the drag resistivity

$$\rho_{xx}^D = \frac{8\epsilon f(1-f)(1-2f)}{\epsilon^2 + 4(1-2f)^2}. \quad (139)$$

As f increases from zero, this drag resistivity grows from zero [or rather, the very small value in the compressible state that is neglected in Eq. (139)] reaching a maximum at $f^* \approx 1/2 - \epsilon/4$ (for small ϵ) and again vanishing at the percolation threshold, in qualitative agreement with the non-monotonic drag observed in Kellogg *et al.* (2003, 2002b).

²² Since the transition between the weakly and strongly coupled quantum Hall states is still poorly understood, one should be speaking in terms of the transition region instead of the precise critical value of d/ℓ_0 .

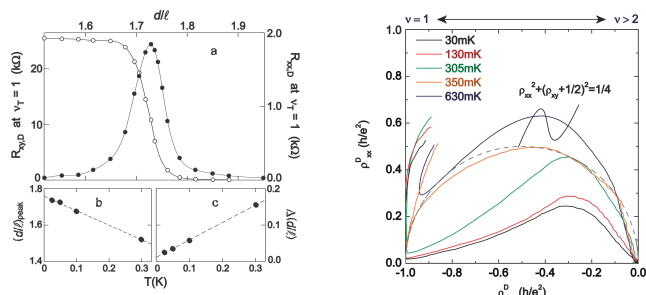


FIG. 33 (Color online) Left: Hall (open dots) and longitudinal (closed dots) drag resistance at $\nu_T = 1$ and $T = 50\text{mK}$ as a function of the ratio d/ℓ_0 . The two lower panels show the temperature dependence of the location and the half-width of the peak in R_{xx}^D . The lines are guides for the eye. [Reproduced from Kellogg *et al.* (2003).] Right: Drag resistivity and Hall drag resistivity in units of h/e^2 for different temperatures. The end points represent the strong- ($\rho_{xy}^D = -1$) and weak-coupling ($\rho_{xy}^D = 0$) regimes. The dashed line represents Eq. (140). [Reproduced from Tutuc *et al.* (2009).]

Furthermore, using the semicircle law (Dykhne and Ruzin, 1994), it can be shown that to the lowest order in ϵ the drag resistivities satisfy the relation (Stern and Halperin, 2002)

$$(\rho_{xy}^D + 1/2)^2 + (\rho_{xx}^D)^2 = 1/4, \quad (140)$$

yielding vanishing Hall drag for the compressible state ($f = 0$) and the quantized value (136) with $n = -1$ for the $(1, 1, 1)$ state at $f \geq 1/2$. Between the two extremes the negative ρ_{xy}^D varies monotonously. The apparent discrepancy in the sign of ρ_{xy}^D obtained by Stern and Halperin (2002) and Kim *et al.* (2001) seem to stem from the alternative definition of drag resistivities. Similar predictions for transport coefficients, in particular Eq. (140), but without the explicit phase separation were obtained by Simon *et al.* (2003). An alternative model invoking the coexistence of the two phases was suggested by Spivak and Kivelson (2005).

The semicircle relation (140) was experimentally tested in Tutuc *et al.* (2009), see Fig. 33. Instead of comparing a number of double-well devices with different interlayer separations (Kellogg *et al.*, 2003), Tutuc *et al.* (2009) varied the electron density and observed the transition between the strong-coupling state at $\nu_T = 1$ and the weakly coupled state at $\nu_T = 2$. The data at intermediate temperatures $T \approx 300\text{K}$ are in a good quantitative agreement with the theory. At the same time, Eq. (140) is only approximate and is expected to hold if the drag resistivity is much larger than the symmetric bilayer resistivity at all fillings. Drag resistivity in the weak-coupling state is also neglected. Given these approximations, the agreement between the data and the phenomenological theory of Stern and Halperin (2002) is satisfactory.

B. Interlayer exciton formation

Further experiments revealed the most intriguing feature of the strong-coupling quantum Hall state at $\nu_T = 1$: the presence of the exciton condensate capable of neutral superfluid transport (Eisenstein, 2014; Eisenstein and MacDonald, 2004). Originally envisioned for optically generated excitons in bulk semiconductors (Blatt *et al.*, 1962; Keldysh and Kopaev, 1964; Keldysh and Kozlov, 1968; Moskalenko, 1962), the phenomenon has been predicted also for indirect excitons in double-layer systems (Lozovik and Yudson, 1976; Shevchenko, 1976).

The quantized Hall effect along with the vanishing longitudinal resistivity at $\nu_T = 1$ indicate a gapped spectrum of charged excitations. In these measurements (Eisenstein, 2014; Eisenstein *et al.*, 1992; Suen *et al.*, 1992), electrical currents in the two layers flow in the same direction. In contrast, the condensate couples to antiparallel or counterflowing currents (Kellogg *et al.*, 2004; Tutuc *et al.*, 2004; Wiersma *et al.*, 2004) and manifests itself through vanishing Hall voltage. The simplest explanation for this observation is based on charge neutrality of excitons: as neutral objects, excitons do not experience the Lorentz force and hence no Hall voltage develops when equal, counter-propagating currents are flowing through the two layers.

Another spectacular manifestation of the exciton condensate is the Josephson-like tunneling anomaly (Finck *et al.*, 2008; Spielman *et al.*, 2000; Tiemann *et al.*, 2008a; Wiersma *et al.*, 2006, 2007; Yoon *et al.*, 2010) that theoretically was predicted in Park and Das Sarma (2006) and Wen and Zee (1992) and later discussed in Dolcini *et al.* (2010).

Finally, the latest experiments revealing the existence of the exciton condensate utilized the multiple connected Corbino geometry (Finck *et al.*, 2011; Nandi *et al.*, 2012; Tiemann *et al.*, 2008a,b). For a theoretical discussion of the superfluid flow in the Corbino geometry see Su and MacDonald (2008). The advantage of the Corbino samples is that they support the exciton flow through the bulk (in contrast to the Hall bar samples where transport is dominated by the edges).

Coulomb drag has played an important role in discovering the interlayer correlated state (Eisenstein, 2014). Quantized Hall drag measured in the simply connected square geometry (Kellogg *et al.*, 2002b) was one of the first indications of anomalous in-plane transport in double-layer systems at $\nu_T = 1$. Remarkably, the quantized Hall voltage has been found to be the same in both layers. At first glance, this contradicts the boundary conditions of the drag measurement: drag experiments involve passing current through one of the layers and measuring the induced voltage in the other, where no current is allowed to flow. The absence of the current seems to yield the absence of the Lorentz force and hence lead to the standard conclusion that no Hall voltage should be

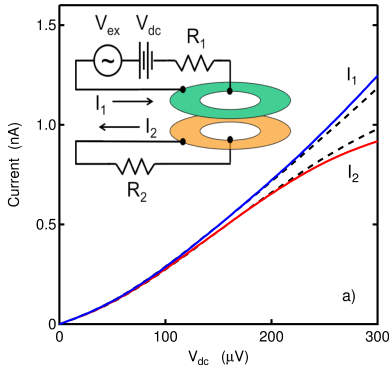


FIG. 34 (Color online) Corbino Coulomb drag. Solid lines show the drive and drag currents. The measurement was performed at $\nu_T = 1$, $T = 17\text{mK}$, and $d/\ell_0 = 1.5$. Dashed lines represent the results of simulations incorporating estimated series resistances and measured Corbino conductivity. The inset shows the measurement schematic. The resistances R_i comprise both external circuit resistors and the resistances intrinsic to the device. [Reprinted by permission from Macmillan Publishers Ltd: Nature, Nandi *et al.* (2012).]

induced in the passive layer, see Sec. II.G. However, this argument does not take into account collective effects. In the presence of the condensate, the driving current can be decomposed into the symmetric and antisymmetric parts (Stern and Halperin, 2002). While the symmetric current carries the electric charge, the antisymmetric – or counterpropagating – current is equivalent to the condensate flow. In the passive layer the two currents cancel each other thus satisfying the boundary condition. At the same time, it is the symmetric, charge-carrying current that can couple to the magnetic field. This current is shared between the layers, yielding the identical quantized Hall voltage across both layers.

Similar arguments lead to the expectation of “perfect” longitudinal drag (Su and MacDonald, 2008): the symmetric current shared between the layers should be responsible not only for the Hall, but also for the longitudinal voltage in the passive layer. This prediction was tested in a dedicated experiment by Nandi *et al.* (2012) using Corbino samples. Deviating from the standard setup, Nandi *et al.* (2012) have closed the electric circuit in the passive layer and measured the induced *current*, rather than the voltage. In this case, perfect drag means that the induced current should be same in magnitude as the driving current passed through the active layer while flowing in the opposite direction. This is exactly what has been observed by Nandi *et al.* (2012), at least for small driving currents, see Fig. 34.

The above arguments neglect the impact of disorder that might affect the presumed dissipationless excitonic transport (Su and MacDonald, 2008) across the bulk of the device (Fertig and Murthy, 2005; Fil and Shevchenko, 2007; Huse, 2005; Lee *et al.*, 2011). Assuming a phe-

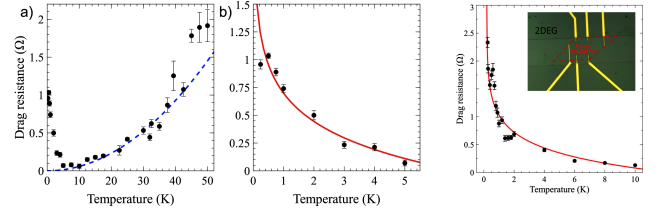


FIG. 35 (Color online) Coulomb drag in a graphene-2DEG vertical heterostructure. Left: measured drag resistivity. The dashed line represents the best fit for the standard temperature dependence $R_D = aT^2$, $a = (5.8 \pm 0.3) \times 10^{-4} \Omega\text{K}^{-2}$. Middle: a fit of the low- T upturn based on Eq. (141). The critical temperature found from the fit is $T_c \sim 10 - 100\text{mK}$. Right: the low- T upturn in a bilayer graphene-2DEG heterostructure. The fit based on Eq. (141) yields $T_c \sim 190\text{mK}$. [Reprinted by permission from Macmillan Publishers Ltd: Nature Communications, Gamucci *et al.* (2014).]

nomenological resistance R_s of the excitonic system, one still finds [neglecting the Corbino conductance (Nandi *et al.*, 2012)] perfect drag $I_1 = I_2 = V/(R_1 + R_2 + R_s)$, where R_i represent the net resistances in series with the Corbino sample, see the inset in Fig. 34. As the magnitude of $R_1 + R_2$ is expected to always exceed $2h/e^2$ (Pesin and MacDonald, 2011; Su and MacDonald, 2008), the ability of the experiment to detect small values of R_s is limited. The issue of dissipation in the excitonic system might be clarified by future multi-terminal measurements.

So far we have discussed experiments on the exciton physics in double-layer systems comprising similar electronic layers (Eisenstein and MacDonald, 2004). It is also possible to create devices with oppositely doped layers, the so-called electron-hole bilayers (Das Gupta *et al.*, 2011; Keogh *et al.*, 2005). Coulomb drag measurements in these systems (Croxall *et al.*, 2008; Seamons *et al.*, 2009) do not provide a direct evidence of interlayer coherence, but nevertheless demonstrate an upturn in ρ_D as the temperature is lowered below 1K. The upturn is seen only in devices with smaller (20nm) interlayer separation suggesting exciton formation.

A microscopic theory of Coulomb drag in proximity to a phase transition was suggested by Hu (2000b) and Mink *et al.* (2012, 2013). As the system approaches the transition temperature T_c from above, the drag resistivity was found to exhibit a logarithmic divergence

$$\rho_D = \rho_0 + A \ln[T_c/(T - T_c)], \quad (141)$$

where ρ_0 and A are two fitting parameters (Gamucci *et al.*, 2014). While qualitatively resembling the upturn observed in electron-hole bilayers (Croxall *et al.*, 2008; Seamons *et al.*, 2009), the theory accounts neither for a subsequent downturn at the lowest temperatures, nor the apparent violation of Onsager reciprocity (Croxall *et al.*, 2008) [although the latter might be related to heating

effects (Seamons *et al.*, 2009)]. The theory also does not make falsifiable predictions regarding the dependence of ρ_D on carrier densities in the two layers (Morath *et al.*, 2009) [at higher temperatures, where the data show the standard T^2 dependence, the density dependence of ρ_D is stronger than expected on the basis of the Fermi-liquid many-body calculations (Hwang and Das Sarma, 2008b)].

The logarithmic temperature dependence (141) fits well with the upturn in the drag resistivity observed in Gamucci *et al.* (2014) in hybrid devices comprising either a monolayer or bilayer graphene sheet and a GaAs quantum well, see Fig. 35. In fact, the search for exciton physics was one of the main motivations for experimental studies of Coulomb drag in double-layer graphene-based structures (Gorbachev *et al.*, 2012; Kim *et al.*, 2011).

Exciton condensation in graphene has attracted considerable theoretical attention (Abergel *et al.*, 2013; Aleiner *et al.*, 2007; Efimkin and Lozovik, 2011; Fil and Kravchenko, 2009; Kharitonov and Efetov, 2008, 2010; Lozovik *et al.*, 2012; Lozovik and Sokolik, 2008; Min *et al.*, 2008; Pikalov and Fil, 2012; Sodemann *et al.*, 2012; Suprunenko *et al.*, 2012; Zhang and Joglekar, 2008). Several contradicting values of the transition temperature in double-layer graphene systems have been reported. The initial estimate (Mink *et al.*, 2012; Zhang and Joglekar, 2008) of T_c close to room temperature appeared to be too optimistic. Screening effects (Kharitonov and Efetov, 2008, 2010) were shown to lead to extremely low values under 1mk ($T_c \sim 10^{-7} E_F$). More recent investigations involving detail analysis of screened Coulomb interaction (Abergel *et al.*, 2013; Lozovik *et al.*, 2012; Sodemann *et al.*, 2012), multiband pairing (Lozovik *et al.*, 2012; Mink *et al.*, 2012), and pairing with nonzero momentum (Efimkin and Lozovik, 2011) suggest somewhat higher values of T_c , making the transition experimentally accessible.

High-temperature coherence and superfluidity has also been suggested in thin films of topological insulators (Efimkin *et al.*, 2012; Mink *et al.*, 2012, 2013; Seradjeh *et al.*, 2009).

The effect of exciton condensation on Coulomb drag has been investigated in graphene numerically by Zhang and Jin (2013) and in topological insulator films analytically in Efimkin and Lozovik (2013). The latter work focused on the drag effect at temperatures exceeding T_c , where the pairing fluctuations are expected to play an important role. In addition to the Maki-Thompson-type contribution (Hu, 2000b; Mink *et al.*, 2012, 2013) to the drag resistivity, Efimkin and Lozovik (2013) have analyzed the Aslamazov-Larkin-type contribution and found

$$\delta\rho_D^{AL} \propto [\ln(T/T_c)]^{-1}. \quad (142)$$

Far away from the transition, the result (142) decays logarithmically, similarly to Eq. (141), but close to the transition exhibits a stronger divergence $\delta\rho_D^{AL} \propto (T - T_c)^{-1}$.

VIII. OPEN QUESTIONS AND PERSPECTIVES

The physics of the Coulomb drag in double-layer systems is well understood if both layers are in the Fermi-liquid state (Flensberg *et al.*, 1995; Kamenev and Oreg, 1995). The current in the passive layer is created by exciting electron-hole pairs (each pair consisting of an occupied state above the Fermi surface and an empty state below) in a state characterized by finite momentum. The momentum comes from the electron-hole excitations in the active layer created by the driving current. The momentum transfer is due to the interlayer Coulomb interaction. Therefore it follows from the usual phase-space considerations that the drag coefficient is proportional to the square of the temperature $\rho_D \propto T^2$. Remarkably, this simple argument is sufficient to describe the observed low temperature dependence of ρ_D . Deviations from the quadratic dependence at higher temperatures are primarily due to the effect of phonons and plasmons (Rojo, 1999).

The universality of the Landau Fermi-liquid theory (Altshuler and Aronov, 1985; Lifshitz and Pitaevskii, 1981) can be traced to the linearization of the quasi-particle spectrum. Within this approximation all details of the microscopic structure of the system are contained in a limited number of parameters, such as the Fermi velocity and density of states (DoS) at the Fermi level. Many observable quantities (e.g. the electronic contribution to the specific heat, spin susceptibility, period of the De Haas-van Alphen oscillations, etc.) can be expressed in terms of these parameters and thus exhibit the “universal” behavior (as a function of temperature or external fields). Same arguments can be applied to elementary excitations in strongly doped graphene ($\mu \gg T$), where the Fermi-liquid theory is expected to be applicable.

Coulomb drag belongs to a different class of observables. In conventional semiconductor devices, it reflects the degree of electron-hole asymmetry in the system vanishing in the approximation of linearized spectrum (Kamenev and Oreg, 1995). The drag coefficient is determined by the subleading contribution taking into account the curvature of the quasi-particle spectrum. Indeed, in the passive layer the momentum is transferred equally to electrons and holes so that the resulting state can carry current only in the case of electron-hole asymmetry. Likewise, this asymmetry is necessary for the current-carrying state in the active layer to be characterized by nonzero total momentum. The electron-hole asymmetry manifests itself (Narozhny *et al.*, 2001; von Oppen *et al.*, 2001) in the energy (or chemical potential) dependence of such quantities as the density of states, single-layer conductivity, and diffusion coefficient. Within the Fermi-liquid theory (Kamenev and Oreg, 1995), the asymmetry is weak, $\partial\sigma_i/\partial\mu_i \approx \sigma_i/\mu_i$, leading to the drag effect, that is much weaker than the single-layer conductivity.

Coulomb drag in non-Fermi-liquid systems is much

more interesting. In particular, it has been used to study novel strongly-correlated, many-body states in double quantum wells (Eisenstein, 2014), graphene (Gamucci *et al.*, 2014), quantum wires (Laroche *et al.*, 2014), and optical cavities (Berman *et al.*, 2014), where practical applications in optical switches have been suggested. In these systems, drag measurements have proved to be an invaluable tool to study the microscopic structure of complex, interacting many-body systems.

At the same time, our understanding of many of these systems is incomplete. In contrast to the Fermi-liquid theory, many aspects of the strongly-correlated many-body states lack a detailed theoretical description. Consequently, their transport properties, including Coulomb drag, can be evaluated only with the help of heuristic or phenomenological models. One can only hope that a proper microscopic theory of these effects will eventually be developed.

This brings us to the list of unresolved questions related to the theory reviewed in this paper and possible direction of the field in the near future.

(i) At low enough temperatures and especially in strong magnetic fields, double-layer systems may host excitonic condensates (Eisenstein, 2014). In monolayer graphene, such condensation is also possible, but for reasonably weak interactions the condensation temperature appears to be rather low (Aleiner *et al.*, 2007; Kharitonov and Efetov, 2008; Mink *et al.*, 2012). Nevertheless, a possibility of interlayer correlated states in graphene-based systems [and possibly in hybrid devices involving other materials, (Geim and Grigorieva, 2013)] is rather exciting and certainly requires theoretical attention.

(ii) The hydrodynamic approach of Sec. IV.B should be extended to include thermoelectric effects in graphene-based double-structures as well as in monolayer and bilayer graphene. As pointed out in Foster and Aleiner (2009) and Narozhny *et al.* (2015), the quasiparticle imbalance in graphene may play a decisive role in thermal transport. Another promising direction may be opened by generalization of the macroscopic linear-response equations to a true, nonlinear hydrodynamics. The relation between the quantum kinetic equation of Zala *et al.* (2001) and the hydrodynamic approach [both in graphene (Narozhny *et al.*, 2015) and in 2DEG (Andreev *et al.*, 2011; Apostolov *et al.*, 2014)] is also of certain theoretical interest.

(iii) Dirac fermions can be found as low-energy excitations not only in graphene, but also in topological insulators (Bernevig and Hughes, 2013; Shen, 2013). An extension of the present theory of Coulomb drag to various possible system configurations involving topological insulators and/or hybrid devices involving topological insulators, graphene, etc. appears to be very promising (Mink *et al.*, 2012).

(iv) Novel aspects of Luttinger liquid physics and role of equilibration processes on drag can be further explored

with the edge states of quantum Hall systems or topological edge liquids of quantum spin Hall effect. Some theoretical predictions have already been made (Zyuzin and Fiete, 2010) and recent experimental advances (Altimiras *et al.*, 2010; Du *et al.*, 2015; König *et al.*, 2013; Roth *et al.*, 2009) bring these exciting perspectives within reach.

(v) Mesoscopic fluctuations of Coulomb drag in ballistic samples should be further analyzed on the basis of the microscopic theory. The theory should be further extended to the cases of Dirac fermions in graphene and composite fermions at the half-filled Landau level. Experimental work in this direction has been already initiated in Kim *et al.* (2011) and Price *et al.* (2010).

(vi) The third-order drag effect (see Sec. IV.F) bears a certain resemblance to the well-known Altshuler-Aronov corrections to single-layer conductivity (Altshuler and Aronov, 1985; Zala *et al.*, 2001). In Zala *et al.* (2001) it was shown that the dominant contribution to conductivity at low (diffusive regime) and high (ballistic regime) temperatures technically comes from different diagrams describing conceptually similar, but at the same time distinct interference processes. Similarly, we expect that the third-order drag contribution in ballistic regime might be governed by scattering processes which are distinct from those considered in Levchenko and Kamenev (2008a).

We would like to close this review by pointing out the surprising richness of the Coulomb drag problem. The original suggestion of a way to observe interwell interactions in semiconductor heterostructures has developed into a vibrant field of research where technological advances go hand in hand with theoretical developments. New experiments with novel materials keep being devised and stimulate new avenues for theoretical thinking. We should be expecting to see further intriguing discoveries being made related to frictional drag in the foreseeable future.

ACKNOWLEDGMENTS

We would like to thank all our collaborators for sharing their insights over the years and especially I.L. Aleiner, A.V. Andreev, S. Apostolov, W. Chen, I.V. Gornyi, A. Kamenev, M.I. Katsnelson, A.D. Mirlin, M. Norman, L. Ponomarenko, P.M. Ostrovsky, M. Schütt, A. Stern, M. Titov, and the late A. Savchenko. While writing this review we have greatly benefited from discussions with M. Foster, G. Gervais, D. Polyakov, and J. Schmalian.

The work of A.L. was supported by NSF grants DMR-1401908 and ECCS-1407875, and in part by DAAD grant from German Academic Exchange Services, SPP 1459 and SPP 1666 of the Deutsche Forschungsgemeinschaft. B.N. acknowledges support from the EU Network Grant InterNoM and the Deutsche Forschungsgemeinschaft under grants SCHO 287/7-1 and SH 81/2-1.

REFERENCES

- Abedinpour, S. H., G. Vignale, A. Principi, M. Polini, W.-K. Tse, and A. H. MacDonald (2011), *Phys. Rev. B* **84**, 045429.
- Abergel, D. S. L., M. Rodriguez-Vega, E. Rossi, and S. Das Sarma (2013), *Phys. Rev. B* **88**, 235402.
- Abrahams, E., P. W. Anderson, D. C. Licciardello, and T. V. Ramakrishnan (1979), *Phys. Rev. Lett.* **42**, 673.
- Abrikosov, A., and S. Beneslavskii (1971), *Zh. Eksp. Teor. Fiz.* **59**, 1280, [*Sov. Phys. JETP* **32**, 699 (1971)].
- Aguado, R., and L. P. Kouwenhoven (2000), *Phys. Rev. Lett.* **84**, 1986.
- Aleiner, I. L., B. L. Altshuler, and M. E. Gershenson (1999), *Waves Random Media* **9**, 201.
- Aleiner, I. L., and K. B. Efetov (2006), *Phys. Rev. Lett.* **97**, 236801.
- Aleiner, I. L., D. E. Kharzhev, and A. M. Tsvelik (2007), *Phys. Rev. B* **76**, 195415.
- Alkauskas, A., K. Flensberg, B. Y.-K. Hu, and A.-P. Jauho (2002), *Phys. Rev. B* **66**, 201304.
- Altimiras, C., H. le Sueur, U. Gennser, A. Cavanna, D. Mailly, and F. Pierre (2010), *Nature Physics* **6**, 34.
- Altshuler, B., and A. Aronov (1979), *Zh. Eksp. Teor. Fiz.* **77**, 2028, [*Sov. Phys. JETP* **50**, 968 (1979)].
- Altshuler, B. L. (1985), *Pis'ma Zh. Eksp. Teor. Fiz.* **41**, 530, [*JETP Lett.* **41**, 648 (1985)].
- Altshuler, B. L., and A. G. Aronov (1985), in *Electron-Electron Interactions in Disordered Systems*, edited by A. L. Efros and M. Pollak (North-Holland, Amsterdam).
- Altshuler, B. L., D. E. Khmelnitskii, A. I. Larkin, and P. A. Lee (1980), *Phys. Rev. B* **22**, 5142.
- Altshuler, B. L., and P. A. Lee (1988), *Physics Today* **41**, 36.
- Altshuler, B. L., P. A. Lee, and R. A. Webb, Eds. (1991), *Mesoscopic Phenomena in Solids* (North-Holland, New York).
- Amo, A., D. Sanvitto, F. P. Laussy, D. Ballarini, E. del Valle, M. D. Martin, A. Lematre, J. Bloch, D. N. Krizhanovskii, M. S. Skolnick, C. Tejedor, and L. Vina (2009), *Nature* **457**, 291.
- Amorim, B., and N. M. R. Peres (2012), *J. Phys.: Condens. Matter* **24**, 335602.
- Amorim, B., J. Schiefele, F. Sols, and F. Guinea (2012), *Phys. Rev. B* **86**, 125448.
- An, S., G. Gopalakrishnan, Y. Shiroyanagi, S. C. Parks, T. J. Gramila, L. N. Pfeiffer, and K. W. West (2006), *Physica E* **34**, 214.
- Anderson, P. W., E. Abrahams, and T. V. Ramakrishnan (1979), *Phys. Rev. Lett.* **43**, 718.
- Ando, T. (2006), *Journal of the Physical Society of Japan* **75** (7), 074716.
- Ando, T., A. B. Fowler, and F. Stern (1982), *Rev. Mod. Phys.* **54**, 437.
- Andreev, A. V., S. A. Kivelson, and B. Spivak (2011), *Phys. Rev. Lett.* **106**, 256804.
- Apalkov, V. M., and M. E. Raikh (2005), *Phys. Rev. B* **71**, 245109.
- Apostolov, S. S., A. Levchenko, and A. V. Andreev (2014), *Phys. Rev. B* **89**, 121104.
- Aristov, D. N. (2007), *Phys. Rev. B* **76**, 085327.
- Arnold, P., G. D. Moore, and L. G. Yaffe (2000), *Journal of High Energy Physics* **2000** (11), 001.
- Asgari, R., B. Tanatar, and B. Davoudi (2008), *Phys. Rev. B* **77**, 115301.
- Aslamazov, L. G., and A. I. Larkin (1968), *Fiz. Tverd. Tela.* **10**, 1104, [*Sov. Phys. Solid State.* **10**, 875 (1968)].
- Badalyan, S. M., and C. S. Kim (2003), *Solid State Commun.* **127**, 521.
- Badalyan, S. M., C. S. Kim, G. Vignale, and G. Senatore (2007), *Phys. Rev. B* **75**, 125321.
- Badalyan, S. M., and F. M. Peeters (2012), *Phys. Rev. B* **86**, 121405.
- Badalyan, S. M., and U. Rössler (1999), *Phys. Rev. B* **59**, 5643.
- Badalyan, S. M., and G. Vignale (2009), *Phys. Rev. Lett.* **103**, 196601.
- Baker, J., and A. G. Rojo (2001), *J. Phys.: Condens. Matter* **13**, 3389.
- Baker, J., G. Vignale, and A. G. Rojo (1999), *Phys. Rev. B* **60**, 8804.
- Balili, R., V. Hartwell, D. Snoke, L. Pfeiffer, and K. West (2007), *Science* **316** (5827), 1007.
- Balram, A. C., J. A. Hutasoit, and J. K. Jain (2014), *Phys. Rev. B* **90**, 045103.
- Berk, Y., A. Kamenev, A. Palevski, L. N. Pfeiffer, and K. W. West (1995), *Phys. Rev. B* **51**, 2604.
- Berman, O. L., R. Kezerashvili, and Y. E. Lozovik (2010a), *Physics Letters A* **374**, 3681.
- Berman, O. L., R. Kezerashvili, and Y. E. Lozovik (2010b), *Phys. Rev. B* **82**, 125307.
- Berman, O. L., R. Y. Kezerashvili, and G. V. Kolmakov (2014), *ACS Nano* **8** (10), 10437.
- Bernevig, A., and T. Hughes (2013), *Topological Insulators and Topological Superconductors* (Princeton University Press).
- Blatt, J. M., K. W. Böer, and W. Brandt (1962), *Phys. Rev.* **126**, 1691.
- Bloch, F. (1930), *Zeitschrift für Physik* **59**, 208.
- Boebinger, G. S., A. Passner, L. N. Pfeiffer, and K. W. West (1991), *Phys. Rev. B* **43**, 12673.
- Boiko, I. I., and Y. M. Sirenko (1988), *Zh. Tekh. Fiz.* **58**, 967, [*Sov. Phys. Tech. Phys.* **33**, 586 (1988)].
- Boiko, I. I., and Y. M. Sirenko (1990), *Phys. Status Solidi B* **159**, 805.
- Boiko, I. I., P. Vasilopoulos, and Y. M. Sirenko (1992), *Phys. Rev. B* **45**, 13538.
- Bonesteel, N. E. (1993), *Phys. Rev. B* **48**, 11484.
- Bønsager, M. C., K. Flensberg, B. Y.-K. Hu, and A. P. Jauho (1996), *Phys. Rev. Lett.* **77**, 1366.
- Bønsager, M. C., K. Flensberg, B. Y.-K. Hu, and A. P. Jauho (1997), *Phys. Rev. B* **56**, 10314.
- Bønsager, M. C., K. Flensberg, B. Y.-K. Hu, and A. MacDonald (1998a), *Phys. Rev. B* **57**, 7085.
- Bønsager, M. C., K. Flensberg, B. Y.-K. Hu, and A. MacDonald (1998b), *Physica B* **249-251**, 864.
- Bønsager, M. C., Y. B. Kim, and A. H. MacDonald (2000), *Phys. Rev. B* **62**, 10940.
- Bostwick, A., F. Speck, T. Seyller, K. Horn, M. Polini, R. Asgari, A. H. MacDonald, and E. Rotenberg (2010), *Science* **328** (5981), 999.
- Braude, V., and A. Stern (2001), *Phys. Rev. B* **64**, 115431.
- Brener, S., and W. Metzner (2005), *Pis'ma Zh. Eksp. Teor. Fiz.* **81**, 648, [*JETP Lett.* **81**, 498 (2005)].
- Bulnes Cuetara, G., M. Esposito, G. Schaller, and P. Gaspard (2013), *Phys. Rev. B* **88**, 115134.
- Burkov, A., J. Schliemann, A. MacDonald, and S. Girvin (2002), *Physica E* **12** (14), 28.

- Büttiker, M., Y. Imry, R. Landauer, and S. Pinhas (1985), Phys. Rev. B **31**, 6207.
- Büttiker, M., and R. Sánchez (2011), Nature Nanotechnology **6**, 757.
- Carr, S. T., B. N. Narozhny, and A. A. Nersesyan (2013), Annals of Physics **339**, 22.
- Carrega, M., T. Tudorovskiy, A. Principi, M. I. Katsnelson, and M. Polini (2012), New J. Phys. **14**, 063033.
- Chakraborty, T., and P. Pietiläinen (1987), Phys. Rev. Lett. **59**, 2784.
- Cheianov, V. V., and V. I. Fal'ko (2006), Phys. Rev. Lett. **97**, 226801.
- Chen, H. Y., and J. Appenzeller (2013), Nano Research **6**, 897.
- Chen, W., A. V. Andreev, and A. Levchenko (2015), Phys. Rev. B **91**, 245405.
- Chudnovskiy, A. L. (2009), Phys. Rev. B **80**, 081309.
- Conway, J. H., and N. J. A. Sloane (1988), *Sphere Packings, Lattices, and Groups* (Springer-Verlag, New York).
- Croxall, A. F., K. Das Gupta, C. A. Nicoll, M. Thangaraj, H. E. Beere, I. Farrer, D. A. Ritchie, and M. Pepper (2008), Phys. Rev. Lett. **101**, 246801.
- Cui, H. L., X. L. Lei, and N. J. M. Horing (1988), Phys. Rev. B **37**, 8223.
- Cuoco, M., W. Saldarriaga, A. Polcari, A. Guarino, O. Moran, E. Baca, A. Vecchione, and P. Romano (2009), Phys. Rev. B **79**, 014523.
- D'Amico, I., and G. Vignale (2000), Phys. Rev. B **62**, 4853.
- Das Gupta, K., A. F. Croxall, J. Waldie, C. A. Nicoll, H. E. Beere, I. Farrer, D. A. Ritchie, and M. Pepper (2011), Adv. Cond. Matt. Phys. **2011**, 727958.
- Das Gupta, K., M. Thangaraj, A. Croxall, H. Beere, C. Nicoll, D. Ritchie, and M. Pepper (2008), Physica E **40** (5), 1693.
- Das Sarma, S., and A. Madhukar (1981), Phys. Rev. B **23**, 805.
- Das Sarma, S., and B. A. Mason (1985), Ann. Phys. (NY) **163**, 78.
- Debray, P., P. Vasilopoulos, O. Raichev, R. Perrin, M. Rahman, and W. C. Mitchel (2000), Physica E **6**, 694.
- Debray, P., V. Zverev, O. Raichev, R. Klesse, P. Vasilopoulos, and R. S. Newrock (2001), J. Phys.: Condens. Matter **13**, 3389.
- Debray, P., V. N. Zverev, V. Gurevich, R. Klesse, and R. S. Newrock (2002), Semicond. Sci. Technol. **17**, R21.
- Deshpande, V. V., M. Bockrath, L. I. Glazman, and A. Yacoby (2010), Nature **464**, 209.
- Dmitriev, A. P., I. V. Gornyi, and D. G. Polyakov (2012), Phys. Rev. B **86**, 245402.
- Dmitriev, I. A., F. Evers, I. V. Gornyi, A. D. Mirlin, D. G. Polyakov, and P. Wölfle (2008), Phys. Status Solidi B **245**, 239.
- Dolcini, F., D. Rainis, F. Taddei, M. Polini, R. Fazio, and A. H. MacDonald (2010), Phys. Rev. Lett. **104**, 027004.
- Donarini, A., R. Ferrari, A. P. Jauho, and L. Molinari (2003), Phys. Lett. A **312**, 123.
- Du, L., I. Knez, G. Sullivan, and R.-R. Du (2015), Phys. Rev. Lett. **114**, 096802.
- Duan, J.-M. (1995), EPL (Europhysics Letters) **29** (6), 489.
- Duan, J.-M., and S. Yip (1993), Phys. Rev. Lett. **70**, 3647.
- Duine, R. A., M. Polini, A. Raoux, H. Stoof, and G. Vignale (2011), New J. Phys. **13**, 045010.
- Duine, R. A., M. Polini, H. Stoof, and G. Vignale (2010), Phys. Rev. Lett. **104**, 220403.
- Duine, R. A., and H. T. C. Stoof (2009), Phys. Rev. Lett. **103**, 170401.
- Dykhne, A. M., and I. M. Ruzin (1994), Phys. Rev. B **50**, 2369.
- Efetov, D. K., and P. Kim (2010), Phys. Rev. Lett. **105**, 256805.
- Efimkin, D. K., and Y. E. Lozovik (2011), Zh. Eksp. Teor. Fiz. **140**, 1009, [JETP **113**, 880 (2011)].
- Efimkin, D. K., and Y. E. Lozovik (2013), Phys. Rev. B **88**, 235420.
- Efimkin, D. K., Y. E. Lozovik, and A. A. Sokolik (2012), Phys. Rev. B **86**, 115436.
- Eisenstein, J. (2014), Annual Review of Condensed Matter Physics **5** (1), 159.
- Eisenstein, J. P. (1992), Superlattices Microstruct. **12**, 107.
- Eisenstein, J. P. (1997), in *Perspectives in Quantum Hall Effects*, edited by S. Das Sarma and A. Pinczuk (Wiley, New York).
- Eisenstein, J. P., G. S. Boebinger, L. N. Pfeiffer, K. W. West, and S. He (1992), Phys. Rev. Lett. **68**, 1383.
- Eisenstein, J. P., and A. H. MacDonald (2004), Nature **432**, 691.
- Elsayad, K., J. P. Carini, and D. Baxter (2008), Solid State Comm. **148**, 261.
- Elzerman, J., R. Hanson, L. W. van Beveren, B. Witkamp, L. Vandersypen, and L. Kouwenhoven (2004), Nature **430**, 431.
- Farina, L. A., K. M. Lewis, C. Kurdak, S. Ghosh, and P. Bhattacharya (2004), Phys. Rev. B **70**, 153302.
- Fei, Z., G. O. Andreev, W. Bao, L. M. Zhang, A. S. McLeod, C. Wang, M. K. Stewart, Z. Zhao, G. Dominguez, M. Thiemens, M. M. Fogler, M. J. Tauber, A. H. Castro Neto, C. N. Lau, F. Keilmann, and D. N. Basov (2011), Nano Letters **11** (11), 4701.
- Fei, Z., A. S. Rodin, G. O. Andreev, W. Bao, A. S. McLeod, M. Wagner, L. M. Zhang, Z. Zhao, M. Thiemens, G. Dominguez, M. M. Fogler, A. H. Castro Neto, C. N. Lau, F. Keilmann, and D. N. Basov (2012), Nature (London) **487**, 82.
- Feng, X. G., S. Zelakiewicz, H. Noh, T. J. Ragucci, T. J. Gramila, L. N. Pfeiffer, and K. W. West (1998), Phys. Rev. Lett. **81**, 3219.
- Fertig, H. A., and G. Murthy (2005), Phys. Rev. Lett. **95**, 156802.
- Fiete, G. A., K. L. Hur, and L. Balents (2006), Phys. Rev. B **73**, 165104.
- Fil, D. V., and L. Y. Kravchenko (2009), Low Temperature Physics **35** (8), 712.
- Fil, D. V., and S. I. Shevchenko (2007), Low Temperature Physics **33** (9), 780.
- Finck, A. D. K., A. R. Champagne, J. P. Eisenstein, L. N. Pfeiffer, and K. W. West (2008), Phys. Rev. B **78**, 075302.
- Finck, A. D. K., J. P. Eisenstein, L. N. Pfeiffer, and K. W. West (2010), Phys. Rev. Lett. **104**, 016801.
- Finck, A. D. K., J. P. Eisenstein, L. N. Pfeiffer, and K. W. West (2011), Phys. Rev. Lett. **106**, 236807.
- Finkelstein, A. M. (1983), Zh. Eksp. Teor. Fiz. **84**, 168, [Sov. Phys. JETP **57**, 97 (1983)].
- Finkelstein, A. M. (1984), Z. Phys. B: Condens. Matter **56**, 189.
- Finkelstein, G., H. Shtrikman, and I. Bar-Joseph (1995), Phys. Rev. Lett. **74**, 976.
- Fischella, G., G. Greco, F. Roccaforte, and F. Giannazzo (2014), Nanoscale **6**, 8671.
- Flensberg, K. (1998), Phys. Rev. Lett. **81**, 184.

- Flensberg, K., and B. Y.-K. Hu (1994), Phys. Rev. Lett. **73**, 3572.
- Flensberg, K., and B. Y.-K. Hu (1995), Phys. Rev. B **52**, 14796.
- Flensberg, K., B. Y.-K. Hu, A.-P. Jauho, and J. M. Kinaret (1995), Phys. Rev. B **52**, 14761.
- Flensberg, K., T. Stibius Jensen, and N. Asger Mortensen (2001), Phys. Rev. B **64**, 245308.
- Foster, M. S., and I. L. Aleiner (2009), Phys. Rev. B **79**, 085415.
- Fredrikse, H. P. R. (1953a), Phys. Rev. **91**, 491.
- Fredrikse, H. P. R. (1953b), Phys. Rev. **92**, 248.
- Fritz, L., J. Schmalian, M. Müller, and S. Sachdev (2008), Phys. Rev. B **78**, 085416.
- Fuchs, T., R. Klesse, and A. Stern (2005), Phys. Rev. B **71**, 045321.
- Furuya, S. C., H. Matsuura, and M. Ogata (2015), ArXiv:1503.02499 (unpublished).
- Gamucci, A., D. Spirito, M. Carrega, B. Karmakar, A. Lombardo, M. Bruna, L. N. Pfeiffer, K. W. West, A. C. Ferrari, M. Polini, and V. Pellegrini (2014), Nature Communications **5**, 5824.
- Geballe, T. H. (1953), Phys. Rev. **92**, 857.
- Geballe, T. H., and G. W. Hull (1954), Phys. Rev. **94**, 1134.
- Geigenmüller, U., and Y. V. Nazarov (1991), Phys. Rev. B **44**, 10953.
- Geim, A. K., and I. V. Grigorieva (2013), Nature **499**, 419.
- Giamarchi, T. (2004), *Quantum Physics in One Dimension* (Oxford University Press).
- Giordano, N., and J. D. Monnier (1994), Phys. Rev. B **50**, 9363.
- Girvin, S. M., and A. H. MacDonald (1997), in *Perspectives in Quantum Hall Effects*, edited by S. Das Sarma and A. Pinczuk (Wiley, New York).
- Giuliani, G., and G. Vignale (2005), *Quantum Theory of the Electron Liquid* (Cambridge University Press).
- Giuliani, G. F., and J. J. Quinn (1982), Phys. Rev. B **26**, 4421.
- Glazman, L. I., G. B. Lesovik, D. E. Khmel'nitskii, and R. I. Shekhter (1988), Pis'ma Zh. Eksp. Teor. Fiz. **48**, 218, [JETP Lett. **48**, 238 (1988)].
- Glazov, M. M., M. A. Semina, S. M. Badalyan, and G. Vignale (2011), Phys. Rev. B **84**, 033305.
- González, J., F. Guinea, and M. A. H. Vozmediano (1999), Phys. Rev. B **59**, R2474.
- Gorbachev, R. V., A. K. Geim, M. I. Katsnelson, K. S. Novoselov, T. Tudorovskiy, I. V. Grigorieva, A. H. MacDonald, S. V. Morozov, K. Watanabe, T. Taniguchi, and L. A. Ponomarenko (2012), Nature Physics **8**, 896.
- Gorkov, L. P., A. I. Larkin, and D. E. Khmel'nitskii (1979), Pis'ma Zh. Eksp. Teor. Fiz. **30**, 248, [JETP Lett. **30**, 228 (1979)].
- Gornyi, I., A. Yashenkin, and D. Khveshchenko (2000), Physica B: Condensed Matter **284 - 288, Part 2**, 1930.
- Gornyi, I. V., A. D. Mirlin, and F. von Oppen (2004), Phys. Rev. B **70**, 245302.
- Gornyi, I. V., and B. N. Narozhny (2014), Unpublished.
- Gornyi, I. V., A. G. Yashenkin, and D. V. Khveshchenko (1999), Phys. Rev. Lett. **83**, 152.
- Gramila, T. J., J. P. Eisenstein, A. H. MacDonald, L. N. Pfeiffer, and K. W. West (1991), Phys. Rev. Lett. **66**, 1216.
- Gramila, T. J., J. P. Eisenstein, A. H. MacDonald, L. N. Pfeiffer, and K. W. West (1992), Surf. Sci. **263**, 446.
- Gramila, T. J., J. P. Eisenstein, A. H. MacDonald, L. N. Pfeiffer, and K. W. West (1993), Phys. Rev. B **47**, 12957.
- Gramila, T. J., J. P. Eisenstein, A. H. MacDonald, L. N. Pfeiffer, and K. W. West (1994), Physica B **197**, 442.
- Greiter, M., X.-G. Wen, and F. Wilczek (1991), Phys. Rev. Lett. **66**, 3205.
- Grigorenko, A. N., M. Polini, and K. S. Novoselov (2012), Nature Photonics **6**, 749.
- Grüneisen, E. (1933), Ann. Phys. (Leipzig) **16**, 530.
- Gubarev, S. I., I. V. Kukushkin, S. V. Tovstonog, M. Y. Akimov, J. Smet, K. von Klitzing, and W. Wegscheider (2000), Pis'ma Zh. Eksp. Teor. Fiz. **72**, 469, [JETP Lett. **72**, 324 (2000)].
- Gurevich, L. E. (1946a), Zh. Eksp. Teor. Fiz. **16**, 193, [J. Phys. (USSR) **9**, 857 (1945)].
- Gurevich, L. E. (1946b), Zh. Eksp. Teor. Fiz. **16**, 416, [J. Phys. (USSR) **10**, 67 (1946)].
- Gurevich, V. L., and M. I. Muradov (2000), Pis'ma Zh. Eksp. Teor. Fiz. **71**, 164, [JETP Lett. **71**, 111 (2000)].
- Gurevich, V. L., and M. I. Muradov (2005), J. Phys.: Condens. Matter **17**, 87.
- Gurevich, V. L., V. B. Pevzner, and E. W. Fenton (1998), Journal of Physics: Condensed Matter **10** (11), 2551.
- Gurevich, Y. G., and O. L. Mashkevich (1989), Phys. Rep. **181**, 327.
- Güven, K., and B. Tanatar (1997a), Phys. Rev. B **56**, 7535.
- Güven, K., and B. Tanatar (1997b), Solid State Comm. **104**, 439.
- Haldane, F., and E. Rezayi (1987), Bull. Am. Phys. Soc. **32**, 892.
- Haldane, F. D. M. (1981a), J. Phys. C **14**, 2585.
- Haldane, F. D. M. (1981b), Phys. Rev. Lett. **47**, 1840.
- Halperin, B. (1983), Helv. Phys. Acta **56**, 75.
- Halperin, B. I., P. A. Lee, and N. Read (1993), Phys. Rev. B **47**, 7312.
- Hänsch, W., and G. D. Mahan (1983), J. Phys. Chem. Solids **44**, 663.
- Herring, C. (1954), Phys. Rev. **96**, 1163.
- Hill, N. P. R., J. T. Nicholls, E. H. Linfield, M. Pepper, D. A. Ritchie, A. R. Hamilton, and G. A. C. Jones (1996), J. Phys.: Condens. Matter **8**, L557.
- Hill, N. P. R., J. T. Nicholls, E. H. Linfield, M. Pepper, D. A. Ritchie, B. Y.-K. Hu, and K. Flensberg (1998), Physica B **249-251**, 868.
- Hill, N. P. R., J. T. Nicholls, E. H. Linfield, M. Pepper, D. A. Ritchie, G. A. C. Jones, B. Y.-K. Hu, and K. Flensberg (1997), Phys. Rev. Lett. **78**, 2204.
- Höpfel, R., and J. Shah (1988), Solid-State Electronics **31**, 643.
- Höpfel, R. A., J. Shah, P. A. Wolff, and A. C. Gossard (1986), Phys. Rev. Lett. **56**, 2736.
- Hruska, M., and B. Spivak (2002), Phys. Rev. B **65**, 033315.
- Hu, B. Y.-K. (1997), Physica Scripta **T69**, 170.
- Hu, B. Y.-K. (1998), Phys. Rev. B **57**, 12345.
- Hu, B. Y.-K. (2000a), Physica E **6**, 611.
- Hu, B. Y.-K. (2000b), Phys. Rev. Lett. **85**, 820.
- Hu, B. Y.-K., and K. Flensberg (1996), in *Hot Carriers in Semiconductors*, edited by K. Hess (Plenum Press, New York).
- Huang, X., G. Bazan, and G. Bernstein (1995), Phys. Rev. Lett. **74**, 4051.
- Huse, D. A. (2005), Phys. Rev. B **72**, 064514.
- Hwang, E. H., and S. Das Sarma (2007), Phys. Rev. B **75**, 205418.

- Hwang, E. H., and S. Das Sarma (2008a), Phys. Rev. B **77**, 115449.
- Hwang, E. H., and S. Das Sarma (2008b), Phys. Rev. B **78**, 075430.
- Hwang, E. H., S. D. Sarma, V. Braude, and A. Stern (2003), Phys. Rev. Lett. **90**, 086801.
- Hwang, E. H., R. Sensarma, and S. D. Sarma (2011), Phys. Rev. B **84**, 245441.
- Imambekov, A., T. L. Schmidt, and L. I. Glazman (2012), Rev. Mod. Phys. **84**, 1253.
- Jacoboni, C., and P. J. Price (1988), Solid-State Electron. **31**, 649.
- Jain, J. K. (1989), Phys. Rev. Lett. **63**, 199.
- Jalabert, R., and S. Das Sarma (1989), Phys. Rev. B **40**, 9723.
- Jauho, A.-P., and H. Smith (1993), Phys. Rev. B **47**, 4420.
- Johnson, A. C., C. M. Marcus, M. P. Hanson, and A. C. Gossard (2004), Phys. Rev. Lett. **93**, 106803.
- Jörger, C., S. J. Cheng, W. Dietsche, R. Gerhardts, P. Specht, K. Eberl, and K. von Klitzing (2000a), Physica E **6**, 598.
- Jörger, C., S. J. Cheng, H. Rubel, W. Dietsche, R. Gerhardts, P. Specht, K. Eberl, and K. von Klitzing (2000b), Phys. Rev. B **62**, 1572.
- Jörger, C., W. Dietsche, W. Wegscheider, and K. Klitzing (2000c), Physica E **6**, 586.
- Ju, L., B. Geng, J. Horng, C. Girit, M. Martin, Z. Hao, H. A. Bechtel, X. Liang, A. Zettl, Y. Ron Shen, and F. Wang (2011), Nature Nanotech. **6**, 630.
- Kamenev, A., and Y. Oreg (1995), Phys. Rev. B **52**, 7516.
- Kashuba, A. B. (2008), Phys. Rev. B **78**, 085415.
- Kasprzak, J., M. Richard, S. Kundermann, A. Baas, P. Jeambren, J. M. J. Keeling, F. M. Marchetti, M. H. Szymanska, R. Andre, J. L. Staehli, V. Savona, P. B. Littlewood, B. Deveaud, and L. S. Dang (2006), Nature **443**, 409.
- Katsnelson, M. I. (2011), Phys. Rev. B **84**, 041407.
- Katsnelson, M. I. (2012), *Graphene* (Cambridge University Press).
- Keldysh, L. V., and Y. V. Kopaev (1964), Fiz. Tverd. Tela. **6**, 2791, [Sov. Phys. Solid State. **6**, 2219 (1965)].
- Keldysh, L. V., and A. N. Kozlov (1968), Zh. Eksp. Teor. Fiz. **54**, 978, [Sov. Phys. JETP **27**, 521 (1968)].
- Kellogg, M., J. P. Eisenstein, L. N. Pfeiffer, and K. W. West (2003), Phys. Rev. Lett. **90**, 246801.
- Kellogg, M., J. P. Eisenstein, L. N. Pfeiffer, and K. W. West (2004), Phys. Rev. Lett. **93**, 036801.
- Kellogg, M., J. P. Eisenstein, L. N. Pfeiffer, and K. W. West (2002a), Solid State Comm. **123**, 515.
- Kellogg, M., I. B. Spielman, J. P. Eisenstein, L. N. Pfeiffer, and K. W. West (2002b), Phys. Rev. Lett. **88**, 126804.
- Keogh, J. A., K. Das Gupta, H. E. Beere, D. A. Ritchie, and M. Pepper (2005), Appl. Phys. Lett. **87**, 202104.
- Khaetskii, A. V., and Y. V. Nazarov (1999), Phys. Rev. B **59**, 7551.
- Kharitonov, M. Y., and K. B. Efetov (2008), Phys. Rev. B **78**, 241401.
- Kharitonov, M. Y., and K. B. Efetov (2010), Semiconductor Science and Technology **25** (3), 034004.
- Khrapai, V. S., S. Ludwig, J. P. Kotthaus, H. P. Tranitz, and W. Wegscheider (2006), Phys. Rev. Lett. **97**, 176803.
- Khrapai, V. S., S. Ludwig, J. P. Kotthaus, H. P. Tranitz, and W. Wegscheider (2007), Phys. Rev. Lett. **99**, 096803.
- Khveshchenko, D. V. (2000), Phys. Rev. B **61**, 7227.
- Kim, S., I. Jo, J. Nah, Z. Yao, S. K. Banerjee, and E. Tutuc (2011), Phys. Rev. B **83**, 161401(R).
- Kim, S., and E. Tutuc (2012), Solid State Commun. **152**, 1283.
- Kim, Y. B., and A. J. Millis (1999), Physica E **4**, 171.
- Kim, Y. B., C. Nayak, E. Demler, N. Read, and S. D. Sarma (2001), Phys. Rev. B **63**, 205315.
- Klesse, R., and A. Stern (2000), Phys. Rev. B **62**, 16912.
- Komnik, A., and R. Egger (2001), Eur. Phys. J. B **19**, 271.
- König, M., M. Baenninger, A. G. F. Garcia, N. Harjee, B. L. Pruitt, C. Ames, P. Leubner, C. Brüne, H. Buhmann, L. W. Molenkamp, and D. Goldhaber-Gordon (2013), Phys. Rev. X **3**, 021003.
- Kozikov, A. A., A. K. Savchenko, B. N. Narozhny, and A. V. Shytov (2010), Phys. Rev. B **82**, 075424.
- Krishnaswamy, A. E., S. M. Goodnick, and J. Bird (1999), Microelectronic Engineering **47**, 81.
- Kukkonen, C. A., and A. W. Overhauser (1979), Phys. Rev. B **20**, 550.
- Kulakovskii, D. V., and Y. E. Lozovik (2004), Zh. Eksp. Teor. Fiz. **125**, 1375, [Sov. Phys. JETP **98**, 1205 (2004)].
- Kvon, Z. D., E. B. Olshanetsky, G. M. Gusev, J. C. Portal, and D. K. Maude (1997), Phys. Rev. B **56**, 12112.
- Laikhtman, B., and P. M. Solomon (1990), Phys. Rev. B **41**, 9921.
- Laikhtman, B., and P. M. Solomon (2005), Phys. Rev. B **72**, 125338.
- Laikhtman, B., and P. M. Solomon (2006), Solid State Commun. **138**, 143.
- Landau, L. D., E. M. Lifshitz, and L. P. Pitaevskii (1984), *Electrodynamics of Continuous Media* (Pergamon Press).
- Landauer, R. (1957), IBM J. Res. Dev. **1**, 223.
- Landauer, R. (1970), Philos. Mag. **21**, 863.
- Laroche, D., E. S. Bielejec, J. L. Reno, G. Gervais, and M. Lilly (2008), Physica E **40**, 1569.
- Laroche, D., G. Gervais, M. P. Lilly, and J. L. Reno (2011), Nature Nanotechnology **6**, 793.
- Laroche, D., G. Gervais, M. P. Lilly, and J. L. Reno (2014), Science **343**, 631.
- Lee, D. K. K., P. R. Eastham, and N. R. Cooper (2011), Adv. Cond. Matt. Phys. **2011**, 792125.
- Lee, P. A., and A. D. Stone (1985), Phys. Rev. Lett. **55**, 1622.
- Lerner, I. V. (1988), Phys. Lett. A **133**, 253.
- Lesovik, G. B. (1989), Pis'ma Zh. Eksp. Teor. Fiz. **49**, 513, [JETP Lett. **49**, 592 (1989)].
- Levchenko, A., and A. Kamenev (2008a), Phys. Rev. Lett. **101**, 216806.
- Levchenko, A., and A. Kamenev (2008b), Phys. Rev. Lett. **100**, 026805.
- Levchenko, A., and M. R. Norman (2011), Phys. Rev. B **83**, 100506.
- Levchenko, A., Z. Ristivojevic, and T. Micklitz (2011), Phys. Rev. B **83**, 041303.
- Lifshitz, E. M., and L. P. Pitaevskii (1981), *Physical Kinetics* (Pergamon Press).
- Lilly, M. P., J. P. Eisenstein, L. N. Pfeiffer, and K. W. West (1998), Phys. Rev. Lett. **80**, 1714.
- Lindhard, J. (1954), Dan. Mat. Fys. Medd. **28** (8).
- Littlewood, P. (2007), Science **316** (5827), 989.
- Lok, J. G. S., S. Kraus, W. Dietsche, K. von Klitzing, F. Schwerdt, M. Hauser, W. Wegscheider, and M. Bichler (2002), Physica E **12**, 119.
- Lok, J. G. S., S. Kraus, M. Pohl, W. Dietsche, K. von Klitzing, W. Wegscheider, and M. Bichler (2001a), Phys. Rev. B **63**, 041305(R).

- Lok, J. G. S., S. Kraus, M. Pohlt, K. Güven, W. Dietsche, K. von Klitzing, W. Wegscheider, and M. Bichler (2001b), *Physica B* **298**, 135.
- Lozovik, Y. E., and M. V. Nikitkov (1999), *Zh. Eksp. Teor. Fiz.* **116**, 1440, [*JETP* **89**, 775 (1999)].
- Lozovik, Y. E., S. L. Ogarkov, and A. A. Sokolik (2012), *Phys. Rev. B* **86**, 045429.
- Lozovik, Y. E., and A. A. Sokolik (2008), *Pis'ma Zh. Eksp. Teor. Fiz.* **87**, 61, [*JETP Lett.* **87**, 55 (2008)].
- Lozovik, Y. E., and V. I. Yudson (1976), *Zh. Eksp. Teor. Fiz.* **71**, 738, [*Sov. Phys. JETP* **44**, 389 (1976)].
- Lunde, A. M., K. Flensberg, and L. I. Glazman (2006), *Phys. Rev. Lett.* **97**, 256802.
- Lunde, A. M., K. Flensberg, and L. I. Glazman (2007), *Phys. Rev. B* **75**, 245418.
- Lunde, A. M., K. Flensberg, and A.-P. Jauho (2005), *Phys. Rev. B* **71**, 125408.
- Lunde, A. M., and A.-P. Jauho (2004), *Semicond. Sci. Technol.* **19**, S433.
- Lung, F., and D. C. Marinescu (2011), *Physica E* **43**, 1769.
- Luo, X., T. Qiu, W. Lu, and Z. Ni (2013), *Materials Science and Engineering: R: Reports* **74** (11), 351.
- Luttinger, J. M. (1963), *J. Math. Phys.* **4**, 1154.
- Lux, J., and L. Fritz (2012), *Phys. Rev. B* **86**, 165446.
- Lyo, S. K. (2003), *Phys. Rev. B* **68**, 045310.
- Manolescu, A., and B. Tanatar (2002), *Physica E* **13**, 80.
- Margenau, H., and N. R. Kestner (1969), *Theory of Intermolecular Forces* (Pergamon Press).
- Maslov, D. L. (1992), *Phys. Rev. B* **45**, 1911.
- Matveev, K. A. (2013), *Zh. Eksp. Teor. Fiz.* **144**, 585, [*JETP* **117**, 508 (2013)].
- Mausser, C., E. D. Como, J. Baldauf, A. L. Rogach, J. Huang, D. Talapin, and J. Feldmann (2010), *Phys. Rev. B* **82**, 081306(R).
- Micklitz, T., J. Rech, and K. A. Matveev (2010), *Phys. Rev. B* **81**, 115313.
- Min, H., R. Bistritzer, J.-J. Su, and A. H. MacDonald (2008), *Phys. Rev. B* **78**, 121401.
- Mink, M. P., H. T. C. Stoof, R. A. Duine, M. Polini, and G. Vignale (2012), *Phys. Rev. Lett.* **108**, 186402.
- Mink, M. P., H. T. C. Stoof, R. A. Duine, M. Polini, and G. Vignale (2013), *Phys. Rev. B* **88**, 235311.
- Mishchenko, E. G., M. Y. Reizer, and L. I. Glazman (2004), *Phys. Rev. B* **69**, 195302.
- Moldoveanu, V., and B. Tanatar (2009), *Europhys. Lett.* **86**, 67004.
- Morath, C. P., J. A. Seamons, J. L. Reno, and M. P. Lilly (2009), *Phys. Rev. B* **79**, 041305(R).
- Morimoto, T., Y. Iwase, N. Aoki, T. Sasaki, Y. Ochiai, A. Shailos, J. P. Bird, M. P. Lilly, J. L. Reno, and J. A. Simmons (2003), *Applied Physics Letters* **82** (22), 3952.
- Mortensen, N. A., K. Flensberg, and A.-P. Jauho (2001), *Phys. Rev. Lett.* **86**, 1841.
- Mortensen, N. A., K. Flensberg, and A.-P. Jauho (2002a), *Phys. Rev. B* **65**, 085317.
- Mortensen, N. A., K. Flensberg, and A.-P. Jauho (2002b), *Physica Scripta* **2002** (T101), 177.
- Moskalenko, S. A. (1962), *Fiz. Tverd. Tela.* **4**, 276, [*Sov. Phys. Solid State.* **4**, 199 (1962)].
- Moško, M., V. Cambel, and A. Mošková (1992), *Phys. Rev. B* **46**, 5012.
- Mott, N. F., and H. Jones (1936), *The Theory of the Properties of Metals and Alloys* (Clarendon, Oxford).
- Müller, M., and S. Sachdev (2008), *Phys. Rev. B* **78**, 115419.
- Müller, M., J. Schmalian, and L. Fritz (2009), *Phys. Rev. Lett.* **103**, 025301.
- Muraki, K., J. G. S. Lok, S. Kraus, W. Dietsche, K. von Klitzing, D. Schuh, M. Bichler, and W. Wegscheider (2004), *Phys. Rev. Lett.* **92**, 246801.
- Murphy, S. Q., J. P. Eisenstein, G. S. Boebinger, L. N. Pfeiffer, and K. W. West (1994), *Phys. Rev. Lett.* **72**, 728.
- Nandi, D., A. D. K. Finck, J. P. Eisenstein, L. N. Pfeiffer, and K. W. West (2012), *Nature* **488**, 481.
- Narozhny, B. N. (2007), *Phys. Rev. B* **76**, 153409.
- Narozhny, B. N., and I. L. Aleiner (2000), *Phys. Rev. Lett.* **84**, 5383.
- Narozhny, B. N., I. L. Aleiner, and A. Stern (2001), *Phys. Rev. Lett.* **86**, 3610.
- Narozhny, B. N., I. V. Gornyi, M. Titov, M. Schütt, and A. D. Mirlin (2015), *Phys. Rev. B* **91**, 035414.
- Narozhny, B. N., M. Titov, I. V. Gornyi, and P. M. Ostrovsky (2012), *Phys. Rev. B* **85**, 195421.
- Narozhny, B. N., G. Zala, and I. L. Aleiner (2002), *Phys. Rev. B* **65**, 180202.
- Nazarov, Y. V., and D. V. Averin (1998), *Phys. Rev. Lett.* **81**, 653.
- Noh, H., S. Zelakiewicz, X. G. Feng, T. J. Gramila, L. N. Pfeiffer, and K. W. West (1998), *Phys. Rev. B* **58**, 12621.
- Noh, H., S. Zelakiewicz, T. J. Gramila, L. N. Pfeiffer, and K. W. West (1999), *Phys. Rev. B* **59**, 13114.
- Nomura, K., and A. H. MacDonald (2006), *Phys. Rev. Lett.* **96**, 256602.
- Nomura, K., and A. H. MacDonald (2007), *Phys. Rev. Lett.* **98**, 076602.
- Onac, E., F. Balestro, L. H. W. van Beveren, U. Hartmann, Y. V. Nazarov, and L. P. Kouwenhoven (2006), *Phys. Rev. Lett.* **96**, 176601.
- von Oppen, F., S. H. Simon, and A. Stern (2001), *Phys. Rev. Lett.* **87**, 106803.
- Oreg, Y., and B. I. Halperin (1999), *Phys. Rev. B* **60**, 5679.
- Oreg, Y., and A. Kamenev (1998), *Phys. Rev. Lett.* **80**, 2421.
- Orgad, D., and S. Levit (1996), *Phys. Rev. B* **53**, 7964.
- Ostrovsky, P. M., I. V. Gornyi, and A. D. Mirlin (2006), *Phys. Rev. B* **74**, 235443.
- Ostrovsky, P. M., I. V. Gornyi, and A. D. Mirlin (2007), *Eur. Phys. J. Special Topics* **148**, 63.
- Park, K., and S. Das Sarma (2006), *Phys. Rev. B* **74**, 035338.
- Patel, N. K., E. H. Linfield, K. M. Brown, M. Pepper, D. A. Ritchie, and G. A. C. Jones (1997), *Semicond. Sci. Technol.* **12**, 309.
- Pereira, R. G., and E. Sela (2010), *Phys. Rev. B* **82**, 115324.
- Peres, N. M. R., J. M. B. L. dos Santos, and A. H. C. Neto (2011), *Europhys. Lett.* **95**, 18001.
- Pesin, D. A., and A. H. MacDonald (2011), *Phys. Rev. B* **84**, 075308.
- Pikalov, A. A., and D. V. Fil (2012), *Nanoscale Research Lett.* **7**, 145.
- Pillarisetty, R., H. Noh, D. C. Tsui, E. P. D. Poortere, E. Tutuc, and M. Shayegan (2002), *Phys. Rev. Lett.* **89**, 016805.
- Pillarisetty, R., H. Noh, D. C. Tsui, E. P. D. Poortere, E. Tutuc, and M. Shayegan (2003), *Phys. Rev. Lett.* **90**, 226801.
- Pillarisetty, R., H. Noh, D. C. Tsui, E. P. D. Poortere, E. Tutuc, and M. Shayegan (2005a), *Phys. Rev. Lett.* **94**, 016807.
- Pillarisetty, R., H. Noh, E. Tutuc, E. D. Poortere, D. Tsui, and M. Shayegan (2004), *Physica E* **22**, 300.
- Pillarisetty, R., H. Noh, E. Tutuc, E. P. D. Poortere, K. Lai, D. Tsui, and M. Shayegan (2005b), *Phys. Rev. B* **71**,

- 115307.
- Pogrebinskii, M. B. (1977), *Fiz. Tekh. Poluprovodn.* **11**, 637, [*Sov. Phys. Semicond.* **11**, 372 (1977)].
- Ponomarenko, L., A. K. Geim, A. A. Zhukov, R. Jalil, S. V. Morozov, K. S. Novoselov, I. V. Grigorieva, E. H. Hill, V. V. Cheianov, V. I. Fal'ko, K. Watanabe, T. Taniguchi, and R. V. Gorbachev (2011), *Nature Physics* **7**, 958.
- Ponomarenko, L. A. (2013), private communication.
- Ponomarenko, V. V., and D. V. Averin (2000), *Phys. Rev. Lett.* **85**, 4928.
- Price, A. S., A. K. Savchenko, G. Allison, and D. A. Ritchie (2008), *Physica E* **40**, 961.
- Price, A. S., A. K. Savchenko, B. N. Narozhny, G. Allison, and D. A. Ritchie (2007), *Science* **316**, 99.
- Price, A. S., A. K. Savchenko, and D. A. Ritchie (2010), *Phys. Rev. B* **81**, 193303.
- Price, P. J. (1983), *Physica (Amsterdam)* **117B**, 750.
- Price, P. J. (1984), *Solid State Communications* **51** (8), 607.
- Price, P. J. (1988), in *The Physics of Submicron Semiconductor Devices*, edited by H. Grubin, D. K. Ferry, and C. Jacoboni (Plenum, New York).
- Principi, A., M. Carrega, R. Asgari, V. Pellegrini, and M. Polini (2012), *Phys. Rev. B* **86**, 085421.
- Profumo, R. E. V., R. Asgari, M. Polini, and A. H. MacDonald (2012), *Phys. Rev. B* **85**, 085443.
- Prunnila, M., S. J. Laakso, J. M. Kivioja, and J. Ahopelto (2008), *Appl. Phys. Lett.* **93**, 112113.
- Pustilnik, M., E. G. Mishchenko, L. I. Glazman, and A. V. Andreev (2003), *Phys. Rev. Lett.* **91**, 126805.
- Pustilnik, M., E. G. Mishchenko, and O. A. Starykh (2006), *Phys. Rev. Lett.* **97**, 246803.
- Raichev, O., and P. Vasilopoulos (2000a), *Phys. Rev. B* **61**, 7511.
- Raichev, O., and P. Vasilopoulos (2000b), *Journal of Physics: Condensed Matter* **12** (30), 6859.
- Raichev, O. E. (1997), *Journal of Applied Physics* **81** (3), 1302.
- Raichev, O. E., and P. Vasilopoulos (1999), *Phys. Rev. Lett.* **83**, 3697.
- Raikh, M. E., and F. von Oppen (2002), *Phys. Rev. Lett.* **89**, 106601.
- Read, N. (1990), *Phys. Rev. Lett.* **65**, 1502.
- Reed, J. P., B. Uchoa, Y. I. Joe, Y. Gan, D. Casa, E. Fradkin, and P. Abbamonte (2010), *Science* **330** (6005), 805.
- Renn, S. R. (1992), *Phys. Rev. Lett.* **68**, 658.
- Reznikov, M., M. Heiblum, H. Shtrikman, and D. Mahalu (1995), *Phys. Rev. Lett.* **75**, 3340.
- Rieder, M.-T., T. Micklitz, A. Levchenko, and K. A. Matveev (2014), *Phys. Rev. B* **90**, 165405.
- Rojo, A. G. (1999), *J. Phys.: Condens. Matter* **11**, R31.
- Rojo, A. G., and G. D. Mahan (1992), *Phys. Rev. Lett.* **68**, 2074.
- Roth, A., C. Brne, H. Buhmann, L. W. Molenkamp, J. Maciejko, X.-L. Qi, and S.-C. Zhang (2009), *Science* **325** (5938), 294.
- Rozhkov, A. V. (2008), *Phys. Rev. B* **77**, 125109.
- Rozhkov, A. V. (2009), *Phys. Rev. B* **79**, 249903(E).
- Rubel, H., A. Fischer, W. Dietsche, C. Jörger, K. Klitzing, and K. Eberl (1997a), *Physica E* **1**, 160.
- Rubel, H., A. Fischer, W. Dietsche, C. Jörger, K. Klitzing, and K. Eberl (1998), *Physica B* **249-251**, 859.
- Rubel, H., A. Fischer, W. Dietsche, K. von Klitzing, and K. Eberl (1997b), *Phys. Rev. Lett.* **78**, 1763.
- Rubel, H., E. H. Linfield, N. P. R. Hill, J. T. Nicholls, D. A. Ritchie, K. M. Brown, M. Pepper, and G. A. C. Jones (1995), *Semicond. Sci. Technol.* **10**, 1229.
- Rubel, H., E. H. Linfield, N. P. R. Hill, J. T. Nicholls, D. A. Ritchie, K. M. Brown, M. Pepper, and G. A. C. Jones (1996), *Surf. Sci.* **361-362**, 134.
- Sakhi, S. (1997), *Phys. Rev. B* **56**, 4098.
- Sánchez, R., R. López, D. Sánchez, and M. Büttiker (2010), *Phys. Rev. Lett.* **104**, 076801.
- Santoro, G. E., and G. F. Giuliani (1988), *Phys. Rev. B* **37**, 937.
- Scharf, B., and A. Matos-Abiague (2012), *Phys. Rev. B* **86**, 115425.
- Schliemann, J., S. M. Girvin, and A. H. MacDonald (2001), *Phys. Rev. Lett.* **86**, 1849.
- Schlottmann, P. (2004a), *Phys. Rev. B* **69**, 035110.
- Schlottmann, P. (2004b), *Phys. Rev. B* **70**, 115306.
- Schmult, S., L. Tiemann, W. Dietsche, and K. von Klitzing (2010), *J. Vac. Sci. Technol. B* **28**, C3C1.
- Schütt, M., P. M. Ostrovsky, I. V. Gornyi, and A. D. Mirlin (2011), *Phys. Rev. B* **83**, 155441.
- Schütt, M., P. M. Ostrovsky, M. Titov, I. V. Gornyi, B. N. Narozhny, and A. D. Mirlin (2013), *Phys. Rev. Lett.* **110**, 026601.
- Seamons, J. A., C. P. Morath, J. L. Reno, and M. P. Lilly (2009), *Phys. Rev. Lett.* **102**, 026804.
- Seeger, K. (2002), *Semiconductor Physics* (Springer).
- Seradjeh, B., J. E. Moore, and M. Franz (2009), *Phys. Rev. Lett.* **103**, 066402.
- Shahbazyan, T. V., and S. E. Ulloa (1997a), *Phys. Rev. B* **55**, 13702.
- Shahbazyan, T. V., and S. E. Ulloa (1997b), *Physica E* **1**, 259.
- Shen, S.-Q. (2013), *Topological Insulators: Dirac Equation in Condensed Matters* (Springer).
- Shevchenko, S. I. (1976), *Fiz. Nizk. Temp.* **2**, 505, [*Sov. J. Low-Temp. Phys.* **2**, 251 (1976)].
- Shimshoni, E. (1995), *Phys. Rev. B* **51**, 9415.
- Shimshoni, E., and S. L. Sondhi (1994), *Phys. Rev. B* **49**, 11484.
- Shon, N. H., and T. Ando (1998), *Journal of the Physical Society of Japan* **67** (7), 2421.
- Shylau, A. A., and A.-P. Jauho (2014), *Phys. Rev. B* **89**, 165421.
- Simon, S. H., E. H. Rezayi, and M. V. Milovanovic (2003), *Phys. Rev. Lett.* **91**, 046803.
- Singwi, K. S., M. P. Tosi, R. H. Land, and A. Sjölander (1968), *Phys. Rev.* **176**, 589.
- Sirenko, Y. M., and P. Vasilopoulos (1992), *Phys. Rev. B* **46**, 1611.
- Sivan, U., P. M. Solomon, and H. Shtrikman (1992), *Phys. Rev. Lett.* **68**, 1196.
- Smith, H., and H. H. Jensen (1989), *Transport Phenomena* (Oxford University Press).
- Snoke, D. W. (2002), *Science* **298**, 1368.
- Snoke, D. W. (2008), *Solid State Physics. Essential Concepts* (Addison-Wesley).
- Sodemann, I., D. A. Pesin, and A. H. MacDonald (2012), *Phys. Rev. B* **85**, 195136.
- Söderström, E., A. V. Buyanov, and B. E. Sernelius (1996), *J. Phys.: Condens. Matter* **8**, 3705.
- Solomon, P. M., and B. Laikhtman (1991), *Superlattices Microstruct.* **10**, 89.
- Solomon, P. M., P. J. Price, D. J. Frank, and D. C. L. Tulipe (1989), *Phys. Rev. Lett.* **63**, 2508.

- Son, D. T. (2007), *Phys. Rev. B* **75**, 235423.
- Song, J. C. W., D. A. Abanin, and L. S. Levitov (2013), *Nanolett.* **13**, 3631.
- Song, J. C. W., and L. S. Levitov (2012), *Phys. Rev. Lett.* **109**, 236602.
- Song, J. C. W., and L. S. Levitov (2013), *Phys. Rev. Lett.* **111**, 126601.
- Sothmann, B., R. Sánchez, A. N. Jordan, and M. Büttiker (2012), *Phys. Rev. B* **85**, 205301.
- Spielman, I. B., J. P. Eisenstein, L. N. Pfeiffer, and K. W. West (2000), *Phys. Rev. Lett.* **84**, 5808.
- Spielman, I. B., M. Kellogg, J. P. Eisenstein, L. N. Pfeiffer, and K. W. West (2004), *Phys. Rev. B* **70**, 081303(R).
- Spivak, B., and S. Kivelson (2005), *Phys. Rev. B* **72**, 045355.
- Spivak, B., S. V. Kravchenko, S. A. Kivelson, and X. P. A. Gao (2010), *Rev. Mod. Phys.* **82**, 1743.
- Stauber, T., and G. Gómez-Santos (2012), *Phys. Rev. B* **85**, 075410.
- Stern, A., and B. I. Halperin (1995), *Phys. Rev. B* **52**, 5890.
- Stern, A., and B. I. Halperin (2002), *Phys. Rev. Lett.* **88**, 106801.
- Stern, A., S. D. Sarma, M. P. A. Fisher, and S. M. Girvin (2000), *Phys. Rev. Lett.* **84**, 139.
- Stern, A., and I. Ussishkin (1997), *Physica E* **1**, 176.
- Stern, F. (1967), *Phys. Rev. Lett.* **18**, 546.
- Stormer, H. L., L. N. Pfeiffer, K. W. Baldwin, and K. W. West (1990), *Phys. Rev. B* **41**, 1278.
- Su, J.-J., and A. H. MacDonald (2008), *Nature Physics* **4**, 799.
- Suen, Y. W., L. W. Engel, M. B. Santos, M. Shayegan, and D. C. Tsui (1992), *Phys. Rev. Lett.* **68**, 1379.
- Suprunenko, Y. F., V. Cheianov, and V. I. Fal'ko (2012), *Phys. Rev. B* **86**, 155405.
- Svintsov, D., V. Vyurkov, S. Yurchenko, T. Otsuji, and V. Ryzhii (2012), *Journal of Applied Physics* **111** (8).
- Swierkowski, L., J. Szymanski, and Z. W. Gortel (1995), *Phys. Rev. Lett.* **74**, 3245.
- Swierkowski, L., J. Szymanski, and Z. W. Gortel (1996), *Surf. Sci.* **361-362**, 130.
- Swierkowski, L., J. Szymanski, and Z. W. Gortel (1997), *Phys. Rev. B* **55**, 2280.
- Takashina, K., K. Nishiguchi, Y. Ono, A. Fujiwara, T. Fujisawa, Y. Hirayama, and K. Muraki (2009), *Appl. Phys. Lett.* **94**, 142104.
- Tan, Y.-W., Y. Zhang, H. L. Stormer, and P. Kim (2007), *Eur. Phys. J. Special Topics* **148**, 15.
- Tanatar, B. (1996), *Solid State Comm.* **99**, 1.
- Tanatar, B. (1998), *Phys. Rev. B* **58**, 1154.
- Tanatar, B., and A. K. Das (1996), *Phys. Rev. B* **54**, 13827.
- Tiemann, L., W. Dietsche, M. Hauser, and K. von Klitzing (2008a), *New Journal of Physics* **10** (4), 045018.
- Tiemann, L., J. G. S. Lok, W. Dietsche, K. von Klitzing, K. Muraki, D. Schuh, and W. Wegscheider (2008b), *Phys. Rev. B* **77**, 033306.
- Titov, M., R. V. Gorbachev, B. N. Narozhny, T. Tudorovskiy, M. Schütt, P. M. Ostrovsky, I. V. Gornyi, A. D. Mirlin, M. I. Katsnelson, K. S. Novoselov, A. K. Geim, and L. Ponomarenko (2013a), *Phys. Rev. Lett.* **111**, 166601.
- Titov, M., B. N. Narozhny, and I. V. Gornyi (2013b), unpublished.
- Tomonaga, S. (1950), *Prog. Theor. Phys.* **5**, 544.
- Tse, W.-K., and S. Das Sarma (2007), *Phys. Rev. B* **75**, 045333.
- Tse, W.-K., B. Y.-K. Hu, and S. D. Sarma (2007), *Phys. Rev. B* **76**, 081401.
- Tso, H. C., D. J. Geldart, and P. Vasilopoulos (1998), *Phys. Rev. B* **57**, 6561.
- Tso, H. C., and P. Vasilopoulos (1992), *Phys. Rev. B* **45**, 1333.
- Tso, H. C., P. Vasilopoulos, and F. M. Peeters (1992), *Phys. Rev. Lett.* **68**, 2516.
- Tso, H. C., P. Vasilopoulos, and F. M. Peeters (1993), *Phys. Rev. Lett.* **70**, 2146.
- Tso, H. C., P. Vasilopoulos, and F. M. Peeters (1994), *Surf. Sci.* **305**, 400.
- Tutuc, E., R. Pillarisetty, and M. Shayegan (2009), *Phys. Rev. B* **79**, 041303(R).
- Tutuc, E., M. Shayegan, and D. A. Huse (2004), *Phys. Rev. Lett.* **93**, 036802.
- Ussishkin, I., and A. Stern (1997), *Phys. Rev. B* **56**, 4013.
- Ussishkin, I., and A. Stern (1998), *Phys. Rev. Lett.* **81**, 3932.
- Varma, C. M., A. I. Larkin, and E. Abrahams (1994), *Phys. Rev. B* **49**, 13999.
- Vignale, G. (2005), *Phys. Rev. B* **71**, 125103.
- Vignale, G., and A. H. MacDonald (1996), *Phys. Rev. Lett.* **76**, 2786.
- Vignale, G., and K. S. Singwi (1985), *Phys. Rev. B* **31**, 2729.
- Vitkalov, S. (1998), *Pis'ma Zh. Eksp. Teor. Fiz.* **67**, 276, [JETP Lett. **67**, 295 (1998)].
- Walter, A. L., A. Bostwick, K.-J. Jeon, F. Speck, M. Ostler, T. Seyller, L. Moerschini, Y. J. Chang, M. Polini, R. Asgari, A. H. MacDonald, K. Horn, and E. Rotenberg (2011), *Phys. Rev. B* **84**, 085410.
- Wang, D.-W., E. G. Mishchenko, and E. Demler (2005), *Phys. Rev. Lett.* **95**, 086802.
- Wang, X., and I. C. da Cunha Lima (2001), *Phys. Rev. B* **63**, 205312.
- Wei, P., W. Bao, Y. Pu, C. N. Lau, and J. Shi (2009), *Phys. Rev. Lett.* **102**, 166808.
- Wen, X.-G. (1995), *Advances in Physics* **44** (5), 405.
- Wen, X.-G., and A. Zee (1992), *Phys. Rev. Lett.* **69**, 1811.
- Wiersma, R., J. Lok, L. Tiemann, W. Dietsche, K. von Klitzing, D. Schuh, and W. Wegscheider (2006), *Physica E: Low-dimensional Systems and Nanostructures* **35** (2), 320, proceedings of the 14th International Winterschool on New Developments in Solid State Physics -Charges and spins in nanostructures: basics and devices.
- Wiersma, R. D., J. G. S. Lok, S. Kraus, W. Dietsche, K. von Klitzing, D. Schuh, M. Bichler, H.-P. Tranitz, and W. Wegscheider (2004), *Phys. Rev. Lett.* **93**, 266805.
- Wiersma, R. D., J. G. S. Lok, L. Tiemann, W. Dietsche, K. von Klitzing, W. Wegscheider, and D. Schuh (2007), *International Journal of Modern Physics B* **21**, 1256.
- Wunsch, B., T. Stauber, F. Sols, and F. Guinea (2006), *New Journal of Physics* **8** (12), 318.
- Yamamoto, M., M. Stopa, Y. Tokura, Y. Hirayama, and S. Tarucha (2002), *Physica E* **12**, 726.
- Yamamoto, M., M. Stopa, Y. Tokura, Y. Hirayama, and S. Tarucha (2006), *Science* **313**, 204.
- Yamamoto, M., H. Takagi, M. Stopa, and S. Tarucha (2012), *Phys. Rev. B* **85**, 041308(R).
- Yan, H., X. Li, B. Chandra, G. Tulevski, Y. Wu, M. Freitag, W. Zhu, P. Avouris, and F. Xia (2012a), *Nature Nanotech.* **7**, 330.
- Yan, H., Z. Li, X. Li, W. Zhu, P. Avouris, and F. Xia (2012b), *Nano Letters* **12** (7), 3766.
- Yang, K. (1998), *Phys. Rev. B* **58**, R4246.
- Yang, K., and A. H. MacDonald (2001), *Phys. Rev. B* **63**,

- 073301.
- Yang, K., K. Moon, L. Zheng, A. H. MacDonald, S. M. Girvin, D. Yoshioka, and S.-C. Zhang (1994), Phys. Rev. Lett. **72**, 732.
- Yang, L., J. D. Koralek, J. Orenstein, D. R. Tibbetts, J. L. Reno, and M. P. Lilly (2011), Phys. Rev. Lett. **106**, 246401.
- Yoon, Y., L. Tiemann, S. Schmult, W. Dietsche, K. von Klitzing, and W. Wegscheider (2010), Phys. Rev. Lett. **104**, 116802.
- Yoshioka, D., A. H. MacDonald, and S. M. Girvin (1989), Phys. Rev. B **39**, 1932.
- Yurtsever, A., V. Moldoveanu, and B. Tanatar (2003), Solid State Communications **125**, 575.
- Zala, G., B. Narozhny, and I. Aleiner (2001), Phys. Rev. B **64**, 214204.
- Zelakiewicz, S., H. Noh, T. J. Gramila, L. N. Pfeiffer, and K. W. West (2000), Phys. Rev. Lett. **85**, 1942.
- Zhang, C., and G. Jin (2013), Journal of Physics: Condensed Matter **25** (42), 425604.
- Zhang, C., and Y. Takahashi (1993), J. Phys.: Condens. Matter **5**, 5009.
- Zhang, C.-H., and Y. N. Joglekar (2008), Phys. Rev. B **77**, 233405.
- Zhang, S. S.-L., and S. Zhang (2012), Phys. Rev. Lett. **109**, 096603.
- Zheng, L., and A. H. MacDonald (1993), Phys. Rev. B **48**, 8203.
- Zhou, F., and Y. B. Kim (1999), Phys. Rev. B **59**, R7825.
- Zhu, J.-J., S. M. Badalyan, and F. M. Peeters (2013), Phys. Rev. B **87**, 085401.
- Ziman, J. M. (1965), *Principles of the Theory of Solids* (Cambridge).
- Zou, Y., G. Refael, and J. Yoon (2009), Phys. Rev. B **80**, 180503(R).
- Zou, Y., G. Refael, and J. Yoon (2010), Phys. Rev. B **82**, 104515.
- Zuev, Y. M., W. Chang, and P. Kim (2009), Phys. Rev. Lett. **102**, 096807.
- Zyuzin, V. A., and G. A. Fiete (2010), Phys. Rev. B **82**, 113305.